Aswath Subramanian

Long-Term Stability of Scalable Perovskite Architecture

TU Delft

SOLLIANCE
10 YEARS OF SOLAR RESEARCH

Long-term Stability of Scalable Perovskite Architecture

By

Aswath Subramanian

in partial fulfilment of the requirements for the degree of

Master of Science
in Sustainable Energy Technology

at the Delft University of Technology,
to be defended publicly on Tuesday August 16th, 2021, at 10:00 AM.

Supervisors:	Prof. dr. ir. O. Isabella	TU Delft
	Prof. dr. ir. L. Mazzarella	TU Delft
Thesis committee:	Prof. dr. ir. A.H.M. Smets,	TU Delft
	Dr. T. Savenije,	TU Delft
	Dr. V. Zardetto,	TNO/Solliance Solar Research

Preface

Let me lead this thesis with an old dialogue signifying the relationship between the Sun and humanity:

"Have you ever seen a beautiful, transparent stone at the druggists', with which you may kindle fire?"
- Strepsiades (The Clouds, By Aristophanes in 419 B.C.E)

The growing dominance of solar energy in today's energy mix is a sufficient motivation to research better solutions outside the conventional silicon-based modules, with perovskite being one of the alternates. For perovskites, the research is currently focused on lab-scale samples with emphasis on performance. There is not sufficient work on devices fabricated with processes adaptable by industry. There is neither sufficient work on long-term stability of the cells. This thesis is an attempt at checking all these boxes, thus aptly titled ***"Long-Term Stability of Scalable Perovskite Architecture"***.

The thesis is targeted at readers with some awareness about photovoltaics and the workings of a solar cell, including recombination processes. An introduction is provided to characterization experiments undertaken without extensive explanation on their principles. An awareness of lab-scale fabrication processes is beneficial to appreciate the necessity of upscaling techniques described in chapter 3. Additional knowledge on the chemistry of the perovskite absorber layer would be beneficial, but not necessary.

These nine months of experiments was a journey unlike any other. Especially with the onset of COVID, the challenges also included simple activities like travel to work or store, conversing in person and scheduling work. The author would like to thank the supervisors from TU Delft, Dr. Olindo and Dr. Luana for their positive academic support during the challenging period of thesis. The Perovskite team in Solliance Solar Research, Eindhoven for their wisdom and wit in performing my experiments and experiencing an enthusiastic work environment. Dr. Valerio, my direct supervisor, for the hours of discussion and the knowledge that has imparted on me. The parents, siblings, and friends for their mental support in keeping me motivated and grounded. The almighty *Brahman*, for providing me with the opportunity to meet these people and learn from them.

Aswath Subramanian
Eindhoven, August 2021

Abstract

Perovskite Solar Cells are an increasing attraction in research with great strides in performance efficiencies. But their commercialization is far from fruition, due to persistent issues. Stability under prolonged exposure to external stresses is a major concern. Furthermore, the adaption of upscaling technologies in research is presently slow.

This research is done on a fully scalable architecture, fabricated with technologies adaptable to mass-production. Variations in active layer (dual cation and triple cation) and Electron Transport Layer are designed into different stack combinations to discriminate the more resilient stack. Long-term stability of these stacks is tested by accelerated thermal test and light-soaking test. Light-soaking test is done from different sides and with a filter to determine the difference in behaviour of samples.

From thermal testing, the dual cation perovskite was found to be more resilient. In light-soaking tests done from side of glass, all stacks failed, while the stacks illuminated from side of ETL showed a far better performance. The dual cation perovskite was again found to be more resilient. Despite the performance loss, none of the stacks demonstrated significant degradation in perovskite layer under XRD or photoluminescence. Therefore, recombination mechanisms were studied under light-intensity measurements. The presence of carrier collection problems across stacks and degradation of HTL particularly in samples of glass-side exposure are determined to be the probable cause.

Contents

1. Introduction

1.1 The Great Electricity Question

The 21st century has the highest ever demand for electricity. The world gets hungrier for energy and electricity day by day. The BP Energy Outlook 2020 estimates an increase in the total final consumption (TFC) share of electricity from little over 20% in 2018 to anywhere between 34% (business as usual) to 50% (Net Zero) [1]. Figure 1.1 provides an insight into the growth of per capita electricity demand over the last two decades as against the GDP of selected nations [2]. A closer look at the figure reveals the increase in per capita electricity consumption is propelled mainly over the last two decades by emerging economies like China, India, and other non-OECD countries. OECD members, on the other hand, have reached a plateau, if not reduction in per capita electricity consumption, in 21st century.

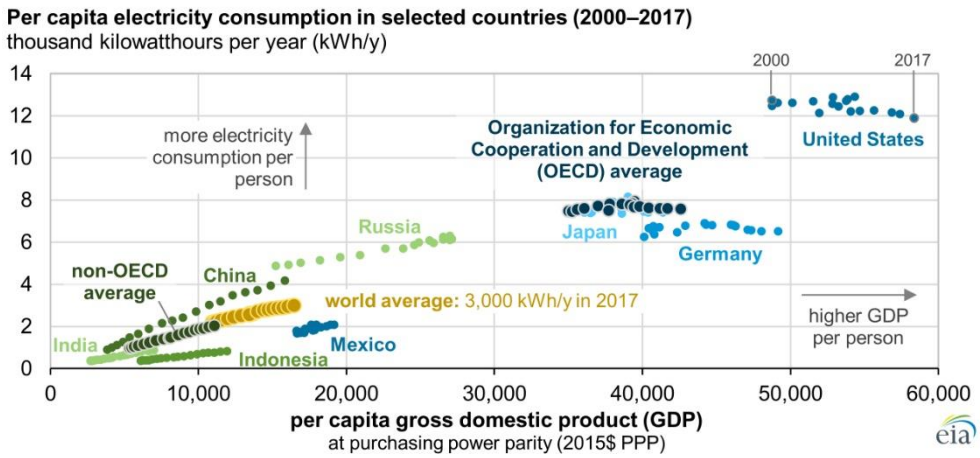

Figure 1.1 Per-Capita Electricity Consumption in selected countries. Courtesy of EIA [2]

To match the demand problem, supply is ramped up in kind. Figure 1.3 shows the production of electricity from various sources of energy. Even until 2019, the fraction of fossil fuels (cumulation of coal, oil, gas) in global energy mix is approximately 62.74%, which is not a great improvement from the 63.9% of 1985 [3]. The relative consumption of gas has increasingly supplanted oil in the global stage but the cumulative share of renewable power (excluding hydropower which is consistently between 16-20%) has risen only in the last two decades, accounting to 10.62% of the total mix as of 2019. The general outlook, presently, is that fossil fuels still dominate the energy generation mix.

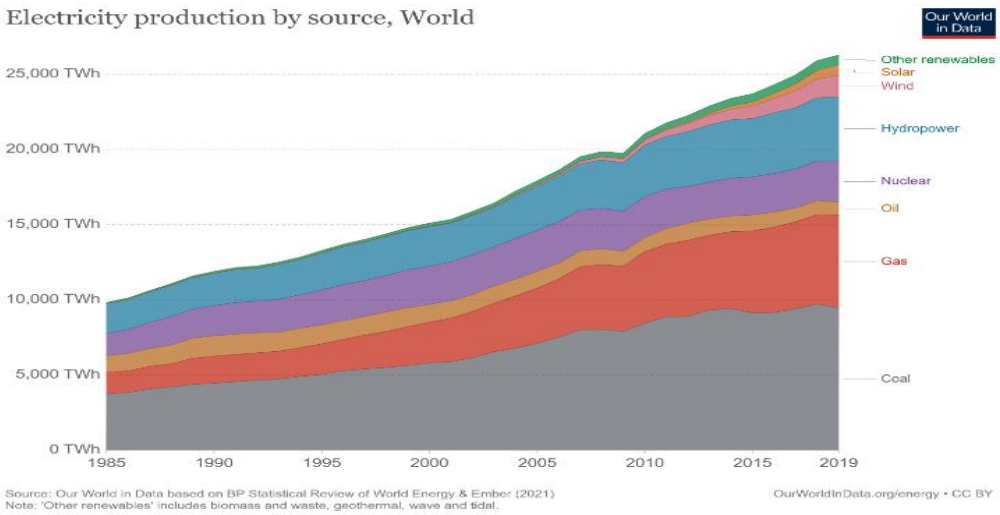

Figure 1.2 Electricity Production By Source, World. Courtesy of Our World In Data

Combustion of carbon-based fuels leads to emission of carbon dioxide. The story of CO_2 emission requires a historical perspective to understand the severity and relevance of its negative externalities in present day. The trend of CO_2 emissions is seen in the figure 1.4. The thrust in coal mining during industrialization era (post 1750s) was the beginning of large-scale CO_2 emission by humans with coal becoming the industry's favorite fuel. The rise in slopes oil emissions in the first half of 20^{th} century, followed by the increasing consumption of gas in the second half is the story of developed nations, while the steep increase in coal-emissions coincides with the increase in industrialization in China and India post 1970s. As of 2019, the cumulative emission of carbon from all fossil fuel sources is at 94.36% (34.36 billion tonnes of 36.42 billion tonnes). An understanding of the growth of CO_2 emission in each sector is shown in figure 1.5. It is pertinent to note the share of electricity/heat in the total emissions which has increased from 8.6 billion tonnes in 1990 to 15.59 billion tonnes as of 2018.

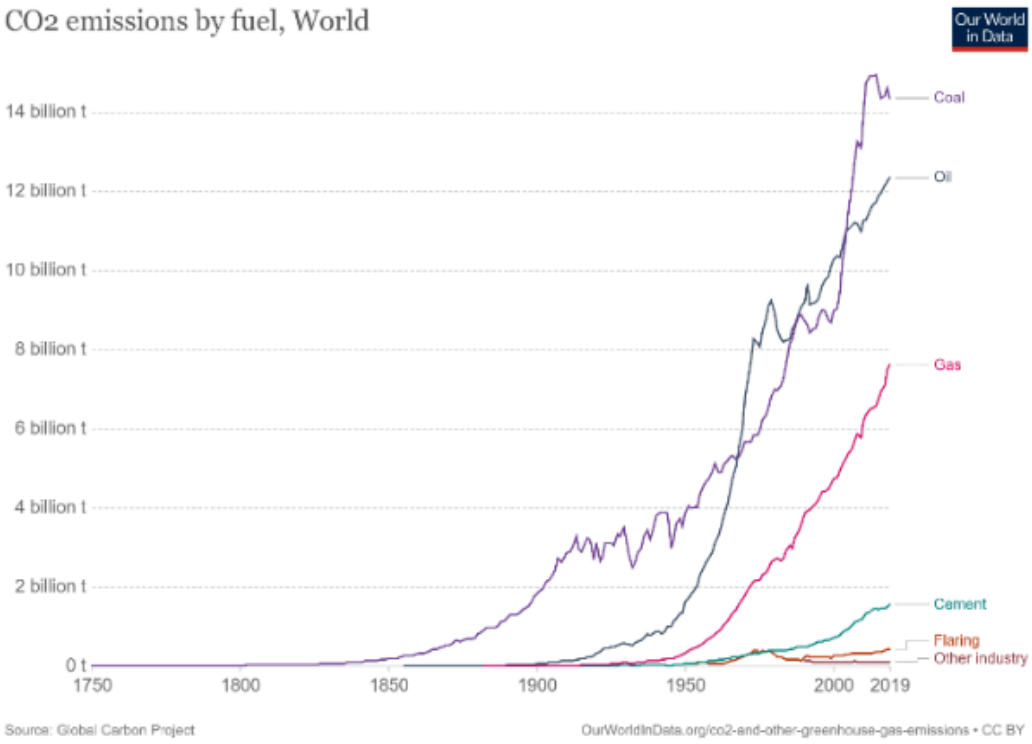

Figure 1.3 Carbon Dioxide emissions by fuel. Courtesy of Our World in Data.

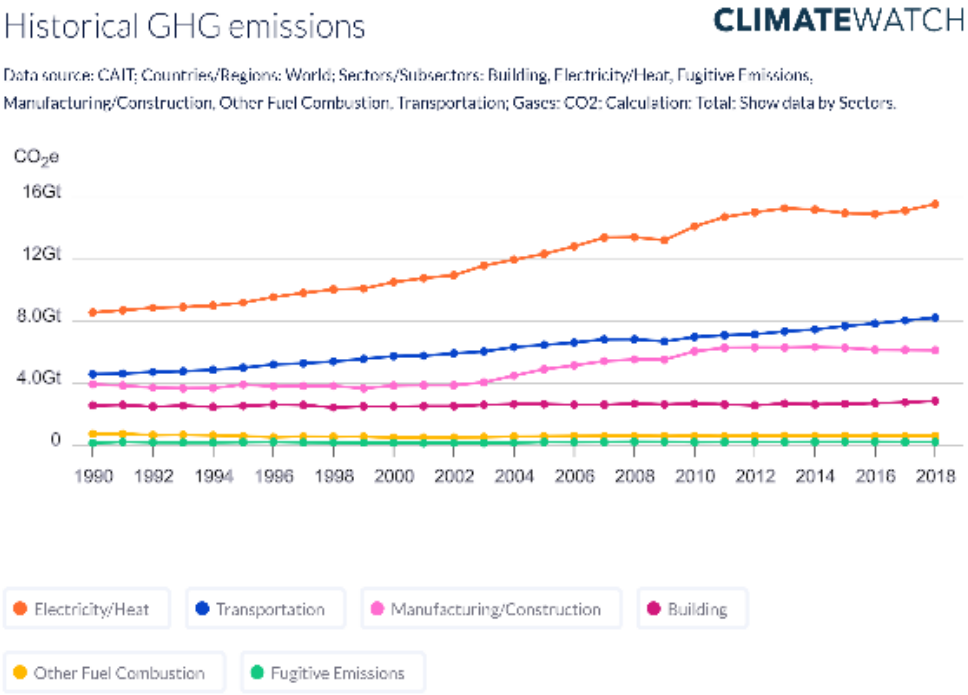

Figure 1.4 GHG Emission per sector. Courtesy of ClimateWatchData.org

The United Nations Framework Convention on Climate Change (UNFCCC) of 1992 defines "climate change" as *"a change of climate which is attributed directly or indirectly to human activity that alters the composition of the global atmosphere and which is in addition to natural climate variability observed over comparable time periods"* [4]. The accelerated emission of greenhouse gases in the last few centuries has increased the surface temperature. According to NASA, there has been a 1°C increase in surface temperature between 1980 and 2019. This so-called "global warming" has been roughly at 0.15-0.20°C per decade since 1975. The various effects of this include melting of polar ice caps, rise in sea levels, submerging of coastal areas, erratic climatic conditions like severe droughts or floods.

International action against global warming took shape with the operationalization of Kyoto Protocol in February 2005. In recent times, the "Paris Agreement" adopted in December 2015 set a global framework towards limiting global warming to below 2°C above pre-industrial levels and aim towards 1.5°C above pre-industrial levels in order to *"significantly reduce the risks and impacts of climate change"*. Figure 1.5 is a representation of the various pathways that may be taken to reduce the global warming by reducing greenhouse gas emissions. The projection for current policies stands at 2.7-3.1°C, which is falling short of the ambitious targets of Paris Summit. Therefore, emphasis is heavily placed on technologies and processes that would help in reducing GHG emissions.

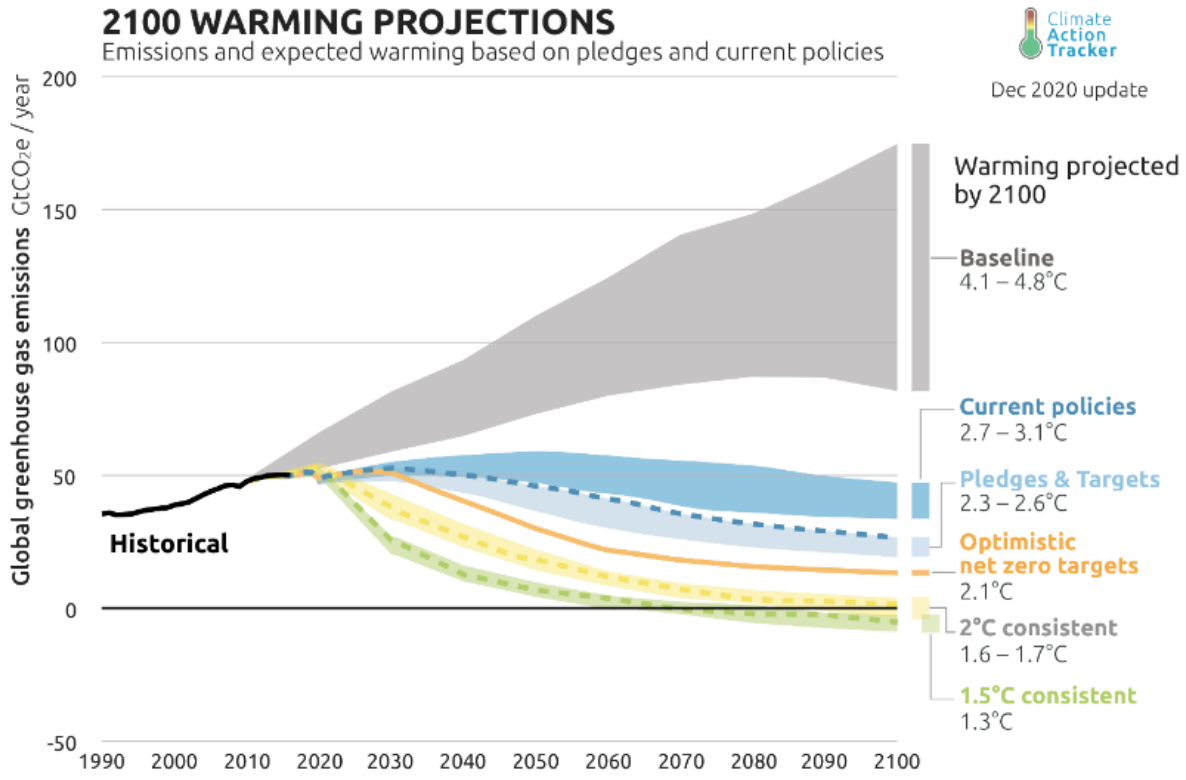

Figure 1.5 Global Warming Projections for 2100. Courtesy of ClimateActionTracker.org

1.2. Going Green, “Chasing The Sun”

Article 2 of the Paris Agreement also recognizes to *“Making finance flows consistent with a pathway towards low greenhouse gas emissions and climate-resilient development”* for addressing climate change. The previous section allows to conclude that global warming is the resultant of an increase in GHG emissions due to an increase in consumption of fossil fuels. The search for low GHG emissions, thus, begins with searching for an alternate fuel source. The potential availability of various energy sources is represented in figure 1.6.

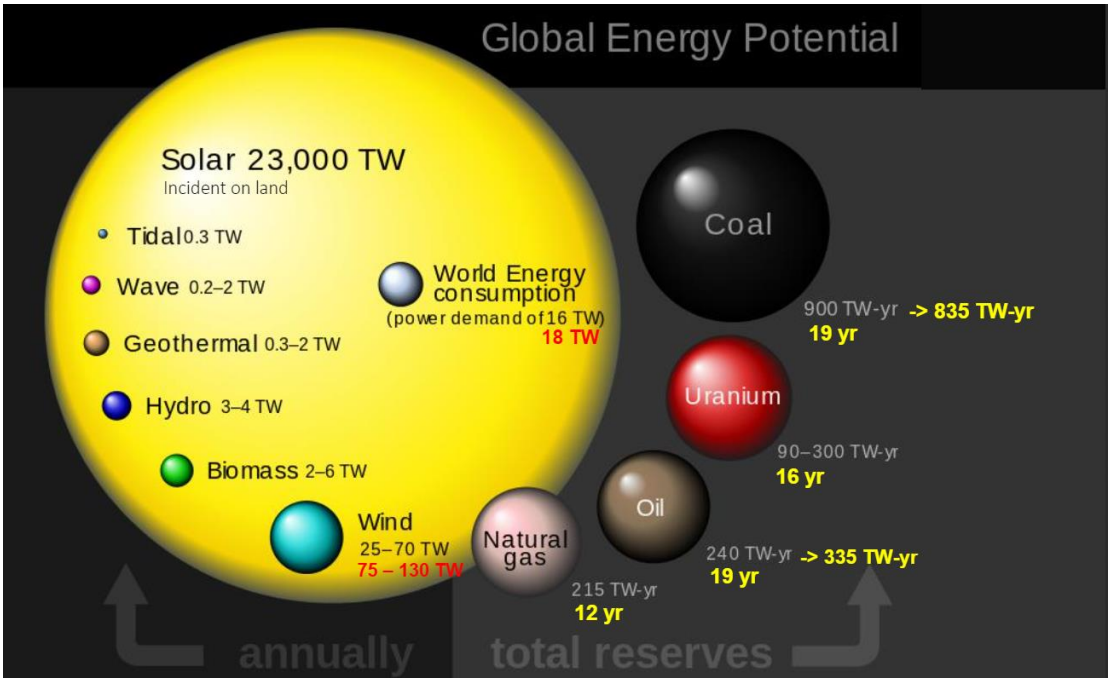

Figure 1.6 Comparing finite and renewable planetary energy reserves- Adapted from “A Fundamental Look At Energy Reserves For The Planet” by Perez et. al., The IEA SHC Solar Update 50(2),2009 [5]

From this figure, the non-replenishable energy sources that emit GHGs (coal, oil and gas) can be seen to have potential alternatives that are non-conventional and have relatively lesser emissions (biomass, geothermal) or significantly lesser emission of GHGs (solar, wind, hydro, wave, tidal). A summary of the various advantages and disadvantages of such potential non-conventional energy sources is listed in table 1.1.

Energy source	Harnessing Technology (examples)	Advantages	Disadvantages
Sun	Solar Cells, Solar thermal plants	Easy installation, low operational costs, abundant supply.	Output influenced by weather.
Wind	Turbines	Low operational costs, abundant supply	High setup costs, inconsistent wind

			patterns.
Water	Dams, Ocean Thermal Energy Generator, Wave Turbine, Tide harnessing	Low operational costs	Very high setup costs, potential ecological issues.
Biomass	Reactors, Powerplants	Low operational costs	Low yield per mass

Table 1.1 Summary of pros and cons - Energy Sources

The generation share of "renewable" energy in electricity has increased consistently year-on-year and the figure 1.7 shows the growth of the various sources with time.

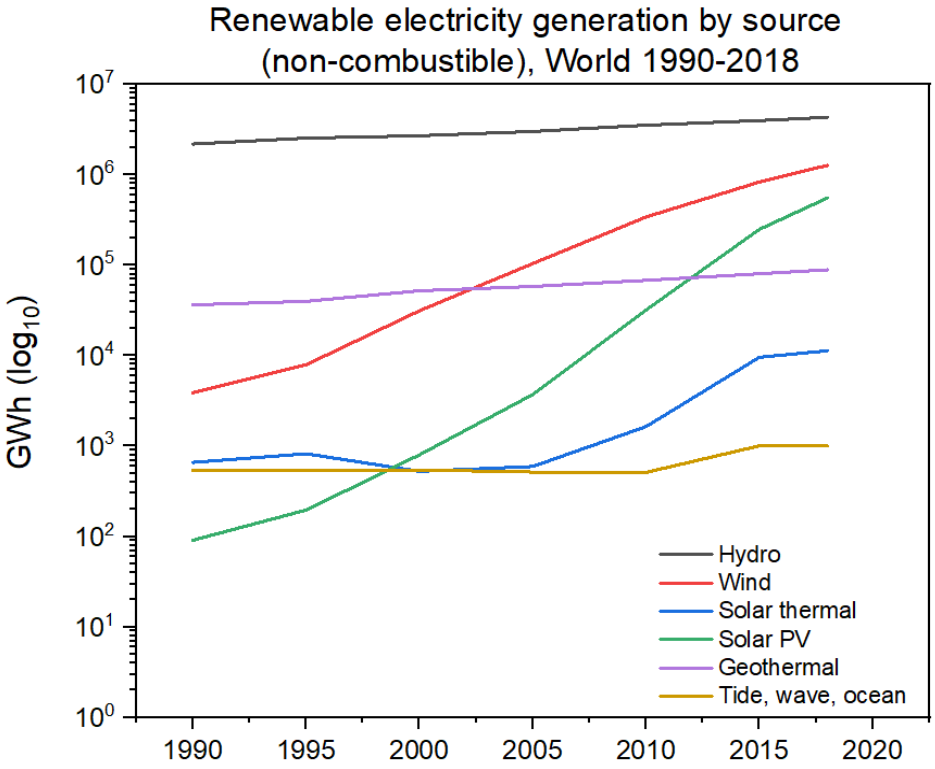

Figure 1.7 Renewable Electricity generation by source. Courtesy of bp Statistical Review of World Energy [6]

The transition towards a decreasing dependence on fossil fuels is the prudent choice for the future of production of electricity is thus stressed on. From the brief glimpse into such alternatives, harnessing energy from the sun is seen as the most prospective option. While sun has always been a traditional source of heat, exploitation of solar energy by directly transforming it into electricity is gaining increasing relevance.

1.3. Photovoltaics – The Engine of Tomorrow

The most lucrative proposition in favor of solar energy is the potential energy that can be harvested from the sun, which is the true perennial source of energy. Figure 1.8 shows how this abundance of

solar power can be exploited across the world. “Photovoltaics” (abbreviated PV) is the phenomenon of conversion of solar energy into electricity. The figure also shows thus, the potential electricity output that may be derived at a geographic location annually. The detraction to this abundant availability is the dependence on weather and the day-night cycle of Earth. This makes it extremely important to anticipate such availability constraints by rigorous prediction methodologies.

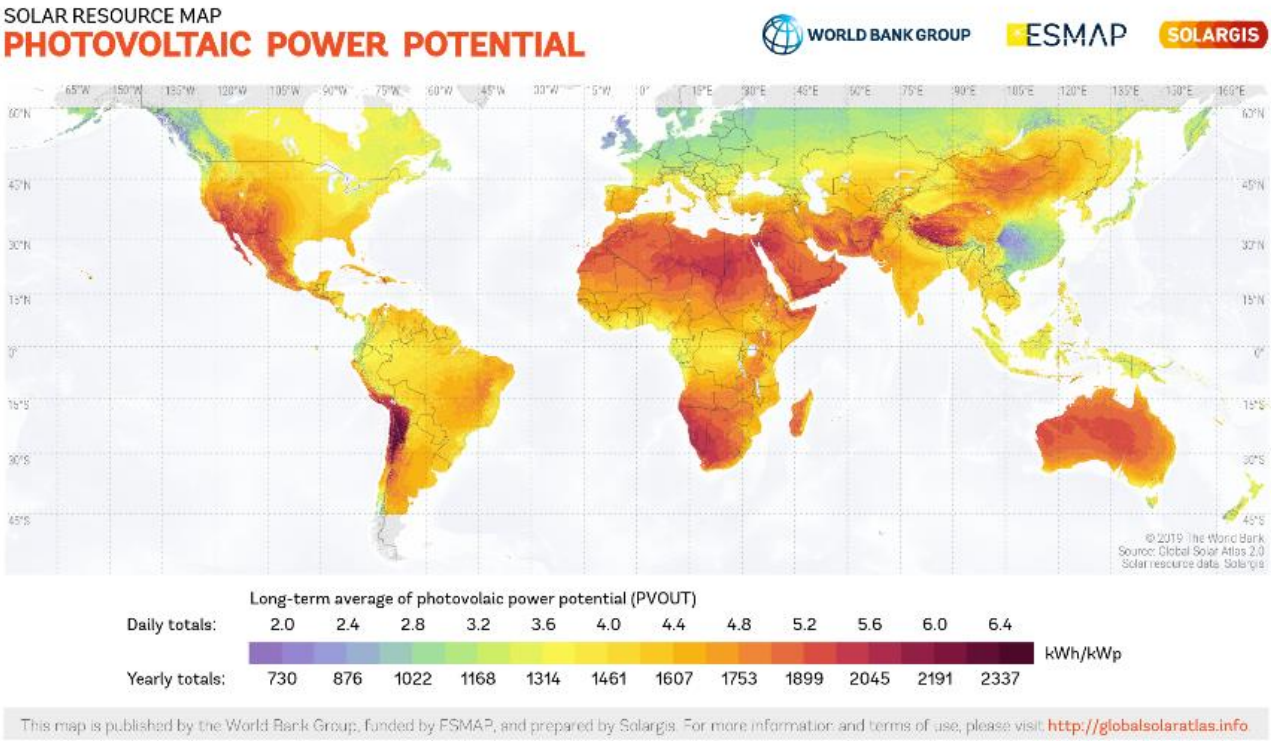

Figure 1.8 Photovoltaic Power Potential. Courtesy of Global Solar Atlas

Several PV technologies are adopted to generate electricity directly from solar energy. And the conversion efficiency of these technologies are heavily researched upon for improvement. Figure 1.9 shows a timeline of the improvement in power conversion efficiency of some of the common (blue labels) and researched (red, yellow labels) technologies. The rapid improvement in efficiency of some of these technologies signify the interest and the potential of PV technology.

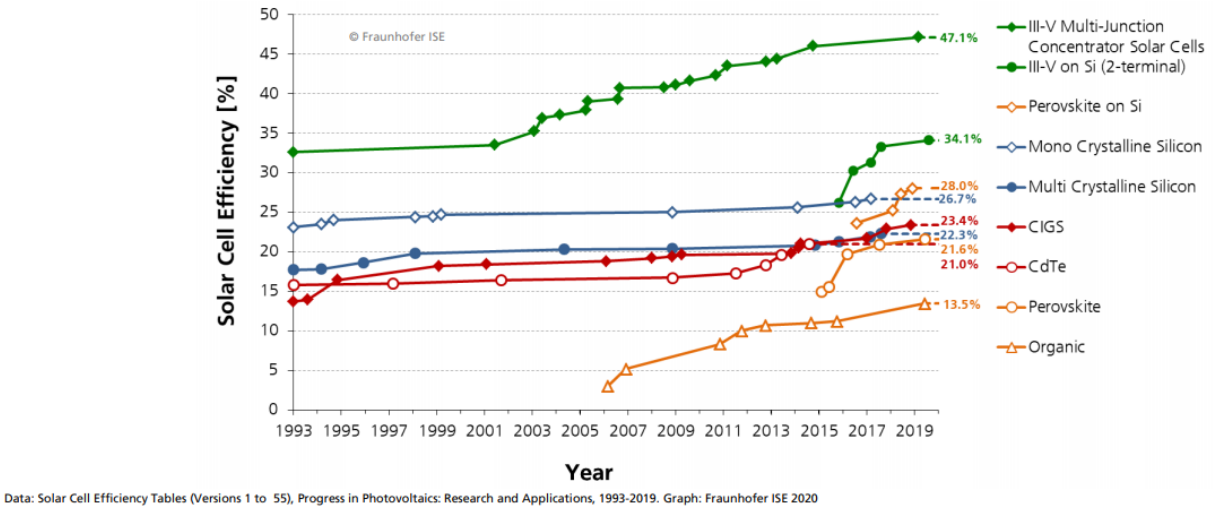

Figure 1.9 Timeline of Record Efficiencies of various PV Technologies. Courtesy of Franhoufer ISE

The installation capacity, usually measured in Watts culminates in global installation capacity, which is represented in figure 1.10.

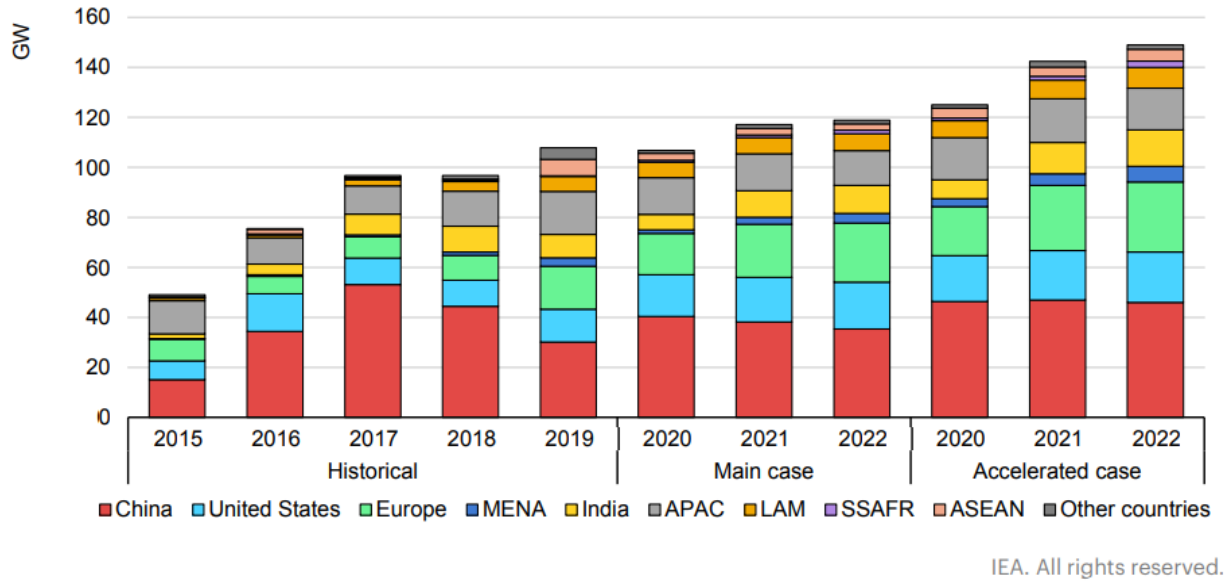

Figure 1.10 Projection for PV Module Installation Capacity. Courtesy of IEA.

Of course, not all the technologies mentioned in figure 1.9 are commercially available, or competitive. The present PV industry is highly dominated by silicon-based technologies, as may be seen from figure 1.11, while the share of thin-film alternatives varies in time and presently accounts for only 5% of the total annual production.

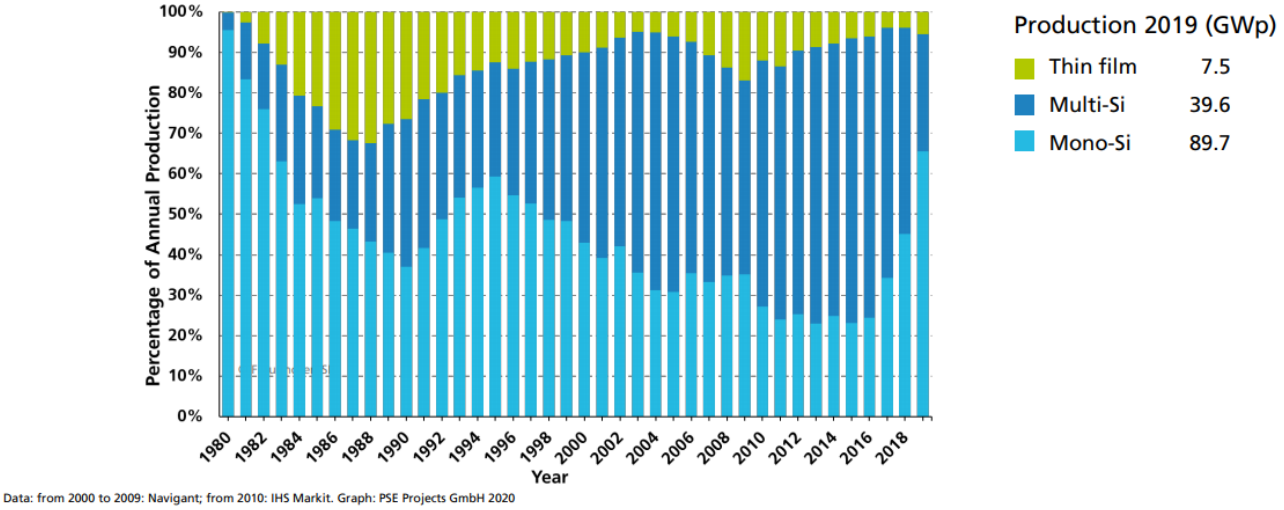

Figure 1.11 PV Production by Technology- Percentage of Global Production. Courtesy of Franhoufer ISE

Revisiting figure 1.9, there is interest in introducing PV technologies that are not based on Si. CIGS (Copper Indium Gallium Selenide) and CdTe (Cadmium Telluride) are some promising inorganic options, while 'organic' cells are usually based on polymers. One of the options listed in the figure that can be organic, inorganic or a hybrid of both, is the perovskite technology. This makes the Perovskite Solar Cell (PSC) an option with better potential for engineering and customization.

1.4 Thesis Outline

This document is written as follows. Chapter 2 elaborates on the fundamentals of perovskite solar cells and outline the various layers deposited on the cells. It also introduces the research questions in section 2.6. Chapter 3 introduces the the various fabarication, testing and experimental conditions and their principles. Chapter 4 and 5 address the RQs listed in section 2.6 and discuss the results of various experiments. This thesis is concluded with chapter 6 on a summary of recommendations. Appendix A1 is added to the document to refer to the figures of the results additionaly discussed in chapters 4 and 5.

2. Perovskite Solar Cells

2.1. Introduction

"Perovskite" is the name given to any material that has the same structure of the mineral of the same name, chemically Calcium Titanium Oxide ($CaTiO_3$). The general formula of perovskite-class materials is denoted by ABX_3. A and B are two cations, usually of two different sizes and X is an anion. As shown in figure 2.1, the idealized perovskite unit cell has a cubic symmetry, with B cations in a 6-fold coordination, surrounded by anions in an octahedral configuration. This is then surrounded by A cation in 12-fold cuboctahedral coordination. Perovskites are researched for their potential application in diverse fields. Their properties like colossal magnetoresistance, ferroelectricity, superconductivity make it a desired candidate in electronic industry. Piezoelectricity of perovskites is being researched for energy storage applications. The other fields of research that investigate perovskites include photocatalysis, lasers, LEDs and scintillation. In 2009, Tsutomu Miyasaka and a team demonstrated the application of perovskites in harnessing solar energy, birthing the era pf perovskite solar cells (PSCs) [7].

This chapter will focus on the basics of perovskite solar cells – Their history, constitution, the advantages and challenges they offer researchers.

2.2. Evolution of PSCs

In line with the general formula, the PSCs have the following species: A is a monovalent organic cation (popularly methylammonium (MA) CH_3NH_3 or Formamidinium (FA) CH_5NH_2) or inorganic (i.e., Cesium), B is a divalent metal cation of carbon family (Pb^{2+}, Sn^{2+}, Ge^{2+}) and X is a monovalent halogen anion (I^-, Cl^-, Br^-). They are thus classified as "metal halide perovskites".

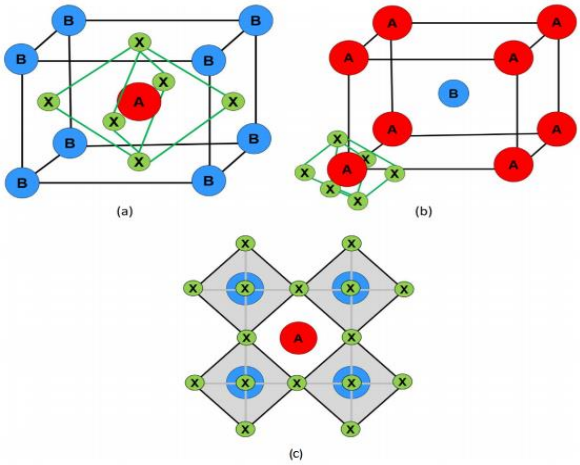

Figure 2.1 Generic Structure of Perovskite Lattice

As noted earlier, the first demonstration of fully functional PSCs with lead halide perovskites was done in 2009 by Kojima *et al*, reporting the application of organometal halide perovskites in DSC as visible-light sensitizer [8]. The figure2.2(a) depicts the DSC technology wherein the mesoporous TiO_2 layer is used as an electron injecting layer. The perovskite forms nanodots on TiO_2 surface and the architecture is completed by iodine/iodine based redox electrolyte and platinum counter-electrode. The team obtained a power conversion efficiency of 3.13% and 3.81% with $MAPbX_3$ with anion I and Br respectively. While the presence of TiO_2 film improved performance relative to DSCs, these cells faced severe degradation due to decomposition of nanocrystalline TiO_2 in the presence of redox electrolyte [9]. In 2012, Park *et al* tried to address the issue of liquid electrolyte by using Spiro-OMeTAD as a solid hole transport material (HTM) and successfully achieved an efficiency of 9.7% [10,11]. The cells showed superior stability over 500 hours with ex-situ storage in air at room temperature without encapsulation. They also compared the performance between deposition on a mesoporous TiO_2 and Al_2O_3 layers, which yielded no significant difference, thus suggesting that PSCs may work even without an electron injecting layer.

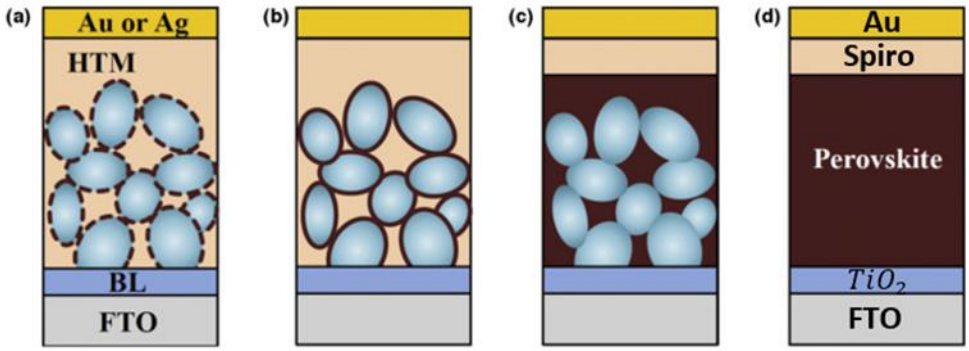

Figure 2.2 Structural evolution of perovskite solar cells: (a) sensitization concept with surface adsorption of nanodot perovskite, (b) meso-superstructure concept with non-injecting scaffold layer, (c) pillared structure with a nano oxide building block, and (d) planar pin heterojunction concept. Spheres represent TiO_2 in (a) and (c) and Al_2O_3 in (b). Adapted from "Perovskite solar cells: an emerging photovoltaic technology" by Park, Materials Today, 18(2), 65-72 [12]

A breakthrough happened in 2012 when PSCs were confirmed to work in the absence of mesoporous TiO_2 layer, i.e., electron transport can happen in perovskite layer without sensitization. Snaith *et al* achieved 10.9% efficiency by depositing $MAPbI_{3-x}Cl_x$ on Al_2O_3 mesoporous film (still on top of TiO_2 compact layer) with spiro-MeOTAD as HTM [13]. The Al_2O_3 layer was itself used as a scaffold to deposit perovskite layer, which granted easier crystallization, superior charge collection and higher V_{oc}. This allowed the option of switching from mesoporous to planar structures depicted in figure 2.2(b). They also showed that using mixed halide perovskites can improve performance because of their higher charge carrying capacity [13]. In 2013, a "pillared" structure was proposed by Heo *et al* to fill the mesoporous TiO_2 film (pillar) with perovskite instead of coating on surface [14]. This approach is represented in figure 2.2(c) and Heo *et al* achieved an efficiency of 12%. Burschka *et al* in 2013 demonstrated a two-step coating procedure for pillared structure that produced PSCs with tremendously improved efficiency of 15%. In this procedure PbI_2 is first introduced to form a solution, which is transformed into perovskite in the second step by exposing to a solution of CH_3NH_3I [15].

Around the same time, research in fully planar devices also saw an upswing [17]. The planar configuration is divided into two categories based on the order of layers deposited on the initial glass/TCO substrate. The stack is called n-i-p planar if the transparent electrode is followed by n-type layer and p-i-n planar if it is succeeded by p-type layer as shown in figure 2.3.

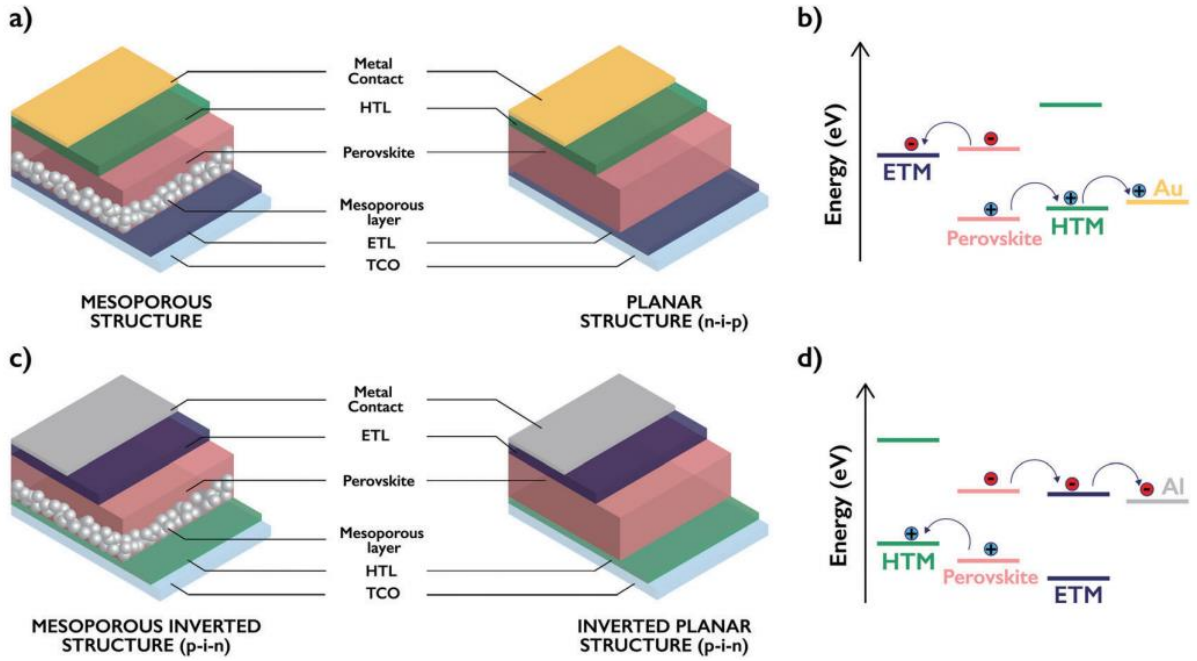

Figure 2.3 Schematic illustration of the most common device architectures of PSCs: (a) (n–i–p) mesoporous and planar structures. (b) Energy diagram of the different components of a conventional PSC. (c) Inverted (p–i–n) mesoporous and planar structures. (d) Energy diagram of the different components of an inverted PSC. Adapted from "Hole transporting materials for perovskite solar cells: a chemical approach" by Urieta-Mora et al, Chemical Society Reviews [16]

In September 2013, Liu *et al* demonstrated an increased efficiency of 15.4% by vapor deposition of the same structure with mixed halide perovskite and silver electrode [18]. In the same year, Docampo *et al* presented an architecture in which the p-layer was deposited first on substrate instead of n-layer [19]. The deposition sequence of FTO/PEDOT:PSS /perovskite/PCBM/TiO_x/Al was referred to as "inverted planar" where holes are collected through FTO, and electrons are collected at the top electrode. In this work, the authors achieved an efficiency of 10% on rigid substrate and 6.5% on flexible substrate with ITO instead of FTO. Malinkiewicz *et al* in December 2013 improved the performance of inverted device with the structure of ITO/PEDOT:PSS/PolyTPD/perovskite/PCBM/Au and demonstrated an efficiency of 12% [20].
From this point, interest in PSC research has increased year on year with record efficiency increasing rapidly. In 2016, Saliba *et al* introduced a triple cation (MA, FA, Cs) mixture of perovskite and achieved an efficiency of 21.1% with high stability and reproducibility [21]. The current world record reported is 25.5% [109]. This rapid growth in efficiency over a relatively short span is indicative of the potential for perovskite solar cells. Due to the band gap compatibility with other commercial technologies, PSCs have been massively investigated also to build up tandem architectures to produce more power per area (yield). Currently monolithic perovskite fabricated on Si tandem, achieved on $1cm^2$ the impressive number of 29.5% which surpass the power conversion efficiency of the single Si cell [109]. Similar has been achieved when fabricating the PSC on top of another commercially available technologies such as copper indium gallium selenide, with a demonstrated 24.2% again on 1 cm^2 [109].

2.3. Structure of PSC

The PSC is made of a number of layers that includes substrate, charge transport layers, perovskite absorber and electrodes. The perovskite (active) layer is discussed in detail in the 'Intrinsic Stability' section. The other layers to be discussed here can be represented by the figure 2.4.

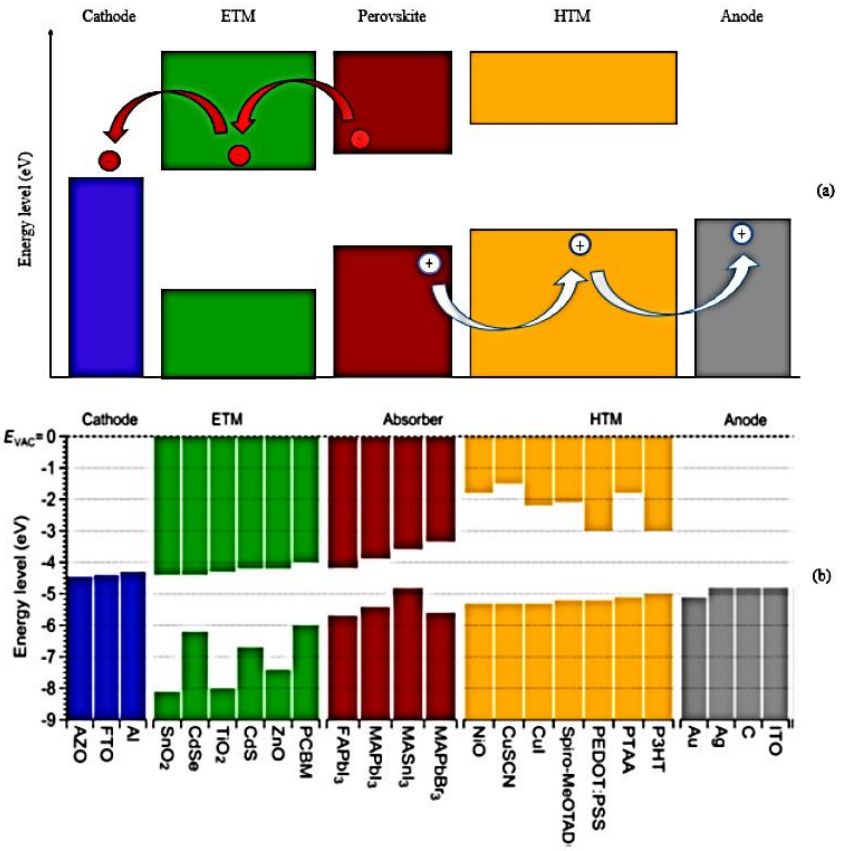

Figure 2.4 (a) Charge movement in a planar PSC (in this case with p-i-n architecture) (b) Diagram showing the energy levels, from left to right, for representative cathode, ETM, absorber, HTM, and anode materials of a PSC. Adapted from "Pathways toward high-performance perovskite solar cells: review of recent advances in organo-metal halide perovskites for photovoltaic applications" by Song et al, J. Photon. Energy, vol. 6, no. 2, 2016 [22]

2.3.1. ETL

ETL or Electron Transport Layer constitutes the n-region of the cell stack. The role of ETL is the extraction and collection of electrons generated in perovskite layer by photoexcitation, while blocking holes to prevent recombination. Therefore, the desired ETL has various properties including high electron mobility, wide band gap, high transmittance, compatibility in energy level with the bandgap of perovskite layer i.e., the conduction band minimum must be closer to that of perovskite while the valence band maximum must be significantly deeper to block the holes. The morphology of ETL is also a factor to consider minimizing current leakage at interfaces. Even since the first PSC, TiO_2 as ETL has been extensively studied in both mesoporous and planar configurations because of its good band alignment. However, TiO_2 had lower electron mobility, which prompted research into other options. Metal oxides, mainly ZnO and SnO_2 and organic materials, especially fullerenes like PCBM and C60 are popularly studied. The deposition techniques for ETLs vary from low-temperature solution processing (spin coating) to thermal evaporation, sputtering, atomic layer deposition.

In literature, it is prevalently seen that inverted planar stacks have adopted organic ETLs and in recent times, it is noted that electron injection/extraction is poor because of the barrier between

the Fermi Level of electrode metal (Au, in particular) and LUMO of organic ETLs. Therefore, significant research has gone into interface engineering, with materials like SnO_2 or BCP being preferred candidates to bolster the performance of organic ETL. The long-term stability of ETLs is yet to be successfully discerned and issues like moisture and oxygen-induced degradation are being studied. [24,25,26,27]

2.3.2 HTL

The Hole Transport Layer (HTL) on the other hand is required to behave in the opposite fashion of ETLs. The hole mobility should be sufficiently high, the valence band maximum should be aligned with that of perovskite layer to efficiently transport photogenerated holes and the conduction band minimum should be sufficiently high to repel electrons. The material used should produce a homogeneous layer and possess high optical, thermal, chemical stability offering resistance to air, water. In inverted planar stacks, the HTL should also be insoluble in solvents such as DMF or DMSO to not be dissolved in case of solution-processed perovskites. The candidates for HTL are typically classified into organic (further into long-polymers, small molecules) and inorganic (metal oxides and others) as given with examples in figure 2.5. From literature, the most adopted HTM is seen to be (2,2',7,7'-Tetrakis[N, N-di(4-methoxyphenyl)amino]-9,9'-spirobifluorene) Spiro-MeOTAD. Spiro-MeOTAD is favored because of its solubility in organic solvents, HOMO level matching the perovskite layer and semi-crystalline nature with low glass transition temperature which allow for a good deposition on the perovskite materials. However, Spiro-MeOTAD has low hole mobility and low conductivity which makes doping strategies necessary. Usually, dopants like 4-tertbutylpyridine (t-BP), lithium salts, FK 209 are used. Next to small molecules, polymer materials have also been researched and adopted, including poly (3,4ethylenedioxythiophene) polystyrene sulfonate (PEDOT:PSS), poly[bis(4-phenyl) (2,4,6trimethylphenyl)amine] (PTAA) and poly (3-hexylthiophene) (P3HT). Among these, PTAA is seen from literature to be the common HTM for p-i-n planar stacks. Alternatively, inorganic materials are also being investigated, including CuSCN, NiO_x, CuO_x, CuI etc. Specifically for p-i-n stacks, NiO_x is preferred for HTL due to their large bandgap and ideal band alignment with perovskite layer. For NiO, it has been observed that post-treatment of the deposited layers (i.e., UV-ozone, O_2 plasma, thermal annealing) is required to increase the p-type behavior and the wettability. [12, 28,29,30].
However, the ongoing research still shows concerns about intrinsic stability towards high temperatures, water and oxygen degradation and batch-to-batch variations especially in upscaling.

2.3.3 Electrodes, TCO

The electrodes are the conduit for transfer of electrons to and from the external circuit. From the architecture of PSCs, it is determined that at least one electrode should possess high transmittance and preferably be a transparent material, in addition to excellent electrical conductivity. Indeed, Transparent Conductive Oxides (TCOs) like Fluorine-doped Tin Oxide (FTO) or Indium Tin Oxide (ITO) are chosen for the electrode deposited directly over the substrate. FTO is cheaper, chemically

more stable, has higher conductivity than ITO. FTO also has high thermal stability while the resistance of ITO increases steadily after 300°C. However, FTO requires very high temperature for deposition (450°C) and is therefore limited to glass substrates. ITO, while inferior in properties, is more ideal for low temperature deposition and is used extensively in flexible substrates.

The second electrode can be another TCO or, more prevalently, a metallic contact such as Au, Ag, Al, or Cu. While these improve the carrier collection of the stack, their band alignment and interface morphology should be considered, along with mobility and chemical nature. For example, the barrier between gold electrodes and ETL in inverted planar architecture is mentioned in a previous section. While gold is a better electrode in n-i-p architecture with Spiro, it is a scarce metal and therefore economical constraints are unavoidable. Silver or Aluminum can be cost-effective alternatives, but they are found to be corrosive and easily react with the iodine species. Copper is being investigated as a more stable and cheaper substitute to gold, but other alternatives being studied include carbon-based options like carbon nanotubes. Carbon nanotubes are particularly interesting due to their excellent optoelectronic and mechanical properties, hydrophobicity, low processing temperature, low cost, scalability, and ability to supplant HTL or even ETL, without either layer relying on very costly alternatives. However, their efficiencies are still lesser than TCOs or metal electrodes, but rapid progress is seen in this field of research. [31,32,33,34,35,36]

2.4. Challenges

From several literature in previous section, it is seen that perovskite solar cells offer excellent intrinsic properties, like an optical absorption coefficient around 10^5 cm^{-1} at 800 nm, direct bandgap, low non-radiative recombination, longer carrier diffusion length and higher carrier mobility. In addition to this, they are also a low-temperature alternative, with potential to reduce costs and increase ease of manufacture [8,48,105,110]. Even as the evolution of performance and rapid improvement in efficiency is evident, PSCs face some serious limitations that are presently detrimental to the technology becoming the next revolution of PV industry. The pertinent issues, like toxicity, stability and hysteresis are discussed in this section.

2.4.1. Toxicity

The application of toxic materials in their manufacturing is a more widespread criticism on perovskite solar cells. The toxicity of lead, which is well-known, poses a potential health hazard during manufacture [37]. Their environmental impact is also under scrutiny in case of encapsulation or recovery during recycling [38] This could lead to prejudiced perception of PSC technology. The various solvents and precursors used at various stages may also pose significant health risks upon unregulated contact. In case of p-i-n architecture, application of NiO_x as hole transport layer might be an issue due to its toxicity, especially upon chronic exposure [39, 40, 41, 42]

The compounds are preferred because they exhibit superior efficiency or stability when used in PSCs, thus posing a challenge in finding a non-toxic alternative with similar performance. But despite this, research is ongoing on finding substitutes or improving encapsulants. Tin is presently the highest-performing alternative to Pb. But Sn-perovskites present a different kind of toxicity. They are extremely susceptible to oxidation of Sn^{2+} into Sn^{4+}, thus liable to release more HI than Pb counterparts when exposed to stresses, becoming more lethal. Some of the inorganic HTL alternatives that are explored for p-i-n architecture along with their efficiencies are shown in the following figure:

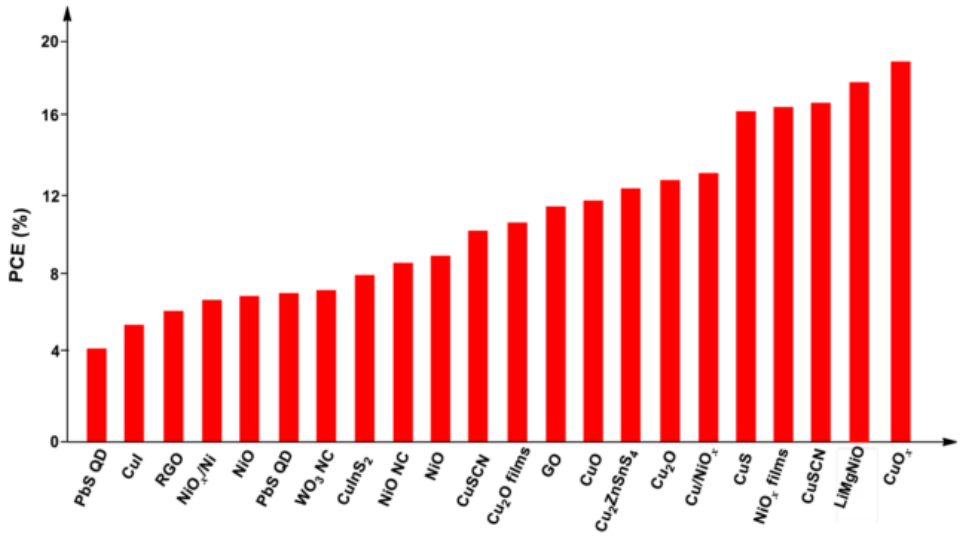

Figure 2.5 Graphical representation of inorganic HTMs vs. PCE in PSCs for the years 2012–2016 Adapted from "Emerging of Inorganic Hole Transporting Materials for Perovskite Solar Cells" by Rajeswari et al, Chemical Record 17(7):681–99 [44]

Copper oxide and copper derivates appear as promising candidates, being low-cost, abundant, non-toxic materials and showing high efficiencies up to 19% [43]. However, further tests need to be done to prove the stability of this material when integrated into a perovskite device.

2.4.2. Stability

Stability is the most pertinent challenge faced by PSCs in commercialization and mass-production. The lack of stability, or degradation, has been reported in literature and is classified into intrinsic stability (the integrity of the solar cell or perovskite layer in absence of external influences) and extrinsic stability (the performance of the solar cell under different influences or "stress factors" like temperature, humidity etc.). The following figure shows a classification and stress factors on PSCs:

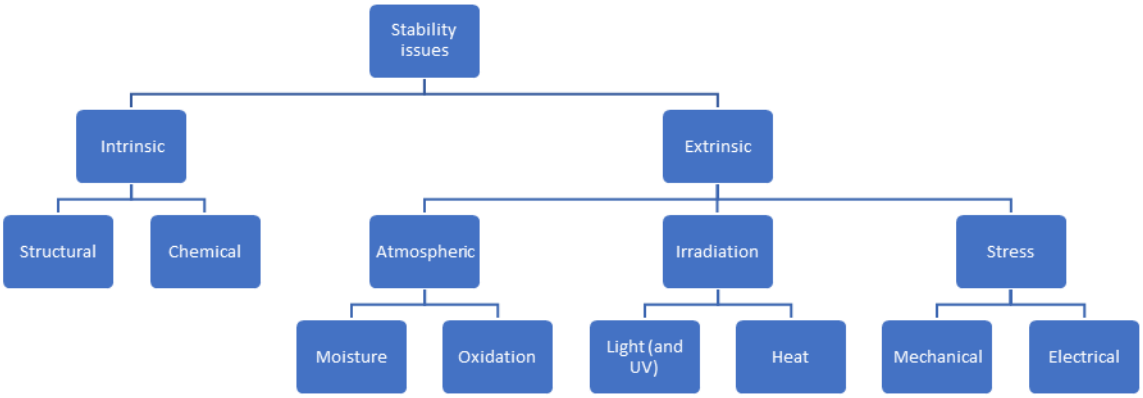

Figure 2.6 Factors affecting stability of Perovskite Solar Cells

In forthcoming sections, the different challenges to stability, the various degradation mechanisms from literature and measures being perused to address these concerns will be discussed.

2.4.2.1 Intrinsic Stability

Crystallinity

The intrinsic stability of ABX3 perovskite structure is assessed by the Goldschmidt tolerance factor, which is a semi-empirical geometrical parameter relating the ionic radii of constituent elements in the following manner

$$t = \frac{r_A + r_X}{\sqrt{2(r_B + r_X)}}$$

Where r_A, r_B and r_X are respectively the ionic radii of A, B cations and X anion. This factor is used to predict the possibility of halide perovskites that may be formed for a given set of ions [45,46]. Another factor to consider is the ability of B cation to fit into the octahedral void, which is denoted by an octahedral factor given by the following relation:

$$\mu = \frac{r_B}{r_X}$$

In an ideal three-dimensional cubic unit cell, the radius of B cation is minimized and therefore t = 1 and μ = 0.414 and 0.732. For 0.7 < t < 0.9, the A cation is small, or B cation is too large, which leads to distortion in the lattice, creating orthorhombic, rhombohedral or tetragonal structures. Also, the basic unit of perovskites is a BX_6 octahedron, a very small μ may lead to instability in the unit cell and thus, the perovskite. For practical purposes, it is reported that μ > 0.442, below which the octahedron will become unstable and not crystallize. From various literature, changing the constituent ions of the perovskite unit cell has reported the range of values for tolerance factor and octahedral factor can respectively be 0.81 < t < 1.12 and 0.44 < μ < 0.90 [37,47]. For structures with

t > 1 layered perovskite structures can also be formed, which exhibit several electrical and optical properties of interest.

The photoactive phase of perovskite is the cubic (or stable tetragonal, orthorhombic phases with comparable bandgaps and mobilities) so-called “black” or α-phase. Therefore, it allows materials in multiple phases to act as absorbers. The other notable phase which occurs as a byproduct of degradation, is an inactive hexagonal “yellow” δ-phase which is a non-perovskite structure usually with t > 1[48]. The δ-phase is accompanied by a drastic decline in the performance of the cell. Thus, it is observed that the perovskite crystal structure is very sensitive to the constituent materials and their optoelectronic, chemical properties and crystallographic phases are also determined by these choices. The formation and retention of the structural integrity of the active layer is thus the primary direction of research in improving intrinsic stability. The tolerance factors and phases of common perovskite materials is given in following figure 2.7.

	Tolerance factor	RT phase, color	RT phase post anneal	E_g	Best PCE (%)	Relevant phase transitions
$MAPbI_3$	0.89	Tetragonal, black	Tetragonal	1.55	20.3 (ref. 30)	⇒cubic, 60 °C
$FAPbI_3$	1.02	Hexagonal, yellow	Cubic	1.49	17 (ref. 1)	⇒cubic, 150 °C
$CsPbI_3$	0.79	Orthorhombic, yellow	Orthorhombic, yellow	1.72	10.77 (ref. 31)	⇒cubic, 300 °C
$CsPb(I_{0.67}Br_{0.33})_2$	0.81	Orthorhombic, yellow	Cubic	1.9	6.5 (ref. 32)	⇒cubic, 250 °C
$FA_{0.85}Cs_{0.15}PbI_3$	0.99	Tetragonal, black	Tetragonal	1.52	17.3 (ref. 27)	
$FA_{0.85}MA_{0.15}Pb(I_{0.85}Br_{0.15})_3$	1.01	Cubic, black	Cubic	1.62	22.1 (ref. 1 and 2)	
$FA_{0.85}Cs_{0.15}Pb(I_{0.83}Br_{0.17})_3$	1.01	Tetragonal, black	Tetragonal	1.74	20.0 (ref. 3)	

Figure 2.7 3D metal halide perovskite compounds commonly used in PV Adapted from “Towards Enabling Stable Lead Halide Perovskite Solar Cells; Interplay between Structural, Environmental, and Thermal Stability” by Leijtens et al, Journal of Materials Chemistry A 5(23):11483–500 [48]

Cation Engineering

MAPbI3 is the first and widely used perovskite absorber material in research, which is tetragonal in room temperature and transitions to cubic phase at higher temperatures (60°C-100°C). This is highly favorable since a photoactive phase can be maintained in real-world applications without structural degradation throughout its lifetime. However, MA is susceptible to organic sublimation due to its acidic nature, which in turn increases the probability of its deprotonation and reaction leading to gaseous HI and a conjugate base (CH_3NH_2 or $NHCHNH_2$). This reaction is accelerated by external stresses, as will be discussed in forthcoming sections. Furthermore, due to high chance of polarization, $MAPbI_3$ has large current-voltage hysteresis [48,49]. These reasons have encouraged research in supplanting MA as the A-site cation.

Formamidinium (FA) became the most investigated alternate to show promising results. FA being a larger cation than MA leads to a larger t-factor and forms at room temperature a hexagonal yellow non-perovskite structure also denoted as δ-phase. Annealing at temperatures above 150°C resulted

in transition to tetragonal black perovskite phase, which was found to be retained even after cooling to room temperature. However, with the possibility of reversion to a more stable δ-phase over time, FA-based perovskites limited the scope for long-term stability. Alternatively, Cs was researched as A-cation to produce fully inorganic perovskite to enhance thermal stability. However, $CsPbI_3$ due to the small size of Cs cation has a low tolerance factor and forms an orthorhombic yellow phase at room temperature. To transition to a photoactive phase, the layer had to be treated at extremely high temperatures (about 300°C) which remained stable in room temperature for 200 days when stored at low RT in inert conditions [50]. Like case of FA, the thermodynamic favorability of inactive phase limits the lifetime. Replacing the iodide anion with bromide was widely researched as well. Br with a smaller radius leads to a more stable lattice but with higher band gaps [51]. For example, CsPbBr3 in room temperature is cubic and structurally stable, but has an unsuitably high bandgap of 2.3 eV, compared to the 1.72 eV of its iodide counterpart. It can be observed that each cation has its own advantage, which led to mixing cations and the advent of "dual" or "triple" cation hybrid perovskites.

Hybrid perovskites

Another line of research involved a mixed halide anion system with changing the stoichiometry between I and Br in the lattice to tune the bandgap and structural stability of the perovskite. "Hybrid perovskites" can be rudimentarily defined as perovskite structures with non-unitary constituent species in one or more ionic sites of the lattice. Such mixtures across various literature are reported to have tolerance factors very close to unity. Dai *et al* in a hybrid $FA_{1-x}MA_xPbI_3$ demonstrated the stabilization of cubic lattice with addition of MA, also improving the structural integrity of the complex higher than pure $MAPbI_3$ or $FAPbI_3$ [111]. The best performance and PL stability was found to be at x = 0.6 which was concurrent with the works of another team [50]. Seok *et al* in December 2014 experimented on a further hybridized $(FAPbI_3)_{1-x}(MAPbBr_3)_x$ architecture and found the most optimal results at x = 0.15 which is dominated by stable α-perovskite and yielded an efficiency of 18% with minimal hysteresis [52]. Although the results were promising, the previously discussed issues of MA volatility and FA transition were present as well. The quantity of MA in the lattice is therefore to be limited, which is also shown in the experiment. In addition, mixed halide perovskites of MA and FA also suffered from a different issue, which is discussed in the next section [52,53]. $FA_{1-x}Cs_xPbI_3$ compounds were investigated to tune the structure by substituting FA with small amounts of Cs with great success [54]. The resultant structure with $0.1 < x < 0.3$ showed an improved structural integrity. Highly efficient and stable compounds were prepared over the entire Br range by tuning the halide composition of $FA_{0.83}Cs_{0.17}Pb(I_{1-x}Br_x)_3$ perovskites [55].

Until this point, the crystallographic structure of the active layer is discussed. However, the formation of perovskite phases is also influenced by the precursor solutions, additives and solvents, salts used in the deposition processes. Wang *et al* [56] demonstrate the superior performance of

DMF/DMSO blended solvent at v/v 4:1 in forming high-quality perovskite due to sufficient lattice expansion as compared to DMSO alone. They further make MA-FA perovskites to demonstrate further improvement at 1:1 ratio of MA:FA. In a different experiment, Liu *et al* create a 2D perovskite at different DMF:DMSO ratios and produce the most stable compound at 1:3 [57].

To summarize, the tuning of A-cation and halide anion is shown to have tremendous influence on the structural integrity, as well as the performance, of the PSC. It is also noted that the conditions of deposition, including chemical nature of precursors and operating parameters, can contribute to the overall structure of the perovskite layer. FA-Cs cation hybrid perovskites appear to be the most promising way forward in the scope of "dual" cations and in the "triple cation" range, the necessity to limit MA in the lattice is understood. Such phases would, while minimizing volatile species, also guarantee improved stability of the black perovskite phase in addition to improving the performance of the PSC. The effect of the stoichiometry of the perovskite layer, in addition to structural integrity, is also seen to affect the stability of the cell while exposed to external stresses like heat or light which are to be anticipated in real-world applications, as can be understood from figure 2.8.

2.4.2.2 Extrinsic Stability

Structural stability of the perovskite compound is but the first step in achieving long-term stability of PSCs. The device must be stable when exposed to external agents, in order to bring this technology towards the commercialization. This section therefore addresses the effect of environmental factors on stability of the PSCs. It also delves into the various degradation mechanisms proposed in literature as a result of exposure to these factors, focusing on atmosphere (oxygen and moisture), temperature(heat) and light (illumination). Other issues, like mechanical stress, electrical stress under load is not discussed as they are beyond the scope of this thesis.

Temperature

Stability of a cell when heated up under the sun is of great importance. In addition to heat, the cell must also be robust under the temperature cycles (from low to high temperature) which varies across the day, locations and the seasons.
As seen in the section discussing intrinsic stability, the most prevalent perovskite materials are able to maintain a stable photoactive phase at room temperatures and high temperatures. $MAPbI_3$, for instance, has a transition temperature around 60°C from tetragonal to cubic. Although both phases are photoactive, the transitions might cause stability issues in long term, especially under continuous thermal cycling [58,59]. Thermal decomposition and their pathways are the focus of study under thermal stability. From various literature, the decomposition route taken by $MAPbX_3$ is debated to be among the following two [60,61]:

1) $MAPbI_3$ -> $PbI_2(s) + CH_3NH_2(g) + HI(g)$
2) $MAPbI_3$ -> $PbI_2(s) + CH_3I\ (g) + NH_3(g)$

While these were done by thermogravimetric analysis at high temperatures, $MAPbI_3$ was found to develop PbI_2 and Pb(0) at 85°C even inside inert conditions (N_2 atmosphere) within 24 hours, which is accelerated in case of presence of water or oxygen [62]. This is attributed to the volatile nature of the methylammonium cation, which was discussed earlier. Therefore, $MAPbI_3$ cannot be considered as a suitable candidate for long-term operation under elevated temperatures.

Thermal stability was seen to be improved by substituting MA with a larger organic cation, FA. The increased stability may be attributed to the hydrogen-bonding in FA and the lower tendency to be deprotonated as against MA. While the short-term stability of FA perovskites is better than MA, they still degrade upon exposure to other stresses, especially moisture [63] which can be mitigated by encapsulation. Long-term thermal stability of FA perovskites is still to be demonstrated, but it is suspected that they undergo a decomposition pathway similar to MAPbI3 [64] Substituting MA with Cs also decreased volatility of the perovskite. $CsPbI_2Br$ was reported to show an enhanced thermal stability, showing no signs of thermal decomposition even after heating for 30 minutes at 180°C [65]. Hybrid FA-Cs perovskites are also a choice for improved thermal stability, with $FA_{0.83}Cs_{0.17}Pb(I_{1-x}Br_x)_3$ compounds being resistant to degradation over 6 hours at 130°C in an inert atmosphere [55]. The effect of partial substitution of MA with FA or Cs on the volatilization of MA is unclear. The decomposition of $(FA_{0.83}MA_{0.17})_{0.95}Cs_{0.05}Pb(I_{0.83}Br_{0.17})_3$ at 150°C was found to occur at two steps, the first of which had kinetics similar to MAPbI3 decomposition [66]. This suggested the presence of MA in lattice as non-ideal for thermal stability in the long term.

Organic HTMs are also prone to thermal stability. Popular options like PEDOT and Spiro-OMeTAD are susceptible to stability issues [67]. t-BP, which was discussed as an additive for Spiro and PTAA, is shown to evaporate as low as 80°C [68,69]. Therefore, more stable oxide layers and dopant-free organic CTLs are pursued [70]. Among them, ZnO is reported to deprotonate the perovskite layer upon heating to 100C for 20 min [71].

Oxygen and Moisture

Among several atmospheric components, oxygen and moisture can affect the performance of solar cells. They provoke oxidation and solubilization, respectively, of many functional components in any solar cell.

Metal halide perovskites have been reported to be relatively stable in presence of oxygen in the dark, with a shelf-life ranging into months. This suggests that the active layer is relatively stable in ground state [11,72]. However, $MAPbI_3$ showed rapid degradation upon exposure to both light and oxygen. The diffusion of oxygen within the perovskite through iodide vacancy as well as at the

interface with the photocatalytic transport layer (like TiO_2) can trigger the formation of oxygen induced degradation mechanism via highly reactive superoxide (O_2^-) which in turn leads to acid-base reactions with the A-site cation [112]. This reaction results in deprotonated A-site gas, PbI_2 and water [73,74,75,76]. Since the reactivity is based on the acidity of A-cation, substituting MA with less acidic options like FA or Cs can mitigate oxidation and concomitant degradation [77]. In transport layers, finding replacement for UV-reactive species with fullerenes or oxides of tin, nickel can improve resistance to oxidation. The use of UV filters can be considered as an alternative [78,79].

Moisture, unlike oxygen, can cause rapid degradation even without illumination (In dark) [35,22,80,81]. Water molecules can permeate into the perovskite lattice and form hydrated phases, which can be reversible in short-term [82]. The stronger interaction of water is the formation of hydrogen bonds with A-site cation, which weakens the bond between the cation and PbI6, thereby allowing faster deprotonation of the cation under other stressors [83]. Like that of oxygen, water also reduces the iodide to form HI and PbI_2. This degradation in $MAPbI_3$ occurs over tens of hours under ambient conditions at 80°C [84]. The similar inference of acidity of A-cation can be applied in the case of moisture as well. However, $CsPbI_3$ or $FAPbI_3$ are, unlike their oxidation resistance, notoriously sensitive to moisture and revert to their respective photoinactive phases [85]. Outside the active layer, transport layers are also susceptible to moisture-induced instability. Common HTMs like Spiro-OMeTAD and PTAA are hygroscopic and induce degradation due to moisture as early as 48 hours [86].

Resistance to moisture in dark storage is improved by incorporating Br^- between 20-29% into the lattice. The reason for this is postulated that Br, being a smaller ion, shrinks the lattice and makes it more cubic, which strengthens the cation-lead halide bonding and reduces permeability [87,88]. Partial introduction of FA into the lattice also reduces moisture volatilization of organic cation [89] because the dipole moment of FA, the larger cation, is ten times lesser than that of MA, which leads to weaker hydrogen bonding with water and therefore lesser chance of deprotonation [90]. Alloying Cs in $FAPbI_3$ improves storability of PSCs [91,92,93] in environments up to 90% RH. In the case of transport layers, hydrophobic alternatives are being perused. Another line of improvement is incorporating multiple layers to CTL, which has shown superior resistance to moisture [94,95]. Employing inert moisture-resistant polymers like polymethylmethacrylate (PMMA) as encapsulation in composite structure with carbon nanotubes have enabled stable performance for hundreds of hours under ambient conditions [96]

Light (Illumination)

The PSC has to be structurally and functionally intact upon prolonged exposure across all range of solar spectrum. $MAPbI_3$ with encapsulation has been shown to have consistent absorption spectrum over 1000 hours [11]. But a consistent spectrum and performance do not necessarily

mean a lack of photoinduced changes in the cell. The various examples of cation and halogen substitution discussed in previous sections that provide bandgap tuning and an improved thermal stability have led to the observation of a new light-induced phenomenon. First observed by Hoke *et al*, $APb(Br_yI_{1-y})_3$ perovskites undergo a segregation into Br- and I-rich perovskite phases upon illumination. This was found to be reversible and attributed to the smaller bandgap of iodine-rich regions acting as trap sites, thus limiting the overall performance of the cell [97]. Since then, this phenomenon was dubbed as "Hoke Effect" and observed when the Br proportion was too high. Partial substitution of Cs into the lattice has shown to improve resistance to light-induced halide segregation [55]. Several models were proposed to explain this effect [98,99,100,101], but the elucidation of mechanism and long-term effects of Hoke Effect are as of yet inconclusive.

A significant part of these tests has been performed using LED light source, which has an emission spectrum after 400 nm and therefore devoid of UV light. An example of PSCs degrading under illumination is given in the following figure 2.8:

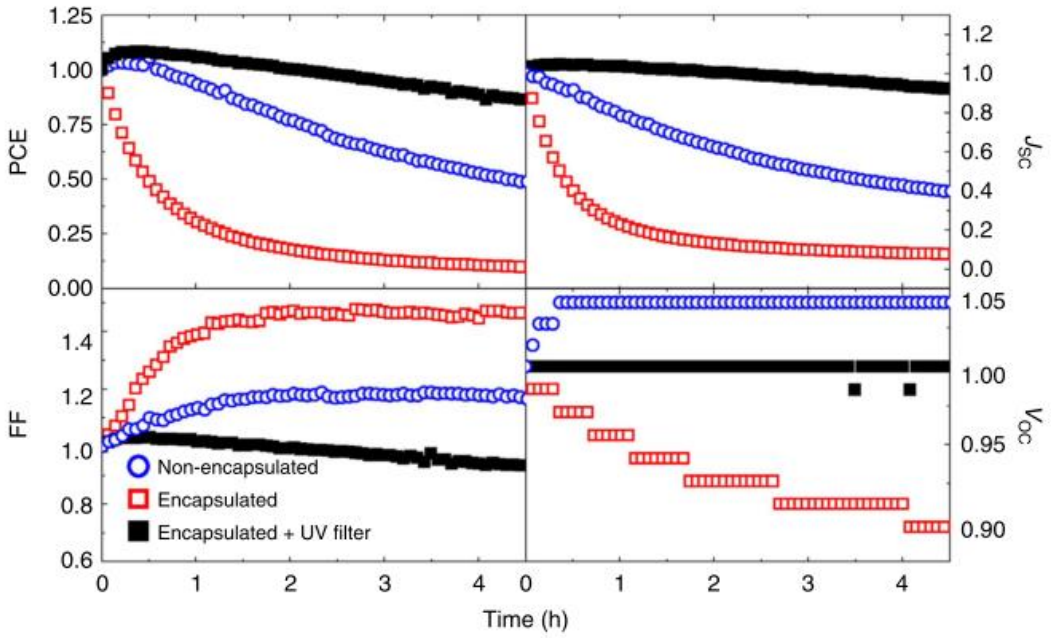

Figure 2.8 Evolution of normalized solar cell performance parameters, power conversion efficiency , short circuit current (J_{sc}), fill factor (FF), and open circuit voltage (V_{oc}) over 5 h of AM1.5 100 mW cm^{-2} solar illumination. Adapted from "Overcoming ultraviolet light instability of sensitized TiO2 with meso-superstructured organometal tri-halide perovskite solar cells" by Leijtens et al, Nature Communications, 4(1). doi: 10.1038/ncomms3885 [102]

The pattern of degradation is typical, with a decrease in efficiency (PCE) following the trend of short circuit current (J_{sc}) with an almost intact open circuit voltage (V_{oc}). This change has occurred within a frame of only four hours. This was traced to the presence of TiO_2, which is photolytically active

under UV light [102]. Irreversible changes in perovskite composition were reported for hybrid cation systems with TiO_2 [103,104]. The degradation pathway which is now well-known is discussed in the previous section and overcome with different materials, for example SnO_2 or PCBM, fullerenes [35,105,22]. Alternatively, UV filters were applied to improve the stability, as can be seen in the figure above.

2.4.2.3 Hysteresis

Apart from the issues discussed above, perovskite solar cells also face an operational issue. The JV curves of the device are dependent on the voltage scan rate and direction, thus producing a pronounced hysteresis between forward and reverse scans. A pictorial representation of this is given in the figure 2.9.

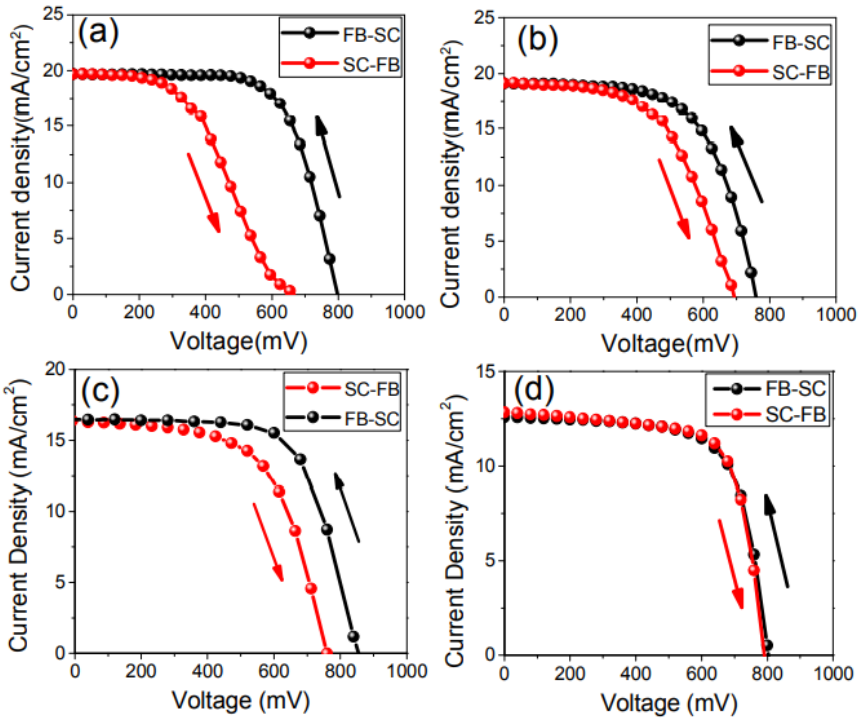

Figure 2.9 Influence of solar cell architecture upon current–voltage hysteresis. Forward bias to short circuit (FB-SC) and short circuit to forward bias (SC-FB) current–voltage curves measured under simulated AM1.5 100 mW cm–2 sun light for: (a) solution-processed planar-structured TiO2-based solar cell; (b) solution-processed mesoscopic TiO2-based solar cell; (c) vapor-assisted planar-structured TiO2-based solar cell; (d) vapor-assisted mesoscopic TiO2-based solar cell. Adapted from "Hysteretic Behavior upon Light Soaking in Perovskite Solar Cells Prepared via Modified Vapor-Assisted Solution Process" by Liu et al [113]

Various plausible sources of JV hysteresis are postulated, like ferroelectricity [106] or unbalanced charge collection due to interstitial and interfacial defects. Ferroelectric behavior is dependent on the applied voltage bias, therefore causing hysteresis. A larger short circuit current and open circuit voltage are generally recorded in sweeps starting from the forward to reverse bias than the opposite [107]. While the effect of hysteresis on performance is unclear and largely regarded

minimal, it poses a significant challenge in algorithms designed to maximize the power point tracking during operation.

2.5. State Of Art

The following table is a summary of the state-of-art results obtained from degradation studies in recent times. Several entries of this table are reproduced from the work of [108]

Table 2.1 State of art stability experimentations in PSCs in literature.

Year	Absorber	PCE (%)	Device stability	Ref
2016	$FA_{0.83}Cs_{0.17}Pb(I_{0.6}Br_{0.4})_3$	17.1	/	[108]
2016	$MAPb_{0.75}Sn_{0.25}(I_{0.4}Br_{0.6})_3$	12.6	30 days storage in inert atmosphere, 5% degradation	
2017	Rb-$FA_{0.75}MA_{0.15}Cs_{0.1}PbI_2Br$	15.4	12 h continuous one-sun illumination under N_2 environment at 25 °C, less than 5% degradation	
2018	$Cs_{0.5}FA_{0.4}MA_{0.1}Pb(I_{0.83}Br_{0.17})_3$	16.0	5 days MPP tracking under AM 1.5 illumination in N_2 without encapsulation, no degradation	
2018	$Cs_{0.12}MA_{0.05}FA_{0.83}Pb(I_{0.6}Br_{0.4})_3$	19.3	Continuous MPP operation under AM 1.5 illumination with a 420-nm UV cut-off filter in N_2 for 11 h, less than 3% degradation	
2018	KI-$(Cs_{0.06}FA_{0.79}MA_{0.15})Pb(I_{0.85}Br_{0.15})_3$	17.5	Stored in a nitrogen glove box over a month and tested regularly under full AM 1.5 simulated sunlight, negligible degradation	
2018	$CsPbBrI_{1.78}F_{0.22}$	10.3	Stored under 20% RH at room temperature without encapsulation for 240 h, less than 30% degradation	
2019	$Cs_{0.925}K_{0.075}PbI_2Br$	10.0	Stored in a constant temperature-humidity chamber (20 °C and RH = 20%) for 20 h, 20% degradation	
2019	$FA_{0.6}Cs_{0.3}DMA_{0.1}PbI_{2.4}Br_{0.6}$	19.2	Under constant bias and illumination in N_2, no degradation	
2020	$Cs_{0.2}FA_{0.8}PbI_{1.8}Br_{1.2}$	16.4	4 h MPP tracking under AM 1.5 illumination in N_2 without encapsulation, no degradation	
2020	KI-$Cs_{0.05}FA_{0.79}MA_{0.16}Pb(I_{0.75}Br_{0.25})_3$	18.38	Stored under ambient air conditions without encapsulation for more than 2000 h, 6% degradation	
2020	$Cs_{0.99}Rb_{0.01}PbI_2Br$	17.16	Stored in ambient condition (<40% RH) without encapsulation for 120 h	
2017	NT p-i-n with ITO (ALD)	19.2	Stable with 80% retention for 500 h in 85°C or 1000 h in light-soaking with 420 nm cutoff.	[114]
2018	NT p-i-n with ALD and Ag	18.7	Retained 86% of PCE in simultaneous thermal stressing (85°C) under 1 Sun illumination in ambient air.	[115]
2018	ST p-i-n with ITO (ALD)	12-13	Stored in 85°C-85% RH for 1000 h.	[116]

2019	ST p-i-n with Ag (and ALD)	16.4	Stored for 1000 h in 85° C, 85°C-85% RH, or 1 Sun illumination each.	[117]
2019	ST p-i-n with ITO (ALD) (LBG)	18	Stored for 678 hours in 60°C under 1 Sun	[118]

2.6. Research Questions

Until now, several positive and negative aspects of PSCs were discussed. However, over the course of this literature review, a dominance of lab-scale research involving processes like spin-coating was observed. To become commercially acceptable, PSCs are expected to be scalable in size and retain their excellent properties observed in the smaller samples in laboratories. This thesis attempts to address in that direction, by experimenting on fully scalable architectures. The following research questions are formulated to answer, which will be recalled in several sections by their serial numbers.

RQ1: How does the choice of perovskite affect the resilience of the scalable architectures?

RQ2: How does the choice of electron transport layer (ETL) affect the resilience of the scalable architectures?

RQ3: What is the significance of the side of illumination on the stability of the PSC?

2.7. Conclusion

This chapter gave a bird's eye view on the technology of perovskite solar cells, their evolution, components and persisting issues. The chapter introduces the effect of choice of A, B and X components on the performance and stability of the PSC to various external stimuli, or intrinsic stability. The hybrid cation and hybrid anion systems are seen to perform better than their standalone counterparts, with Cesium and Formamidinium combination for A-site being very promising. The limited addition of Bromine in X-site is also seen to be beneficial.

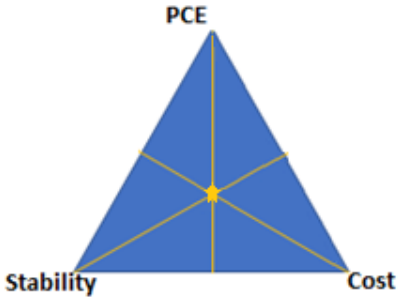

Figure 2.10 Golden Triangle for PSC Upscaling

While performance of PSCs is rapidly improving, they are far from being a commercial success due to their persistent issues of toxicity and stability. An approach to upscaling requires balancing performance with costs and life of the product, as illustrated in the following golden triangle in figure 2.11.

3.Experimental methods, characterization methods

In this section, the technologies adopted for cell manufacturing, characterizing and experimentation are discussed. The stacks fabricated throughout this thesis are made from scalable technologies within Solliance Solar Research. A typical cell can be seen in the following figure 3.1 to introduce the manufacturing processes.

Top Electrode	Sputtering
Metal Oxide Buffer Layer	ALD
Electron Transport Layer	Slot-die Coating
Perovskite absorber layer	
Hole Transport Layer	
Substrate	

Figure 3.1 Schematic of a typical stack in this thesis

3.1 Solution processing Deposition

3.1.1 Slot-Die Coating

In literature, a majority of samples studied are in laboratory scale and employ spin-coating deposition technique. While it is cost-effective and good for initial screening of materials, spin-coating is limited to small area substrates, and it is not continuous, thus unviable as an upscaling technology. Slot-die coating (SDC), on the other hand, is the technique where a continuous deposition of a material is pumped through the blade, throughout the motion of the blade, as shown in figure 3.2 [172]. Whilst deposition of transport layers is relatively straightforward (deposition and annealing to remove the solvents) SDC of perovskite active layer requires an additional drying step to control the crystallization of the absorber over large area. [119,120] In this work slot die coating has been used to deposit the HTL, the perovskite material.

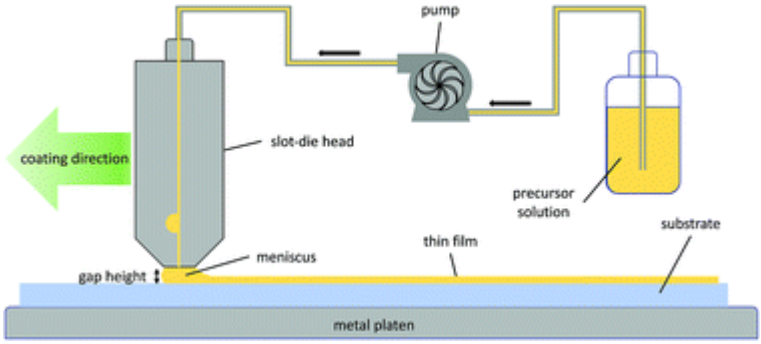

Figure 3.2 Slot Die Coating. Adapted from "Scalable slot-die coating of high performance perovskite solar cells" by Whitaker et al, Sustainable Energy and Fuels, 2018 [126]

3.1.2 Atomic Layer Deposition (ALD)

Atomic Layer Deposition (ALD) is a chemical phase deposition method where the chemical precursors are exposed to the substrate in a sequential, non-overlapping manner, as depicted in figure 3.3. Each exposure step is followed by a "purging" step, usually flushing with an inert gas like N_2, to prevent reaction of precursors in gaseous phase (parasitic CVD). The reaction of precursor molecules to the substrate is self-limiting in the sense that it terminates after all reaction sites on the surface are consumed. This allows to acutely control the thickness of the film by regulating the number of exposure steps and yet maintain high density of deposition. The aforementioned sequential "temporal" approach of ALD, while resulting in layers with excellent properties, it is generally time consuming and most likely not ideal in case of high throughput line such as roll to roll (R2R) line for flexible perovskite solar cells for instance. Spatial ALD (sALD) is the variation wherein the substrate is moved between precursors which are separated by inert gas "curtains" to avoid parasitic CVD and purging regions sequentially. In this work spatial ALD has been used to fabricate the buffer layer prior to the deposition of the sputtered TCO. [121]

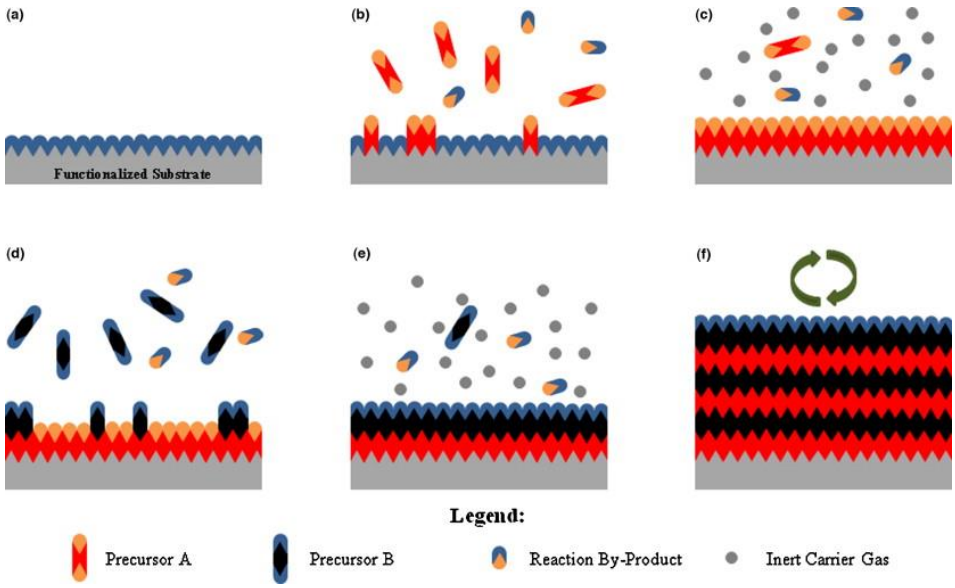

Figure 3.3 Schematic of ALD process. Adapted from "A brief review of atomic layer deposition: from fundamentals to applications" by Johnson et al, materialsToday,Volume 7, 2014 [125]

3.1.3 Physical Vapor Deposition - Sputtering

Sputtering is a method pf physical vapor deposition. It involves ejection of atoms from a target material by bombarding heavy ions (Ar^+, for example) to be deposited onto a substrate. In PSCs sputtering is used commonly for deposition of TCO material or other inorganic oxides like NiO_x [122,123,124]. The principle of sputtering is summarized in figure 3.4

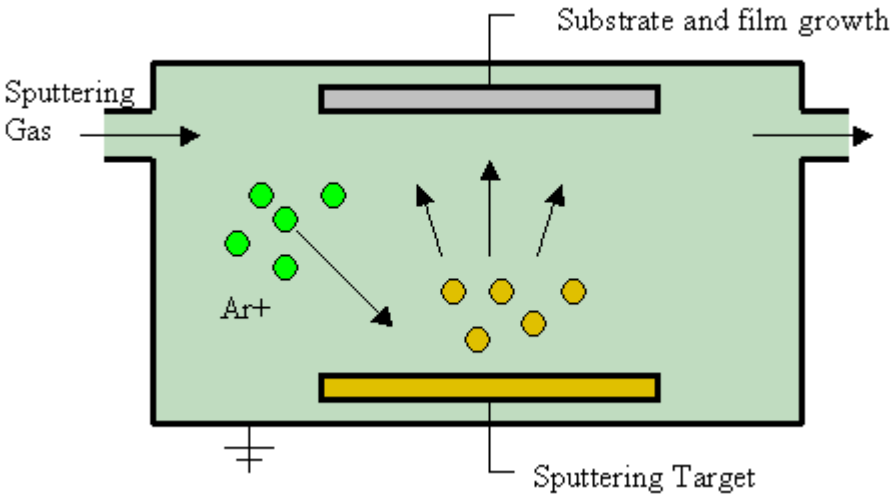

Figure 3.4 Principle of Sputtering. Courtesy of Wikipedia.

3.2 Characterization Techniques

3.2.1 Characterizing the performance of PSC [128]

The most fundamental characterization of any solar cell is the current-voltage curve (termed JV curve). A specimen of JV and the insights derived from it is presented in figure 3.5

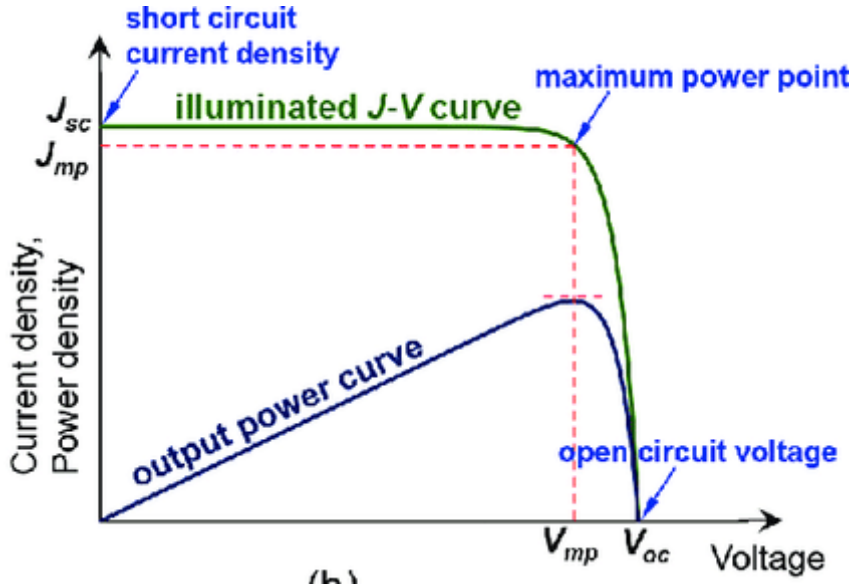

Figure 3.5 A typical JV Curve, Adapted from " Screen-Printed Front Junction n-Type Silicon Solar Cells " by Tao [127]

Current

J_{sc} is the current density of the cell under short circuit condition. It is a function of the incident photon flux density, the absorptance of active layer, the parasitic absorption and interference of the other layers deposited prior to the perovskite absorber, and also by the recombination mechanism in the perovskite bulk and at the interface perovskite/transport layer.

Voltage

The highest voltage, V_{oc}, is the voltage at open circuit condition in which current flow is zero. It corresponds to the forward bias voltage at which dark current density compensates the photocurrent density, i.e., the carrier generation rate is equal to recombination rate. V_{oc} is approximated to the following relation:

$$V_{oc} = \frac{k_B T}{q} \, ln\left(\frac{J_{ph}}{J_0}\right)$$

The voltage is proportional to the exponential J_{ph}/J_0 factor, which means there must be a high disproportion between the two to maximize Voc. While the relation shows a positive linear correlation between V_{oc} and temperature, it must be noted that with increase in T, J_0 increases exponentially and the exponent term therefore reduces to offset any T increase, leading to a cumulative drop in V_{oc}.

MPPT

The point of maximal power output is denoted as MPP (Maximum Power Point) in figure 3.5. MPP is the optimal operational point. Therefore, algorithms for tracking MPP (denoted MPPT) are used, either by static encoding MPP into a device (indirect MPPT) or by dynamic reading of I-V data to determine MPP (direct MPPT). A description of the MPPT algorithm in the experiment apparatus will be given in following sections.

FF

In JV curve, the ratio between power at MPP and product of V_{oc} and J_{sc} is called fill factor (FF). It is a measure of the realization of output as compared to the ideal scenario.

Efficiency

All aforementioned electrical parameters are used to find the power conversion efficiency (PCE) by the following relation:

$$\eta\ (PCE) = \frac{J_{sc} V_{oc} FF}{I_{in}}$$

Efficiency is the most discussed parameter of a solar cell because it is the hallmark of a solar cell. However, for the same cell, under different operating conditions, the efficiency varies. Therefore, a set of Standard Test Conditions (STC) are adopted to benchmark the efficiencies of all solar cell technologies. A cell is operated under STC when it is irradiated with a light source of AM1.5G spectrum at an intensity of 1000 W/m^2 in a fixed cell temperature of 25°C.

In common practice, the issues that could cause resistance to current flow are divided into two categories: Series and Shunt. “Series resistance” models the defect density, recombination losses, trap states etc. in the bulk of the active later and is in series to the current source. Therefore, it has to be minimized for optimal performance i.e., the absorber layer should be homogeneous. “Shunt resistance” on the other hand represents issues pertaining to interface like scratches, grain boundary orientation, interface orientation (or lack thereof) that may offer an alternative path for current flow. Therefore, shunt resistance should be sufficiently high to not create potential gradient

enabling current flow in such undesired paths, making it a parallel component to the current source.

3.2.2 Photoluminescence

Photoluminescence Spectroscopy (referred to as PL) is a non-contact, nondestructive method for studying various electrical and structural properties of a surface. The process works on the principle of photoluminescence - Upon excitation by an incident photon with energy greater than band gap, the charge carriers are generated, a fraction of which undergo nonradiative relaxation towards the valence band maximum (hole) and conduction band minimum (electron) wherein they undergo radiative recombination to release a photon. These photons constitute an emission spectrum that can provide information about band edge, presence of trap states, exciton peaks and electron-phonon interactions [129].

A Horiba Scientific LabRAM ARAMIS is used for characterizing the PL spectrum within this thesis. PL is carried out between 600 and 800 nm over time. The output of the experiment gives the wavelength of peaks and their corresponding intensity. The peaks are associated with the bandgap energy of the perovskite film and tracking the peak shift over time allows to define the increase (blue shift) or decrease (red shift) of the bandgap energy. This is indicative of the composition of the active layer. The intensity, on the other hand, is indicative of the radiative recombination of charge carriers and thus an evaluation of charge recombination within the active layer. Measured over time, the change in intensity gives insights about the quality of the active layer [129].

3.2.3 XRD

To understand the lattice characteristics of a material, crystallographic analysis at the level of unit cell, like X-Ray Diffraction (XRD) is used. The XRD apparatus consists of a cathode ray tube housing a filament that is heated to produce electrons. These electrons are collimated and accelerated towards a target by high voltage. When electrons have sufficient energy to dislodge inner shell electrons of the target material, secondary spherical waves are produced. Most of these waves annihilate each other by destructive interference and the remaining, which add constructively, are counted, and processed on a detector. The sample and detector are both rotated, and the intensity of the reflected X-Rays is recorded. The conditions to satisfy for producing a constructive interference are related by Bragg Equation:

$$n\lambda = 2d\ sin\theta$$

In an XRD setup, λ, n are fixed and for each angle, $\theta = \theta_B$ can be considered. By measuring the X-Ray spectra for the range of 2θ angles, all possible diffraction directions of the sample should be

attained due to random orientation of the sample. The output of XRD is an intensity-angle plot which shows diffraction peaks at angles with constructive interferences. By Bragg equation, each peak yields a corresponding d-spacing. Both angle and d-spacing are unique to each mineral and therefore by comparing the result against standard reference patterns, the crystal properties and constituents can be discerned. XRD is fairly quick and non-destructive. However, the penetration depth of incident X-Rays is limited to the order of micrometers. Therefore, when measurement in deeper layers is required, material removal is needed. An example of this case would be to measure the bulk material because of a modification on surface that is not indicative of the bulk properties, or if a study on phase contents or depth profile of residual stresses are needed. In such instances, it must be ensured that the layer removal does not influence the XRD measurement or the morphology of the material.

3.2.4 Absorbance and EQE [128]

Absorptance denotes the part of incident light that is absorbed i.e., not reflected, or transmitted. It can be represented by the following relation:

$$A + R + T = 1 \rightarrow A = 1 - R - T$$

This principle of exclusion is applied in measuring absorptance. A Cary 5000 UV-Vis-NIR is used to measure the reflectance and transmittance in the samples. The measurements are done within the UV and visible components of the spectrum. A wide-spectrum lamp emits light which goes through a series of filters, monochromators, and collimators (mirror and lens) to fall on the solar cell sample. The results are measured in %T and %R varied with wavelength for transmittance and reflectance respectively. Absorptance is then calculated by aforementioned equation.

EQE can be defined as the fraction of photons incident on a photoactive surface that is absorbed to generate electron-hole pairs which are successfully collected. EQE is a function of wavelength of incident light and determined by illuminating the solar cell with a monochromatic light and measuring the photocurrent generated by this irradiation. The relation for EQE can be given as

$$EQE\ (\lambda) = \frac{I_{ph}(\lambda)}{q\Psi_{ph,\lambda}}$$

Where $\Psi_{ph,\lambda}$ is the wavelength-dependent incident spectral photon flow. The device measuring EQE usually comprises of a wide-spectrum lamp to cover the relevant wavelengths in case of solar cell (usually xenon gas discharge lamp) which is proceeded by a series of filters and monochromators to emit a narrow spectrum of irradiation to be incident on the solar cell. EQE is done to determine the short circuit current density using the following relation:

$$J_{sc} = -q \int_{\lambda_1}^{\lambda_2} EQE(\lambda) \Phi_{ph,\lambda}^{AM1.5}\, d\lambda$$

It also provides a picture on which component of the spectrum is utilized the best. EQE is zero for wavelengths below the bandgap of the perovskite material because the light is not absorbed due to their inability to generate photoexcitation on account of low energy.

EQE measurements in this thesis are carried out in RERA Solutions setup. A xenon discharge lamp is set to emit light at AM1.5 spectrum. The range of measurement is fixed at 300nm-900nm to simulate the irradiation from sunlight. The setup measures the spectral response from the sample which is then converted to EQE.

3.3 Experimental Setup

The various layers of the PSC in successive order introduced in figure 3.1. The deposited samples are stressed thermally and under light. The samples are measured at intervals of time under the characterization techniques listed in the previous section. Thermal stress is done by placing the samples on a hot plate at 85°C in the inert N_2 atmosphere within glove box.

Figure 3.6 Representative image of thermal stress testing apparatus

Accelerated ageing by light soaking is done in inert atmosphere. The samples are placed under the soaking apparatus under 1 Sun illuminaiton of AM1.5 spectrum lamp as shown in the following representative image. The tests are done in three versions:

i) Light Soaking Test 1 – Irradiation of samples incident to glass substrate.
ii) Light Soaking Test 2 – Irradiation of samples incident to top electrode.
iii) Light Soaking Test 3 – Irradiation of samples incident to glass substrate, with a cutoff filter.

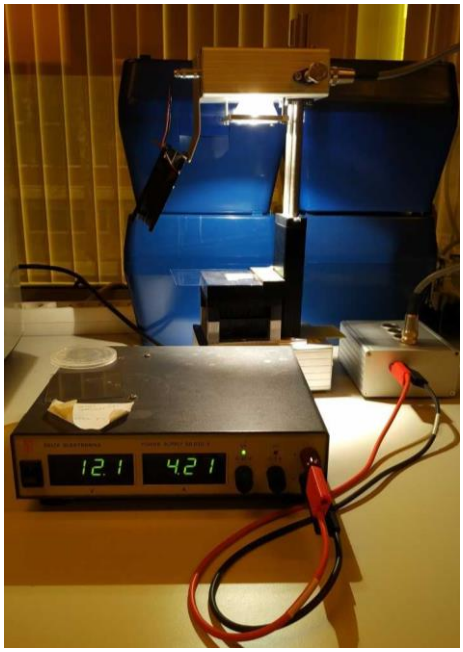

Figure 3.7 Representative image of illumination stress testing apparatus

Over the course of the discussion in results, the notation adopted is as follows:

Item	Terminologies used
CsFA Perovskite	2C, Dual Cation
MAFACs Perovskite	3C, Triple Cation
Thermal Stress test	TH
Illumination stress/light soaking	LS (exp. Suffix)

4. Choosing the Upscaling Architecture

This chapter addresses the experiments revolving RQ 1 and RQ 2, wherein the results obtained in performance and characterization of PSCs aged under thermal and illumination stresses are discussed. These results are considered in choosing the perovskite-ETL architecture with the most potential for upscaling. The chapter is divided into two major sections: i) thermal stability in section 4.1 and ii) light soaking stability in section 4.2. In each section the comparison between the ETLs and then the different perovskite stoichiometry is carried out.

The target of at least 80% of the initial power conversion efficiency (T0, initial time/0-hour measurement) after 1000 hours of accelerated stress tests (T1000) was chosen as internal target withing this project to discriminate and select the most promising architecture. Before proceeding with this chapter, it is recommended to revisit the notations for sample descriptions as listed in section 3.3.

4.1 Thermal Stability

As discussed in section 3.3 the evaluation of the thermal stability of the perovskite architecture under investigation consists of exposing the perovskite device to a continuous thermal budget defined by a constant temperature of 85°C in inert atmosphere, specifically the environment inside a glove box. The variation of parameters on intermediate measurements at different points of time for the same comparison is shown in figure 4.1. To address the issue of hysteresis in measuring PCE, only the efficiency at Maximum Power Point (MPP) is presented. In the other three quadrants, the cell parameters are shown with the values from both forward and reverse scans.

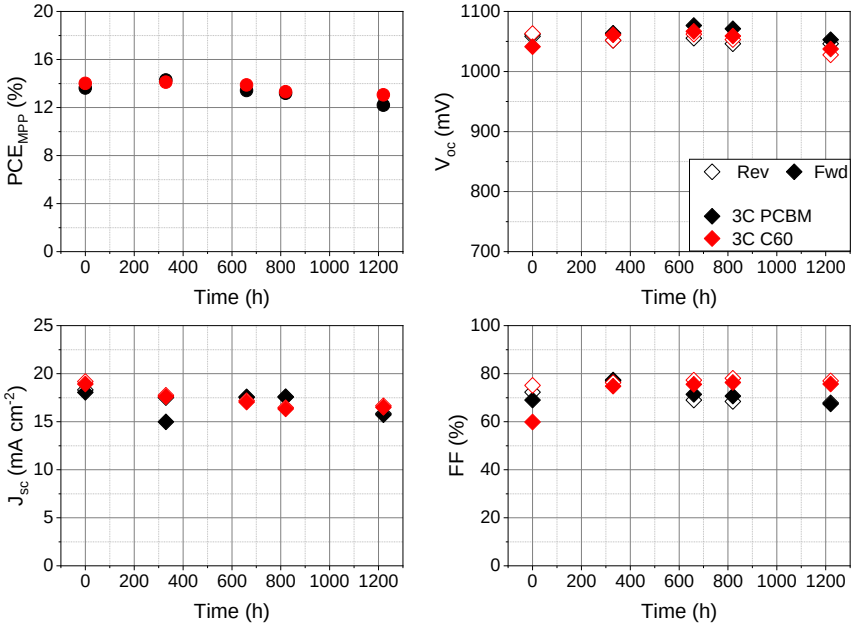

Figure 4.1 Trends for 3C Thermally Aged PSC

Whilst the PV parameters change in overall duration, both the architecture with the two fullerene layers under consideration appears to retain more than 80% of PCE at T0. Ideally a PV stable device should exhibit no variation in the V_{OC}, J_{SC} and FF. However, in the investigated case it can be observed that during the intermediate measurements the PV parameters vary.

An initial increase in V_{oc} is observed in both ETLs which then starts reducing over time, only in the last measurement point. This increase is also reported in literature for long-term thermal stability tests [130,131,132]. The increase in V_{oc} could be a consequence of the prolonged thermal budget applied to the perovskite absorber leading to neutralization of defects or improvement in work function due to suppression of recombination [133]. However, in long-term, the performance does go down mostly due to the JSC trend, which is reported in these literature as an outcome of the degradation of HTL layer [130-133]. As thermally stable perovskites are seen to retain their most of the initial Jsc [134,135], the observed decline in short circuit current density could be ascribed to the presence or increase of defects that can hamper carrier extraction [136].

From comparing the FF values presented in the trends, a decrease in hysteresis between T0 and T1000 is noticed. This can be quantified by introducing a 'Hysteresis Index' (HI) which can be written as follows [137,138]:

$$HI = \left|\frac{PCE_R - PCE_F}{PCE_R + PCE_F}\right|$$

Where F and R are subscripts denoting forward and reverse scans respectively. A HI < 0.01 (1%) is desirable and fixed as the target. The evolution of HI over time is given in the following figure 4.2:

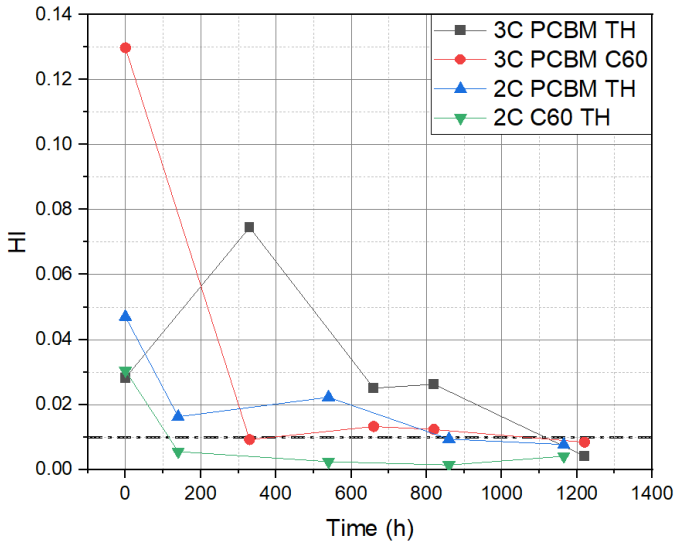

Figure 4.2 Hysteresis Index in thermally aged stacks

At T1000 for all four architectures, the HI is less than 1% and the trend shows a decrease over time. In case of C60, the T0 measurement displays large hysteresis between two scans (~13%). However, between 330 hours and 1220 hours, hysteresis is largely reduced. There is an initial increase in FF and V_{oc} between 0 and 330 hours, wherein FF has improved, and the hysteresis is minimized. Fill

Factor, as known, is the effective utilization of incident light that is affected by various resistances [139]. As proposed by Unger *et al*, illumination under JV-measurement would then lead to a transient polarization within the absorber layer affecting the carrier collection efficacy at these interfaces/carrier-selective contacts. This results in the hysteresis observed in figure 4.2. Such a case could be avoided by preconditioning the samples before T0 measurement by stabilizing the FF (and J_{sc}) with sufficient biasing [140,141]. Interestingly, the measurements presented in the trends are taken after MPP tracking, which exposes the sample to some preconditioning. The presence of hysteresis despite the initial illumination could likely be influenced by the C60-perovskite interface developed during deposition. Also, any state achieved in dark storage is suggested to be reversible, as hysteresis is reduced after the initial thermal budget (330 hours) and consistently remains low. This could indicate the rearrangement of the perovskite-ETL interface. But the initial energy required to overcome the relaxation appears to be higher in the case of C60 rather than in the case of PCBM.

Similar to what observed in the case of the triple cation mixed halide-based PSC devices, also the devices including the dual cation mixed halide perovskite stoichiometry also retain above 80% of the initial T0 PCE at T1000 as reported in the variation of parameters in time (see Figure 4.3). A reduction of hysteresis can also be observed from previous Figure 4.2.

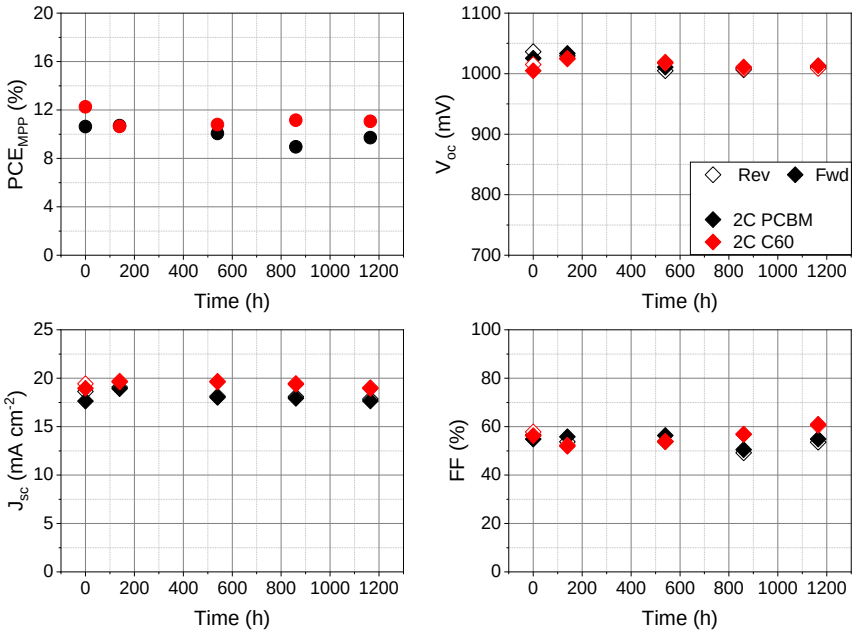

Figure 4.3 Trends for 2C Thermally Aged PSC

After initial measurement, an increase in J_{sc} and V_{oc} is noted for both PCBM and C60, with a drop in FF in case of C60. This trend is not observed in case of triple cation PSC. The difference could be due to the difference in perovskite stoichiometries, leading to different interface behaviors. From the measurements, V_{oc} is stabilized and does not have a significant change. J_{sc} on the other hand shows marginal decrease, which could also be attributed to the reasons discussed in the case of triple cation PSC.

Whilst both type of ETL can assure that at least 80% of the initial PCE can be retained after 1000 hours of thermal monostress, the use of C60 can deliver higher PCE with respect to PCBM most likely due to the difference in deposition and coverage of the perovskite surface. A similar consideration can be done in the case of the perovskite stoichiometry since all combination retained more than 80% of PCE at T0.

To shed light into the evolution of the PV parameters during this ageing tests, XRD and steady state PL have been carried out to assess whether these variations could have been ascribed to crystalline or optoelectronic modification of the perovskite absorbers. X-ray diffraction (XRD) pattern have been evaluated at T0 and T1000 to assess whether crystalline structural changes occur at the different perovskite architectures because of the thermal budget applied to it. Thermal monostress on PSC is expected to bring about the changes described in section 2.4.2 This would mean an increase in PbI_2 at the expense of photoactive bulk perovskite material. Such a change can be detected by comparing the peak angles and intensities in the XRD pattern for the two materials (PbI2, perovskite

The results for XRD analysis of 3C is shown in figure 4.4. Table 4.1 is attached to show specifically the change in intensity and peak angle of PbI2 and the photoactive α-Perovskite between T0 and end time. In case of 3C samples, even from T0, a peak s registered at 12.7° corresponding to PbI_2. This is due to the excess of PbI_2 taken into the precursor solution while fabricating the PSC would have remained in the active layer after deposition. Lack of the same in case of dual cation sample is due to no excess of PbI_2. The comparison however shows no discernable shift in peaks to suggest any loss of α-perovskite, or indicative of thermal decomposition that may be expected. Thus, the loss in performance may be ascribed to the effect of the thermal budget on other layers, like evaporation of additives in HTL [134]

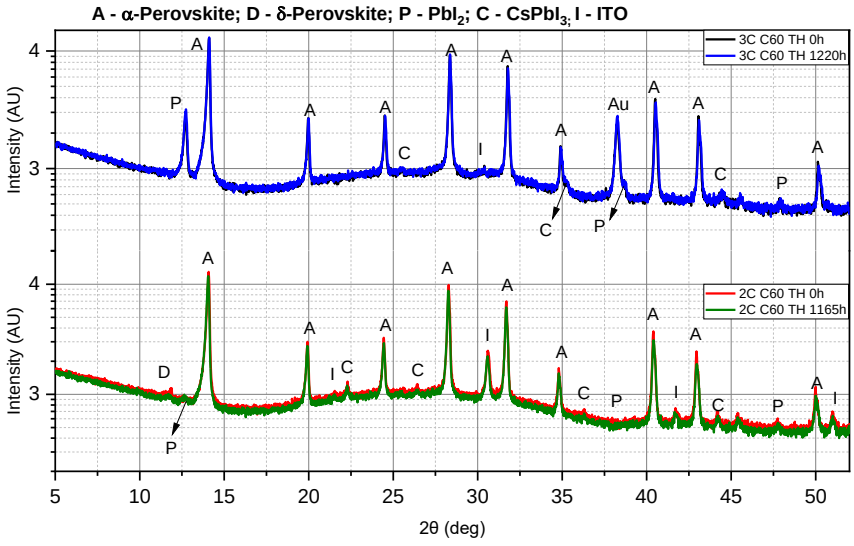

Figure 4.4 XRD Results for thermally aged triple and dual cation PSC stacks. The difference between 3C and 2C in both ITO peak at 30.6° and Au peak at 38.18° is explained by the difference in the layers deposited. The 3C samples have Au deposition on the top to increase carrier collection and minimize FF losses, which is not present in 2C samples.

Sample	XRD Component	Peak Angle (°)		Peak Intensity (AU)	
		T0	T1000	T0	T1000
3C C60	A	14.1	14.11	4.11	4.11
	P	12.69	12.74	3.43	3.5
2C C60	A	14.07	14.05	4.1	4.07
	P	12.68	12.64	2.98	2.99

Table 4.1 XRD Peaks for PbI_2 and α-Perovskite at T0 and T1000

One other reason for the increase in V_{oc} and decrease in J_{sc} could be a bandgap widening due to blue-shift induced by temperature [142], which can be enhanced by a fullerene ETL [143]. Since no structural crystalline changes were observed in XRD, steady state photoluminescence measurements were carried out to understand whether the impact of the thermal stress modified the optoelectronic properties of the perovskite layer.

Figure 4.5 shows the variation in time of the PL peak for the 4 variations under investigation. The 2C samples have PL peaks at ~15nm higher than 3C samples due to the different band gaps. In all four architectures, the shift in peak wavelength between T0 and T1000 is seen to be lesser than ±3 nm (±5meV) with no clear trends despite initial soft blue shift for the triple cation formulation, it can be concluded that the absence of significant red or blue shifts indicates no massive change in stoichiometry of the bulk absorbers to be associated at this stage to the variation in J_{SC} and V_{OC}.

A potential explanation to justify the variations in the PV parameters can arise from the perovskite modification which are not detectable with the type of techniques used during this project. Formation of defects in the bulk and/or at the interface as well as the rearrangement in time of the mobile ions could be feasible mechanism for the type of behavior observed here [136,144]

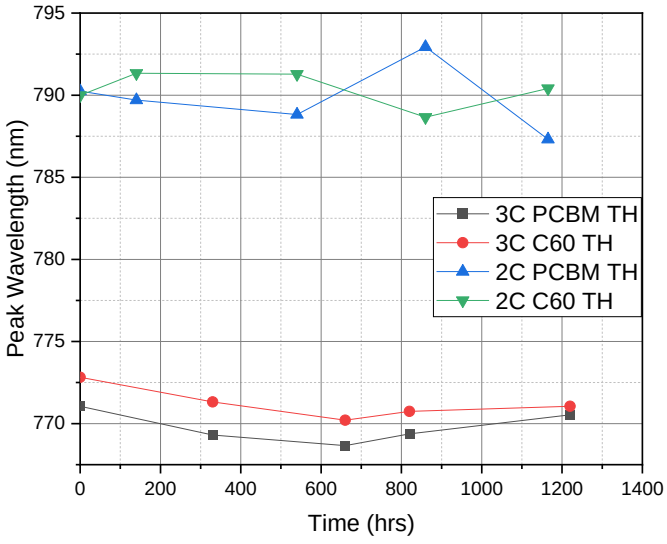

Figure 4.5 Trend in photoluminescence peaks for triple and dual cation thermally aged stacks.

To summarize, the perovskite architecture including the triple or dual cation mixed halide perovskite absorbers and different fullerene layers show no significant change in the intrinsic structure of the lattice that may be expected from thermal stressing as observed by the XRD and PL measurements.

Therefore, to identify the most promising architecture, different strategies can be followed:
i) To increase the duration of investigation further; ii) to define stricter target (i.e., 90% of initial PCE); iii) To evaluate also the photostability of the solar cell, as it is expected to work under illuminated condition. This is indeed what is discussed in the forthcoming section.

So far, from the trends, the 3C seems favorite because the higher initial PCE, and the highest PCE at T1000.

4.2 Light Soaking

The various types of light-soaking tests are discussed in section 3.3. For convenience, this section is continued with PCBM samples. The appendix section A2 has figures relevant to the results of C60 samples, which show similar trends as those discussed in this chapter. The variation of parameters on intermediate measurements at different points of time for the same comparison is shown in figure 4.6.

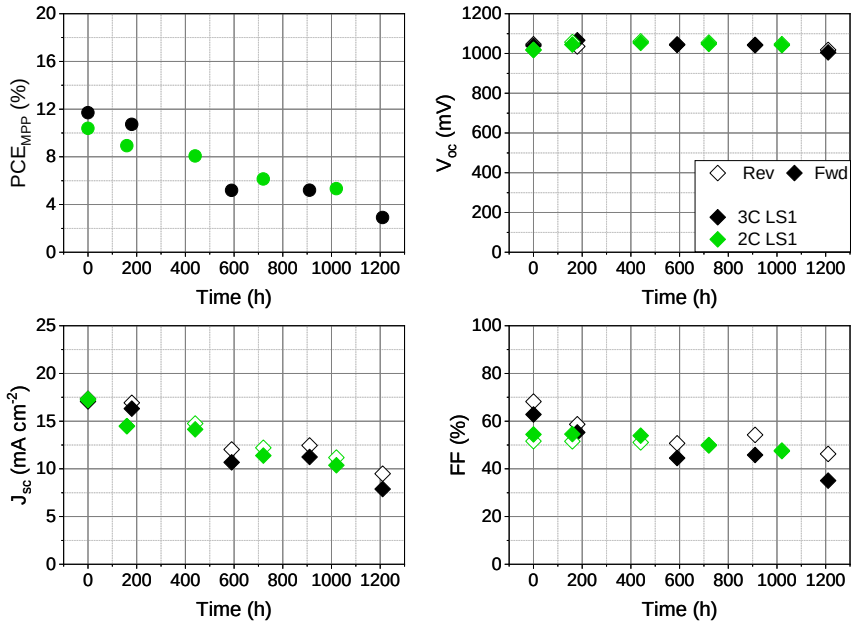

Figure 4.6 Trends for Glass-side light soaked PSC

In case of LS1 (illumination from the side of glass substrate), a drastic drop in performance for both architecture including the two types of perovskite absorbers is observed. This loss in PCE is

accompanied by a drop in J_{SC} and FF, which could point to a severe degradation within the perovskite cell.

The increase in V_{OC} could be due to an expansion in the band energy (blue-shift), which is caused by light-induced halide segregation [97,147,148]. Characterization tests are performed to study this hypothesis. Figure 4.7 and table 4.2 show the results for XRD test for LS1 samples.

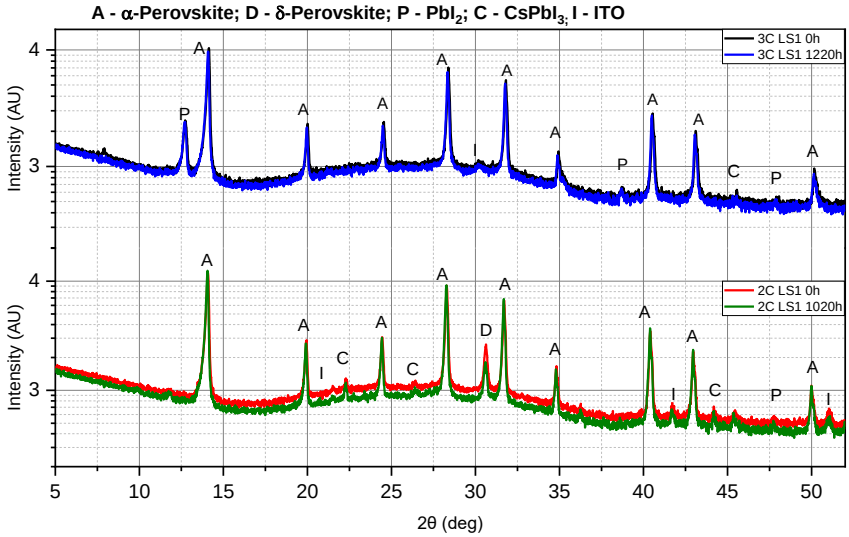

Figure 4.7 XRD Results for glass-side light soaked triple and dual cation PSC stacks. A high presence of δ-perovskite at T0 at 30.6° can be explained by the storage of the PSCs in dark for an extended period. Since FA and Cs-based perovskites favor the δ-phase for natural state, it is suspected that a fraction of α-perovskite has reversed during this stored time.

Sample	Peak Angle (°)		Peak Intensity (AU)	
	T0	T1000	T0	T1000
3C LS1	14.14	14.1	4.01	3.98
2C LS1	14.07	14.06	4.11	4.1

Table 4.2 XRD Peaks for α-Perovskite for LS1 samples.

In case of irreversible phase segregation induced by the continuous irradiation, α-perovskite XRD peaks should manifest a shift. However, as evident in the Figure and Table it is hard to conclude that this is the case. Thus, from XRD, no significant evidence of peak shift is observed to confirm the presence of halide rearrangement. A similar conclusion can be drawn from the steady state PL peak position analysis that indeed shows no clear trend (see Figure 4.8).

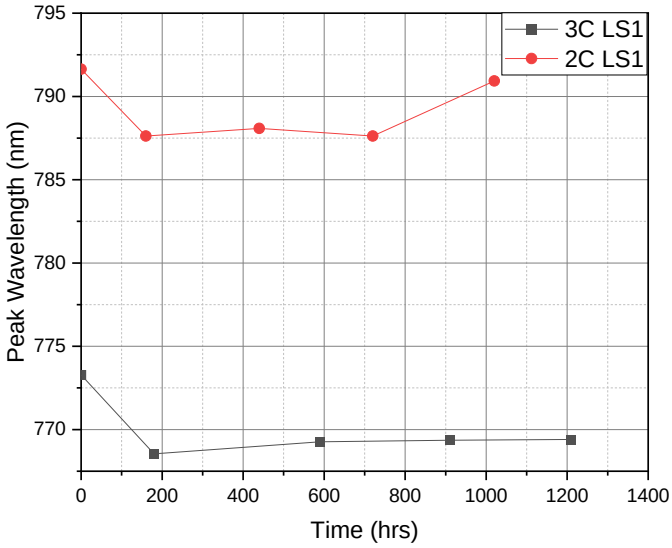

Figure 4.8 Trend in photoluminescence peaks for triple and dual cation LS1 stacks

However, the drop in J_{sc} and FF could be due to recombination losses through generation of sub-energy bands (trap states) [145] in the bulk or out of the interface alignments between perovskite and CTL [146]. Furthermore, an increase in hysteresis is observed between T0 and T1000, which is quantified by HI in figure 4.9. As it can be seen, there is a steady increase over time, which could be due to the irreversible changes caused by migration of mobile ions accelerated by light soaking, leading to losses in J_{sc} and FF [149,150]. The more drastic response of 3C sample could also be due to the segregation of MA-rich phase accelerated by light [151].

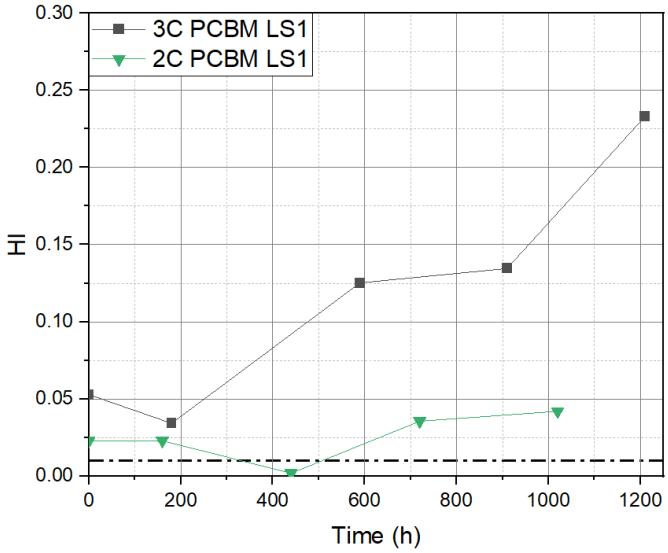

Figure 4.9 Hysteresis Index in LS1 stacks

So far, not significant difference among the architecture can be highlighted neither when the samples are light soaked from the glass side. Therefore, the attention was shifted to evaluate the stability of the cells when illuminated from the TCO side (top side of the cells).

The trends for LS2 samples are given in following figure 4.10. To reiterate, LS2 is the set of experiments where the light passes in the order of TCO-ETL-Perovskite-HTL.

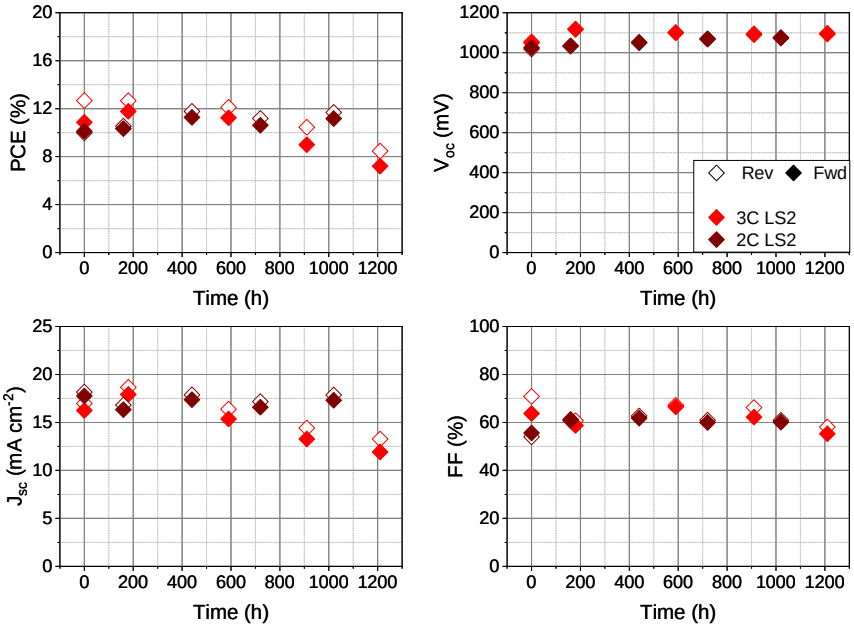

Figure 4.10 Trends for TCO-side light soaked PSC

First of all, it clearly appears that the architectures are more light stable when illuminated from the TCO side with respect to the previous case. The dual cation formulation retains 80% of their initial PCE at T0, while triple cation formulation is between 70-80%. There is an increase in V_{oc} in both cases. However, while there is a steady decline in J_{sc} in case of 3C PSC which affects the PCE, in the case of the dual cation formulation the J_{SC} remains roughly constant throughout the test. Furthermore, a rise in hysteresis between T0 and T1000 is seen is more evident again in the case of the triple cation mixed halide formulation as reported in figure 4.11

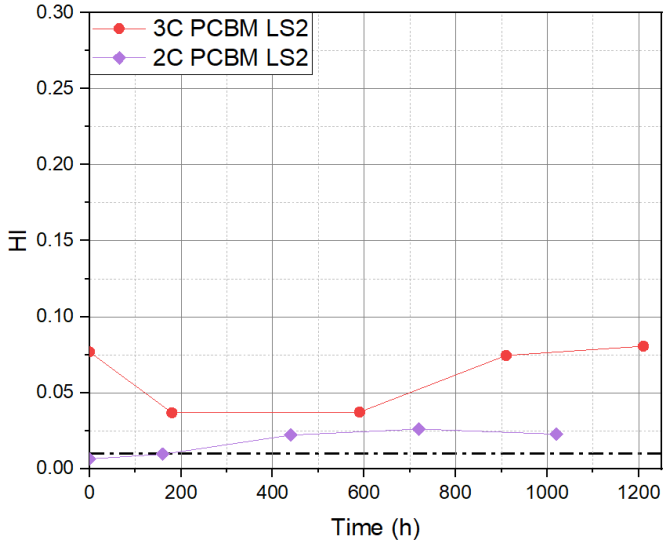

Figure 4.11 Hysteresis Index in LS2 stacks

As previously observed neither in this case XRD and PL show significant differences among the two formulation nor on the initial and the final spectra

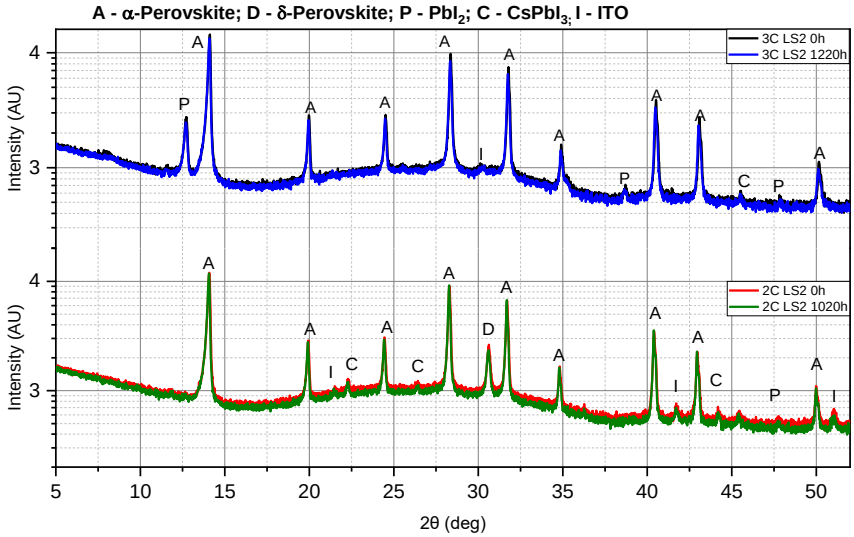

Figure 4.12 XRD Results for LS2 test samples

Sample	Peak Angle (°)		Peak Intensity (AU)	
	T0	T1000	T0	T1000
3C LS2	14.1	14.09	4.16	4.13
2C LS2	14.06	14.07	4.1	4.09

Table 4.3 XRD Peaks for α-Perovskite for LS2 samples

So far, the main result consists in the observation that the illumination from the TCO/ETL side is more stable than illuminating from the side of HTL. The type of characterization used in this project points out that no massive bulk degradation occurs at the perovskite absorber. A potential clue to understand this behavior can be obtained the external quantum efficiency (EQE) of the cells illuminated from both side (Figure 4.14)

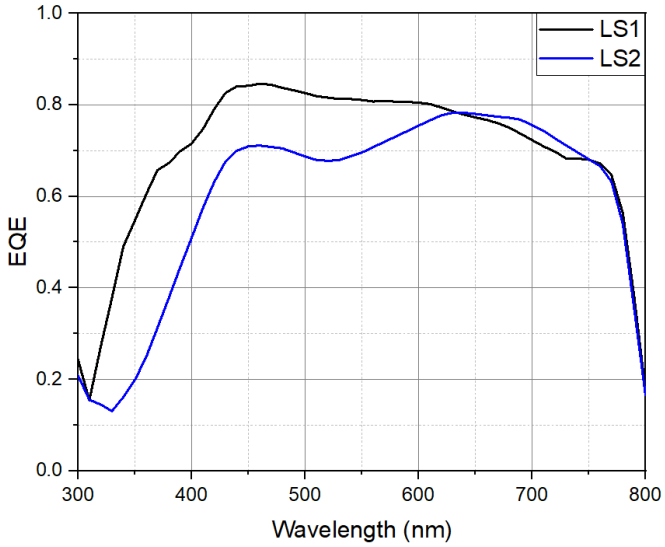

Figure 4.14 EQE measurement of LS1 and ls2. The 2C PSC has a bandgap of 1.61eV and 3C of 1.57eV, which translates approximately to a cut-off wavelength of 770 and 790 nm respectively.

The main difference is that the cell illuminated from the glass side generates and collects much more carriers in the UV-blue region than the one illuminated from the TCO side, since the top TCO and the fullerene typically absorbs the photons in these spectral regions [152,153,154,155].

To evaluate the impact of the energetic photons (UV-blue) on the long-term light stability of the cell, LS3 is conducted with glass-side orientation placing a PEN foil just in front. PEN has been chosen due to an onset of 375nm which therefore cuts at least the UV the component. A comparison of all three tests is shown for 3C and 2C in figures 4.15 and 4.16 respectively.

The drop in J_{sc} is the biggest difference between the two architectures. This drop in case of 3C between LS1 and LS3 is 9.2mAcm^{-2} and 7.8 mAcm^{-2} respectively, while the same in case of 2C is 6.8 mAcm^{-2} and 3.3 mAcm^{-2}. This shows the possible impact of the UV-filter on the cell. However, the decrease in J_{sc} still occurs, despite the presence of UV-filter. Therefore, it is presently unclear how UV light affects these architectures. The results for characterization in case of LS3 shown in appendix figures A1.1, A1.2 also do not show significant changes between T0 and T1000 to show the presence of degradation.

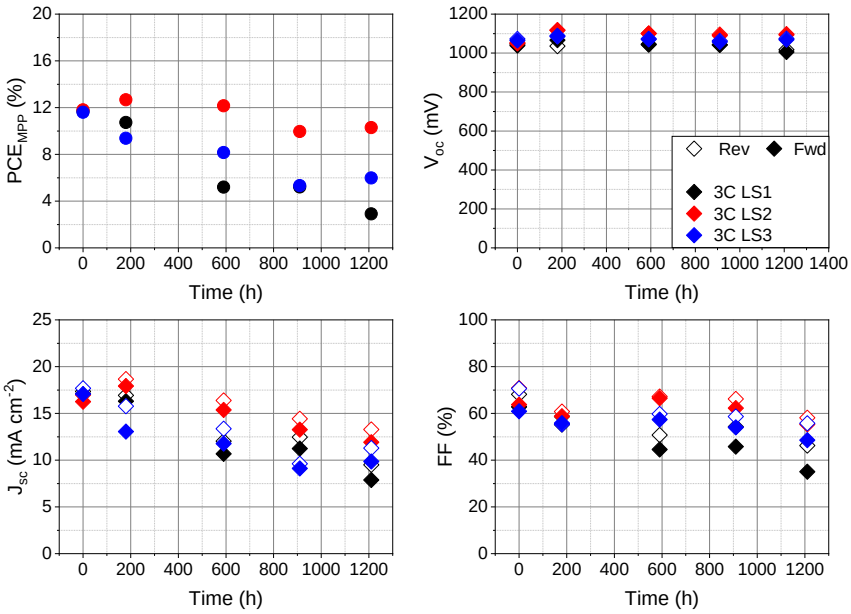

Figure 4.15 Comparison of LS experiments for triple cation stacks

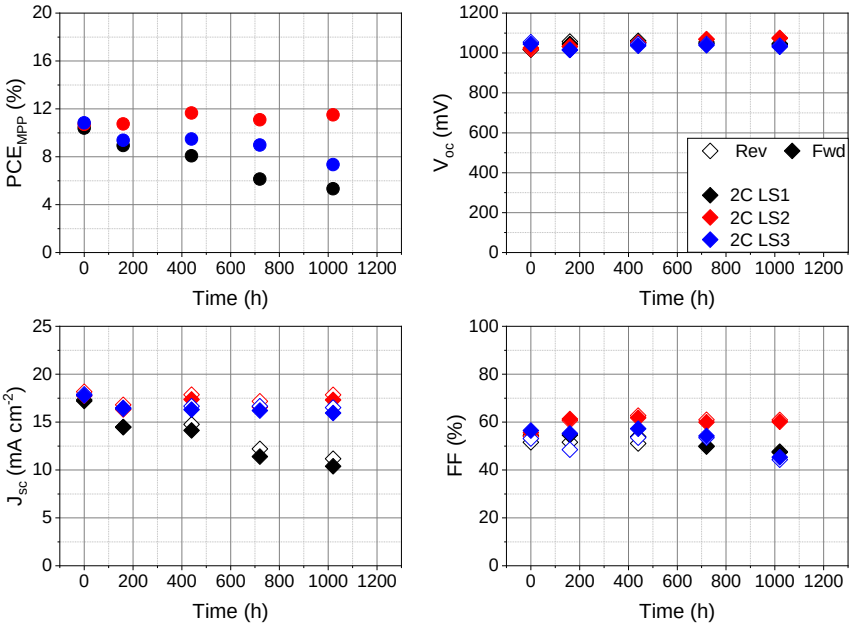

Figure 4.16 Comparison of LS experiments for dual cation stacks

To summarize, the results for accelerated illumination tests in different orientations lead to different results. The LS2 configuration is seen to be the most performing and most stable among the three cases investigated. 2C perovskite sample is seen to perform superior to 3C. The LS1 configuration shows a severe drop in performance, which is seen to be slightly ameliorated by the presence of UV-filter in case of dual cation perovskites. A potential pathway for future research could be to incorporate alternative UV-filters with different cut-off wavelengths.

Interestingly, the samples do not show sufficient evidence to indicate significant degradation or halide segregation in the active layer that could validate the change in performance. As suggested earlier, the driving factor behind loss of performance may therefore not be limited to the chemical composition of the active layer itself, but to issues not explored in this chapter. Possible explanations can include trap-assisted recombination within the bulk and surface/interface recombination mechanism as well as degradation of the HTL material. Further investigation in this direction is thus recommended.

4.3 Conclusion

This chapter dealt with the results from thermal stressing and light-soaking tests conducted on various perovskite samples. The initial expectations to observe heat-induced decomposition (in case of thermal monostress) or light-induced halide segregation (in case of light-soaking) were not observed to satisfactorily suggest these degradation mechanisms were indeed happening in their respective samples. The trends in performance, along with the results from characterization experiments, suggest the presence other sources of losses as mentioned in this chapter. Proper selection of ABX3 components for the active layer is seen to be of vital importance to achieve long-term stability and resilient performance. The choice of electron transport layer is seen to have an impact on the performance, but over the course of these experiments, it is observed that the hole transport layer might have a more immediate role in the results that were obtained. This chapter answers RQ1 and RQ2, with dual cation architecture being selected for superior combination of thermal and light-soaking stability and C60 electron transport layer selected for its overall superiority.

5.Elaboration on Light Soaking Orientations

The previous chapter presents the difference in performance and stability after light soaking stress. Specifically, the PSCs devices exhibited more stable PV parameters when illuminated from the TCO-side with respect to the case when the solar cell is illuminated from glass side. Chapter 5 takes a closer look at the results of light soaking experiments, which addresses RQ 3. According to the previous results, the tests and analysis carried out in this chapter focus exclusively on the architecture based on the dual cation mixed halide perovskite formulation and the evaporated C60 as fullerene material.

The behaviors observed might be expected to vary with batch. Therefore, ensuring reproducibility of the trends in chapter 4 is important. Therefore, a new batch (batch 2) is prepared and aged under LS experiment for 1000 hours. The following figure 5.1 shows a comparison of the trends from both batches of 2C-C60 samples in LS3 experiment. Similar figures for LS1 and LS2 can be found in appendix figures A1.3 and A1.4.

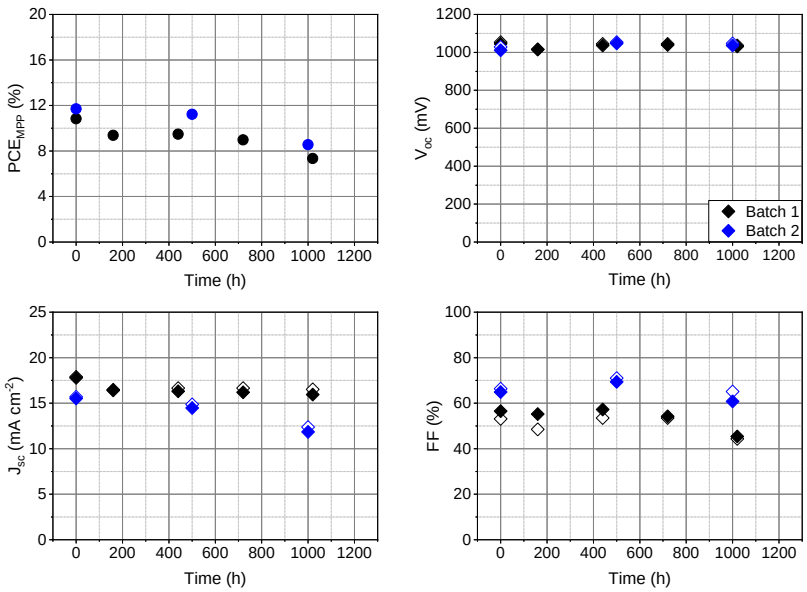

Figure 5.1 Reproducibilty of trends - LS3 test.

As observed in these figures, the trends for LS1 and LS2 are similar to those obtained in batch 1. The V_{oc} is increased in all cases, J_{sc} and FF dropped for LS1 and LS3 while the same for LS2 are retained in case of J_{sc} and increased in case of FF.

Consequently, PCE drops for LS1 and LS3, however, compared to the previous batch, the presence of UV-filter does not appear to have improved the J_{sc} measured over time. Instead, LS3 results are similar to LS1. This could be due to other factors beyond the materials in the cells themselves. Some possible sources could be handling issues (scratches on filter or sample, for example),

uncontrolled equipment malfunctions or material issues of other kind (substrates, precursors, solvents etc.). The successful reproduction of LS1 and LS2 trends show consistency in observations and therefore leads to consider that degradation is indeed minimal in the case of light exposure from TCO/ETL-side.

The lack of evidence to prove sufficient material degradation in the active layer suggests the issue with performance may be due to factors outside the crystallographic nature of the active layer.
This could include degradation at the interfaces of ETL-Perovskite, HTL-Perovskite, recombination, degradation in the transport layers themselves.

5.1 Spectral Response of architecture

From the trends of batch 2 (appendix figure A1.5), it is observed that J_{sc} is the more influential parameter affecting PCE. A tabular summary of forward-scan J_{sc} from JV measurement for three LS experiments of batch 2 is given below.

	J_{sc} ($mAcm^{-2}$)		
Time (hours)	LS1	LS2	LS3
0	17.62	18.55	15.51
1000	12.56	16.58	11.85

Table 5.1 Jsc Measured in batch 2 of LS samples.

One of the possible issues causing this drop in J_{sc} could be a change in spectral response. This can be quantified by measuring the behavior of a sample under a wide spectrum irradiation incident upon it. This is done in two levels: i) The actual component of incident light that is absorbed and ii) The part of absorbed light that is converted into electricity. These are denoted by absorptance and External Quantum Efficiency (EQE) respectively.

Figure 5.2 shows the results for EQE measurement for all LS samples along with the calculated J_{sc}. Before discussing the results, one point of interest is also the difference in the J_{sc} values noted in table 5.1 and figure 5.2. This may be explained by a combination of various factors like difference in experimental setup, ambient setup, time difference between two experiments or ageing-driven delay in response of the sample [156]. The measurements show a drop in EQE in all LS cases, across the spectrum. The drop in EQE can be the outcome of light-induced carrier collection issues in the bulk or the interfaces, or photoinduced degradation of active layer, which may shift the bandgap of the cell [157,158,159,160,161]. An easy option to verify this is to observe the changes in light absorbed by the cell. Therefore, the trend of 1-R is also compared alongside EQE. LS3 sample, which has not registered any noticeable change in 1-R or absorptance in the visible region, is an indication of carrier collection problems. The case of LS1 does not register any change in 1-R. However, in figure 5.3, a clear reduction in absorptance is seen. There is a larger drop in J_{sc} relative to LS3, which could indicate at additional issues besides carrier collection. The case of LS2 however,

has a drop in 1-R in the yellow-red region of spectrum. This could indicate a combination of increase in R and decrease in A or T. From figure 5.3, it is indeed seen that absorptance goes down. This could hint at a change in the TCO layer due to light-soaking or leading to the perovskite becoming more transparent, which is to be investigated further. From an initial look, the case of LS2 appears to not have carrier collection problems.

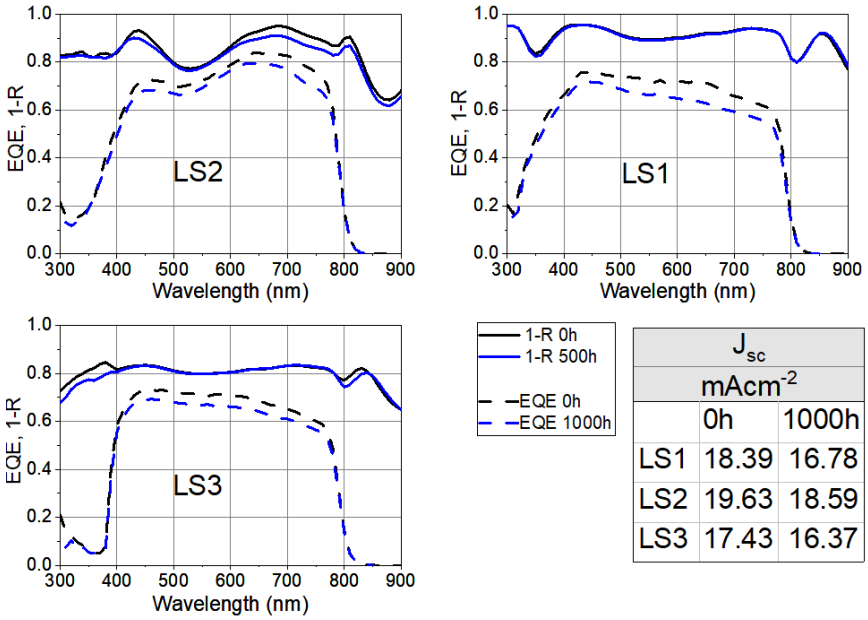

J_{sc} mAcm^{-2}	0h	1000h
LS1	18.39	16.78
LS2	19.63	18.59
LS3	17.43	16.37

Figure 5.2 Result for EQE measurements of LS samples

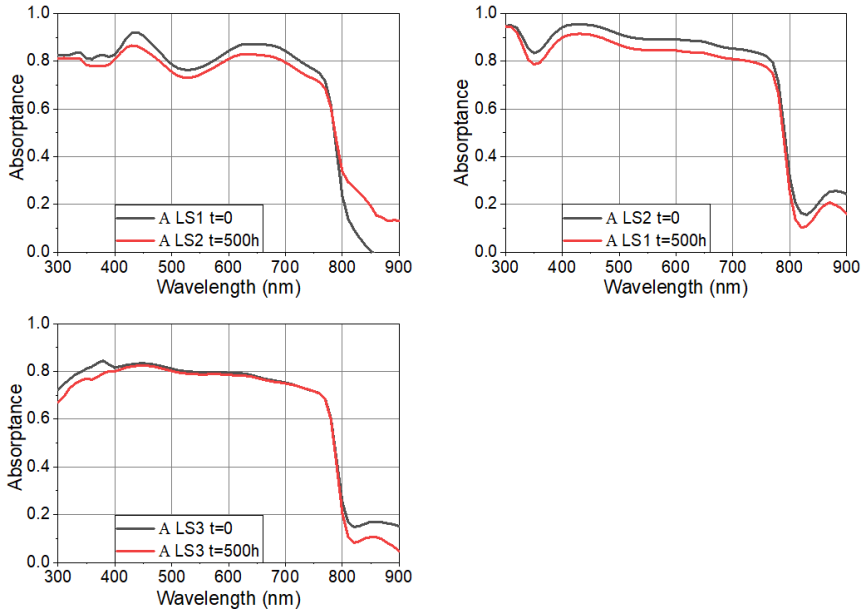

Figure 5.3 Result for Absorptance of LS samples.

The discrepancy in J_{sc} values measured in EQE setup and JV setup was mentioned and several potential reasons were listed [156]. Figure 5.4 shows the absolute difference in J_{sc} between T0 and T1000 for the light-soaking experiments. It is interesting to note the margin of deviation which is

significant at higher intensities, is very little in lower intensities. This difference arising from the experimental setup, could be the reason for the EQE setup registering a higher J_{sc} than JV.

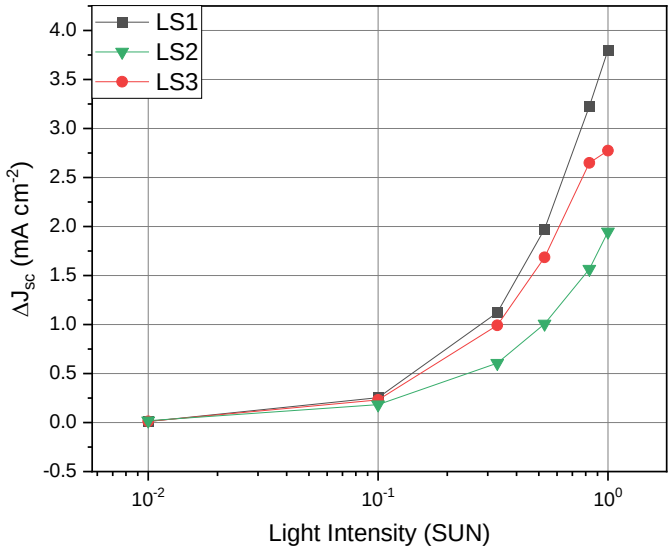

Figure 5.4 $|\Delta J_{sc}|$ between T0 and T1000 for LS samples.

The carrier collection issues, which cause this loss in absorptance, may originate from defects that are not radiative, i.e., non-radiative recombination in the bulk or interfaces. To determine the type of recombination mechanism occurring in the cell, the Ideality Factor of the samples are evaluated and discussed in the next section.

5.2 Light Intensity Measurements

To shed light on the PSC recombination mechanism, the ideality factor (IF) of the cells is evaluated. In particular, the IF is extrapolated by the analysis of the V_{oc} as a function of illumination intensity [162]. The basis of this analysis is the logarithmic relationship between V_{oc} and intensity (through carrier generation rate) by the following relation:

$$eV_{oc} = E_g - n_{ID}k_B ln\left(\frac{I_o}{I}\right)$$

Where n_{ID} is IF and I_o is a constant with the same unit as I (Wm^{-2}). The IF which is determined is usually within the range of 1-2. The implications of this on the type(s) of recombination mechanism in the PSC are summarized in figure 5.5. In short, an IF closer to unity usually denotes the dominance of surface recombination which observed in cases of low built-in voltage [163]. IF greater than unity but closer to 2 denotes to the presence and domination of non-radiative recombination mechanisms like trap-assisted Shockley-Reed Hall (SRH).

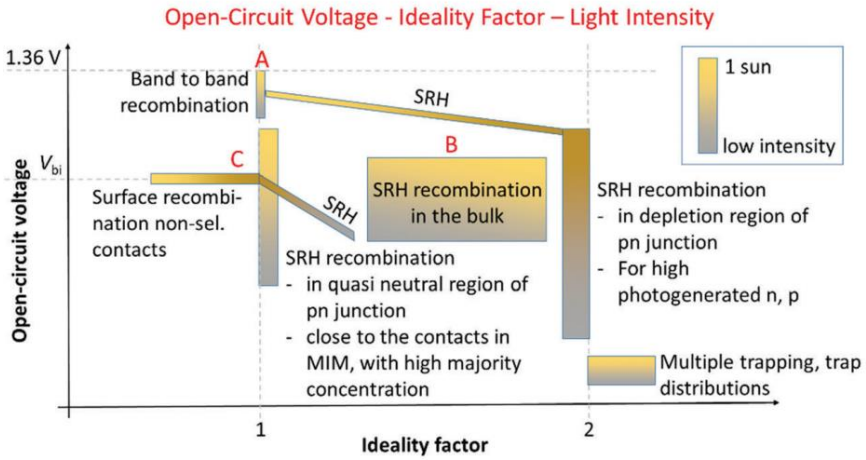

Figure 5.5 Ideality factor for different recombination mechanisms and corresponding trends, Adapted from "Interpretation and evolution of open-circuit voltage, recombination, ideality factor and subgap defect states during reversible light-soaking and irreversible degradation of perovskite solar cells†" by Tress et al, Energy Environ. Sci., 2018, 11, 151 [162]

Next to the ideality factor, the relationship between photocurrent and light intensity can give information about the quality of the charge carrier collection, although not possible to discriminate in case which interface is responsible for. They follow a power law relationship, i.e., $J \propto I^{\alpha}$, with α in a range between 0.85 and 1 [164]. α is determined by the slope of a logarithmic plot between J_{sc} and light intensities. The closer α is to unity, the superior is the charge extraction and suppression of non-radiative recombination in the solar cell [165]. This power law relationship is attributed to the space-charge that is built up in the device that could be brought about by the variation in charge carrier mobilities under different intensities.

For this thesis, the V_{oc}-light intensity and J_{sc}-light intensity measurements are done in the same apparatus for JV measurement by setting up neutral filters to obtain 1, 0.83, 0.53, 0.33, 0.1 and 0.01 Sun intensities.

The factors IF and α are determined by the slope of linear fitting of V_{oc} and J_{sc} as a function of light intensity as reported in figures 5.6, 5.7 respectively and presented in table 5.2.

The α parameter shows significant difference between LS tests. Specifically, there is a massive decrease in α for both LS tests illuminated from glass-side (LS1 and LS3, without and with PEN filter respectively). As already mentioned, when α is closer to 1, it is indicative of effective charge carrier extraction and suppression of non-radiative recombination [165]. Therefore, it is plausible to say that the PSC illuminated from ETL-side maintain a more efficient charge carrier collection which would explain also the retention of the J_{SC} during the light soaking tests with respect to the other 2 cases [166].

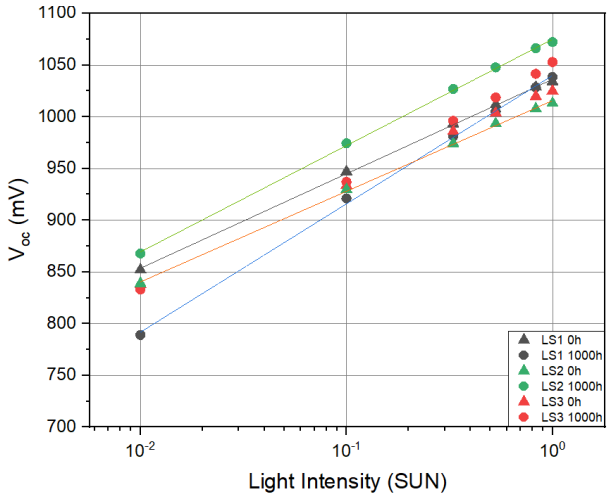

Figure 5.6 V_{oc}-Light Intensity Curve for LS samples.

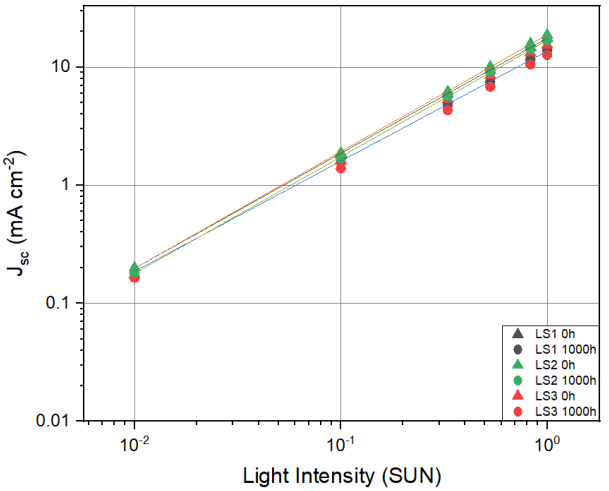

Figure 57 J_{sc}-Light Intensity Curve for LS samples.

Experiment	Time	IF	α
LS1	0h	1.52	0.975
	1000h	2.07	0.932
LS2	0h	1.46	0.988
	1000h	1.72	0.986
LS3	0h	1.58	0.975
	1000h	1.83	0.942

Table 5.2 Summary of IF, α

As a consequence of the results it can be concluded that the interface HTL/perovskite in this work is responsible for the charge collection issue with an impact in the J_{SC} value measured with the JV scan. The issue in this interface could be the generation of trap states due to formation of smaller perovskite crystals near the interface is reported by Ni *et al* [167], or the degradation of the PTAA/perovskite interface and potentially also its delamination lead to a massive decrease of the performance despite mild ageing conditions (35°C, dark) reported by Perrin *et al* [168]. The degradation of HTL or HTL-Perovskite interface would clearly explain the decrease in J_{sc} observed in both batches of PSCs. The initial reduction of J_{SC} also in the case of the illumination from the TCO side can on the other hand be related to the photoinduced modification under light soaking as explained by Zhao *et al* [166]. Next to the impact on the charge accumulation at the interface, the authors point out that a complementary effect is the decrease of the bulk-electrical polarization which causes a decrease on J_{SC}.

The samples in batch 2 for LS3 experiment did not reproduce the retention of J_{sc} demonstrated by batch 1. One explanation for this behavior could be that UV radiation is not the most contributing component of the spectrum to accelerate defects in HTL/Perovskite interface. Alternatively, the non-impact of UV-filter could be exclusive to this batch alone. This difference could have originated

from the preparation of HTL precursors, or the process and operating conditions of the fabricating technique, leading to localized defect sites that cannot be detected by present capacity.

The decrease in α, which indicates higher presence of carrier collection problems and non-radiative recombination, is expected to affect the V_{oc} negatively. However, there is no signifncant decrease in V_{oc} for LS1, and in case of LS2 and LS3, V_{oc} actually increases. To understand this behavior, the IF of LS tests is calculated.

As observed by the extrapolated values, the IF tends to increase for all the light-soaking conditions investigated in this project. The initial values among all LS are similar between 1.5 and 2 which, according to Tress *et al*, should be attributed to SRH recombination in the bulk of a mostly intrinsic or depleted perovskite film [162]. The devices stressed when illuminated from the ETL side (TCO side) exhibits actually a slightly lower IF, which might indicate that illumination direction and where most of the electron-hole pairs are photogenerated has an impact on the formation on the SRH mechanism and therefore that trap states can indeed photoinduced. After light soaking the ideality factor increases for all the investigated architectures which indicates the formation on new recombination channels in the perovskite [162], mostly related to SHR bulk state formation. What it is interesting is that whilst Tress *et al* observed a decrease of V_{OC} upon light soaking, all the three investigated scenarios within this projects exhibit an increase of V_{OC}. This behaviour has been reported mostly in the case of p-i-n architecture rather than the n-i-p studied by Tress *et al* [169,170]. In these two contributions, the V_{OC} increase is attributed to a redistribution of mobile ions after light soaking towards the interfaces. This rearrangement which can change the built-in electric field modifying the charge accumulation at electrode interfaces, can therefore neutralize interfacial defects [170]. This increase in V_{oc}, alongside FF, is attributed to the defect suppression in interface also in the works of Kim *et al* and Zhao *et al* [171,166]

Different from the paper, where a recovery of the PCE have been measured when storing the sample in dark after the light soaking, within this projects the modification seems irreversible after storing in dark (2hrs). A potential explanation can be attributed to the extremely longer light soaking test carried out within this project, or the type of defects created upon light soaking. It could be interesting to perform FTPS analysis to shed light to the energy level position of the bulk defects as reported by Tress *et al* [162]. Whilst a higher IF indicates more SRH recombination, it is also observed that the IF tends to decrease for higher illumination intensities (an example provided in figure 5.8 from the work of Tress *et al*) which highlights that still surface recombination becomes relevant for higher V_{oc} (or higher light intensity and therefore during the JV scans measurements).

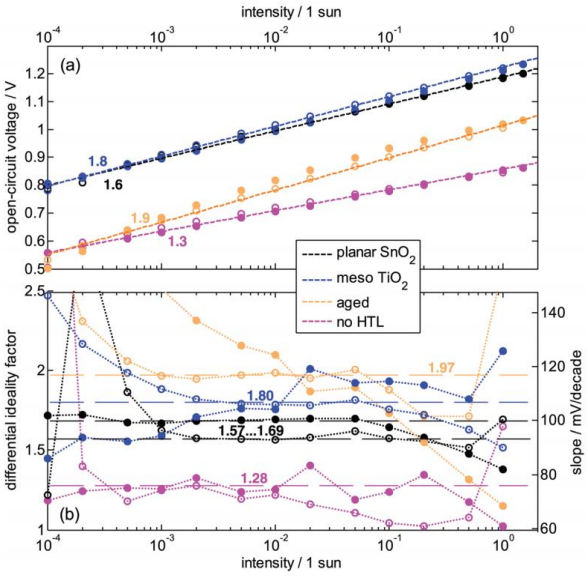

Figure 5.8 Differential IF across light intensities, Adapted from "Interpretation and evolution of open-circuit voltage, recombination, ideality factor and subgap defect states during reversible light-soaking and irreversible light-soaking and irreversible degradation of perovskite solar cells†" by Tress et al, Energy Environ. Sci., 2018, 11, 151 [162]

However, the IF does not change in orders of magnitude with light intensity, thus not be influenced by radiative recombination or change with intensity of light exposed [162]. The IF exhibit similar trends for all of the investigated cases, therefore making it complicated to draw a possible explanation on the difference in behavior observed with direction of illumination.

5.3 Conclusion

The chapter attempts at answering RQ3, which involves understanding the recombination mechanisms of the various light-soaked samples. The behavior of samples under varying illumination intensities is studied and found to display their dominant recombination mechanisms. All three tests show an increase in IF, which is indicative of the growing dominance of bulk recombination. On the other hand, the α is seen to decrease drastically for glass-side illumination. This is in agreement with the results from EQE and UV-Vis, which hinted towards carrier collection issues. This leads to the conclusion that ETL/perovskite interface is possibly more resilient than HTL/perovskite interface. The behavior of PTAA in long-term stability tests must therefore be studied further.

6. Conclusions and Remarks

Perovskite solar cells are a promising technology for harnessing solar energy. Although their performance is increasingly positive, their commercial feasibility is limited by stability issues and costs of components in small-scale fabrication. This thesis is written about the experiments conducted on PSCs made wholly from fabrication techniques that can be upscaled for commercialization. The cells are tested for stability at >1000 hours in the two most important stresses faced by a PSC – Heat and light. The inert atmosphere of stress tests precludes the effect of the other important stresses like oxygen and moisture. To select the most prospective architecture for upscaling, a comparison is done between two perovskites (triple cation and dual cation) and two electron transport layers (PCBM and C60). Their performance and structural changes are characterized by various tests.

The results of thermal stress tests show resilience (>80% PCE) in PCE for all configurations, but 2C architecture is preferred for better retention of J_{sc} than 3C architecture. Light-soaking tests done from glass-side did not retain 80% initial PCE for both dual and triple cation architectures. Light-soaking done from ETL/TCO-side showed retention of 80% initial PCE in case of 2C perovskite. Among the tested configurations, it is concluded that dual cation-C60 architecture is the more resilient option. The characterization done by XRD, and photoluminescence did not show sufficient evidence for material degradation that may be from long-term exposure to stressors.

To justify this difference in performance with illumination side, their recombination mechanisms are studied to determine IF and α by light intensity measurements. The α parameter drops for glass-side illumination but does not change significantly for ETL/TCO-side. This establishes the presence of carrier collection problems and potential degradation of HTL layer under UV or blue spectrum over long-term exposure from glass-side exposure.

For further studies, several recommendations are presented. i) To conduct further experiments to study the possibility of ion migration, like XPS ii) To perform advanced microscopy tests like cross-section SEM to detect interface issues like delamination iii) Incorporation of FTPS, capacitance-voltage and electroluminescence methods to throw more light on the recombination mechanisms iv) Performing trap density calculations by measuring Space Charge Limited Current (SCLC) v) Incorporation of alternative UV filters to discriminate wavelength dependency of degradation mechanism vi) Replacement of HTL material.

A1. Appendix 1

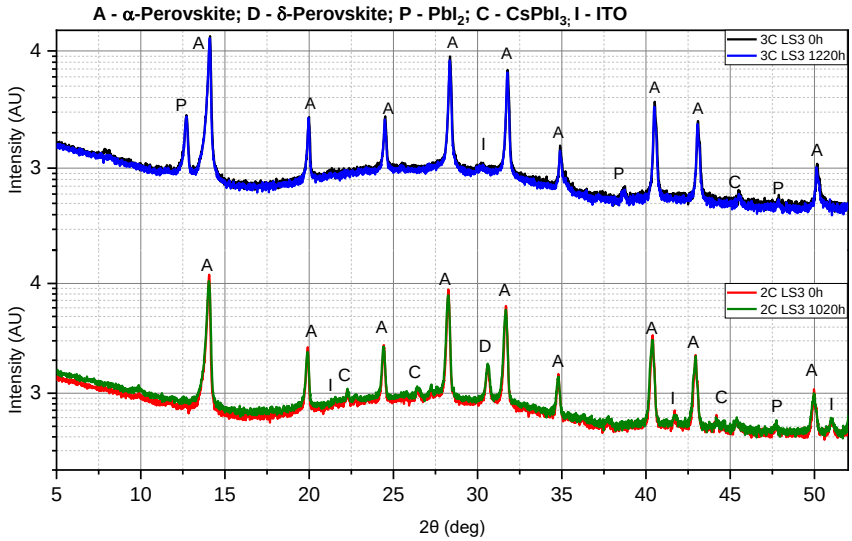

Figure A1.1 XRD Results for LS3 samples

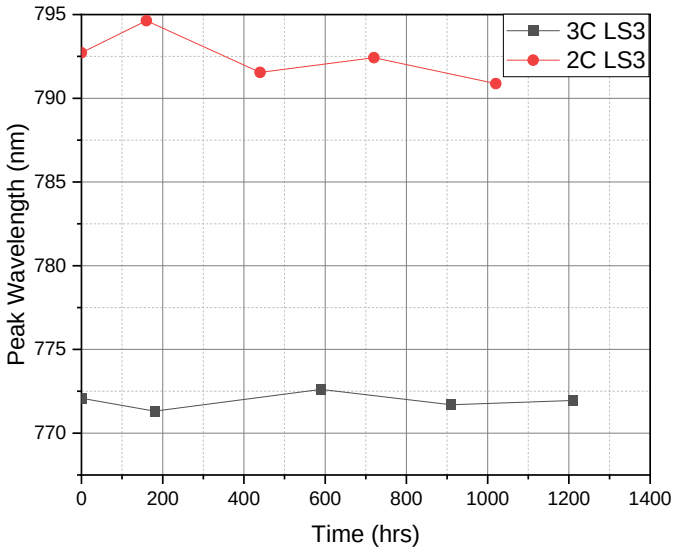

Figure A1.2 Trends in photoluminscnence for LS3 samples

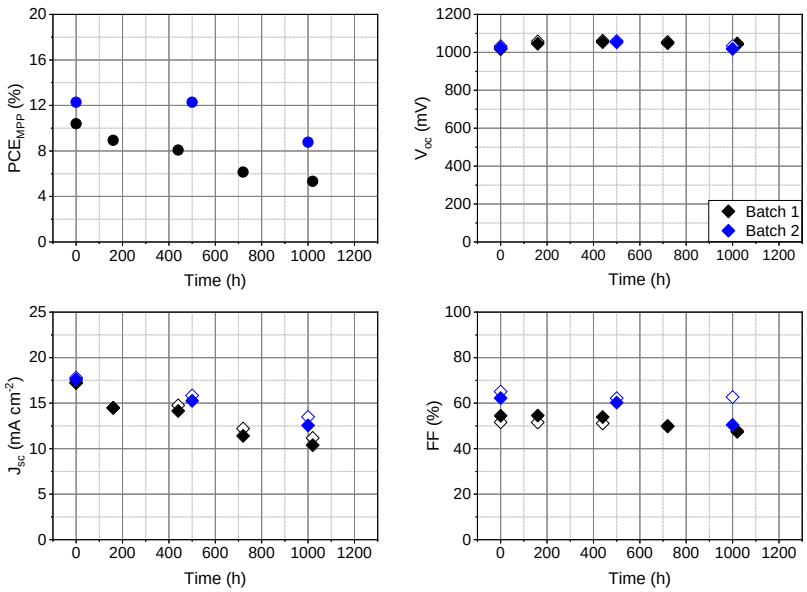

Figure A1.3 Reproducibilty of trends - LS1 test.

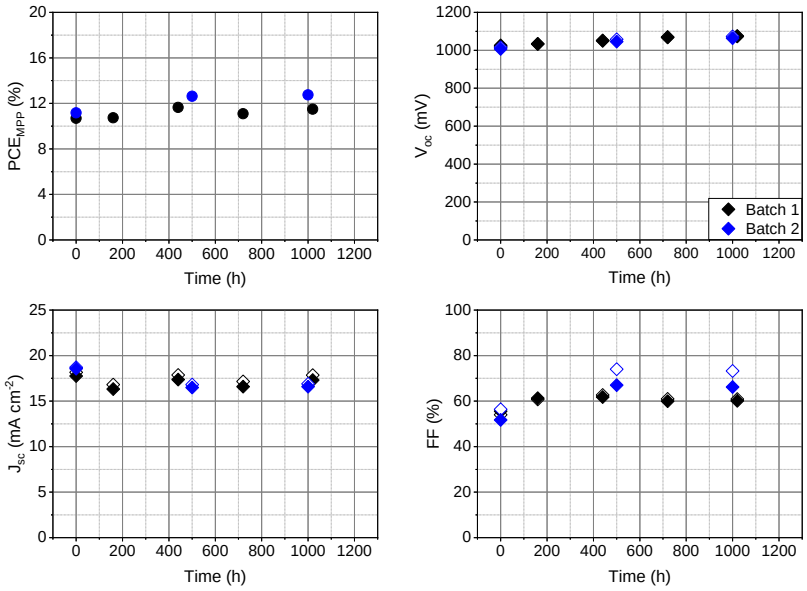

Figure A1.4 Reproducibilty of trends - LS2 test.

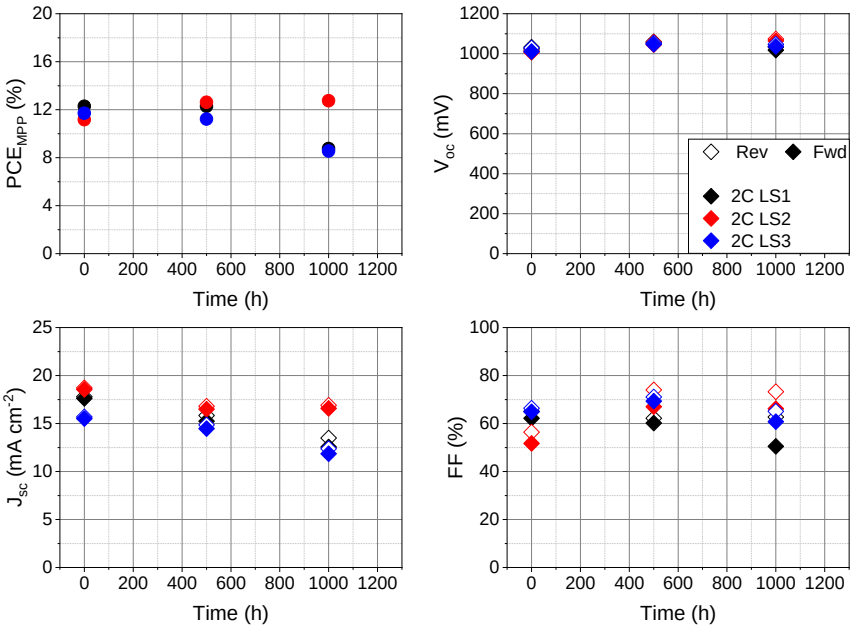

Figure A1.5 Comparison of LS tests for Batch 2

A2. Appendix 2

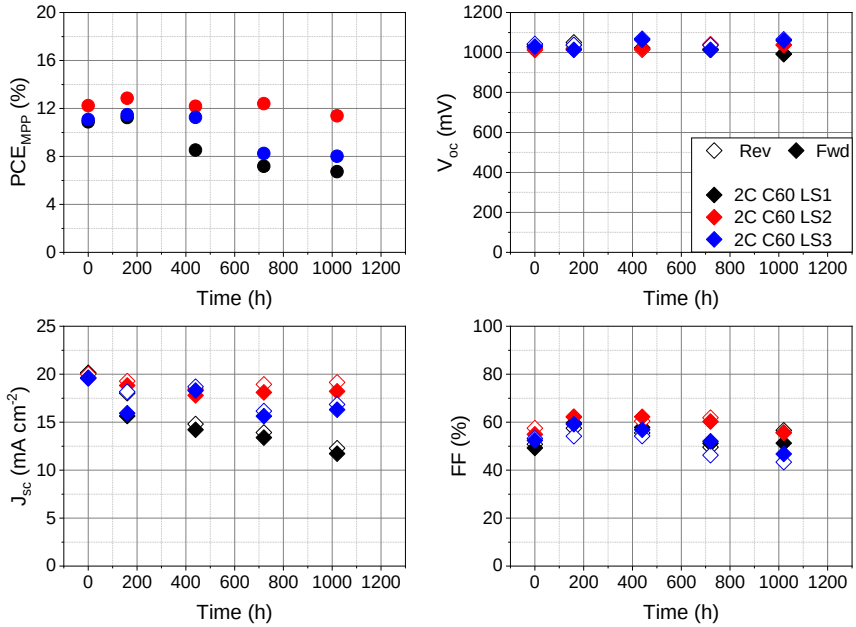

Figure A2.1 Trends for Light Soaked samples with C60 ETL

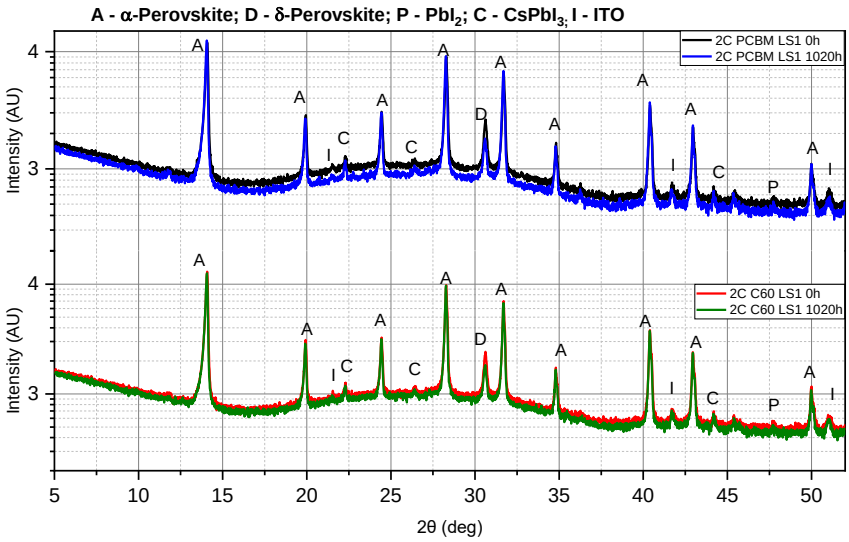

Figure A2.2 XRD results for 2C C60 samples light soaked from glass-side

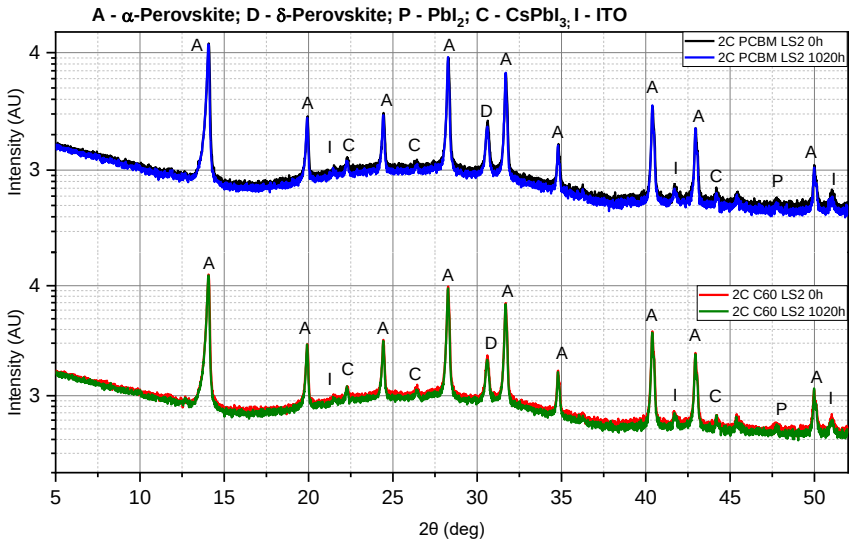

Figure A2.3 XRD results for 2C C60 samples light soaked from TCO-side

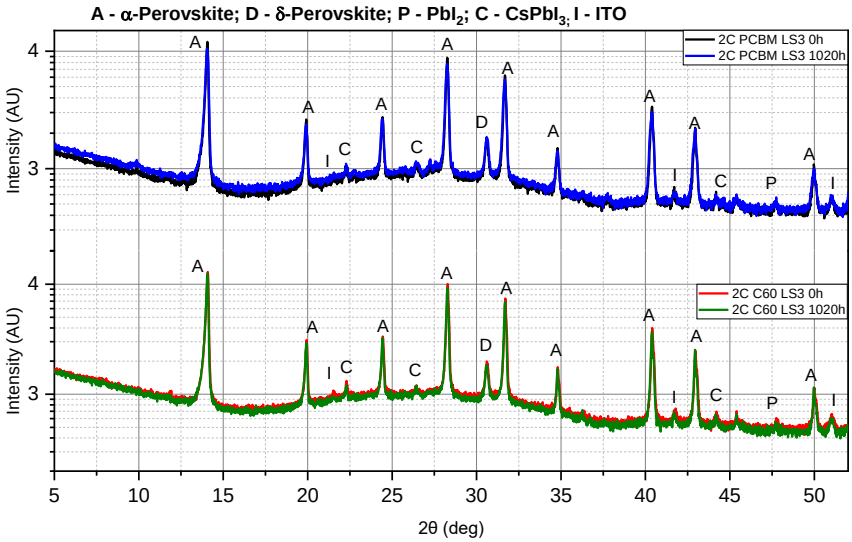

Figure A2.4 XRD results for 2C C60 samples by LS3

Bibliography

1. BP Global. 2020. Energy Outlook. [online] Available at: <https://www.bp.com/en/global/corporate/energy-economics/energy-outlook.html> [Accessed 5 August 2021].
2. Kahan, A., 2020. Global electricity consumption continues to rise faster than population. [online] Eia.gov. Available at: <https://www.eia.gov/todayinenergy/detail.php?id=44095> [Accessed 5 August 2021].
3. Our World in Data. 2021. Electricity production by source. [online] Available at: <https://ourworldindata.org/grapher/electricity-prod-source-stacked> [Accessed 5 August 2021].
4. Unfccc.int. 1992. UNITED NATIONS FRAMEWORK CONVENTION ON CLIMATE CHANGE. [online] Available at: <https://unfccc.int/resource/docs/convkp/conveng.pdf> [Accessed 5 August 2021].
5. Perez, R., & Perez, M. (2009). A fundamental look at energy reserves for the planet. The IEA SHC Solar Update, 50(2).
6. Bp.com. 2021. Statistical Review of World Energy 2021 70th Edition. [online] Available at: <https://www.bp.com/content/dam/bp/business-sites/en/global/corporate/pdfs/energy-economics/statistical-review/bp-stats-review-2021-full-report.pdf> [Accessed 6 August 2021].
7. Kojima, Akihiro, Kenjiro Teshima, Yasuo Shirai, and Tsutomu Miyasaka. 2009. "Organometal Halide Perovskites as Visible-Light Sensitizers for Photovoltaic Cells." Journal of the American Chemical Society 131(17):6050–51. doi: 10.1021/ja809598r
8. Green, Martin A., and Anita Ho-Baillie. 2017. "Perovskite Solar Cells: The Birth of a New Era in Photovoltaics." ACS Energy Letters 2(4):822–30. doi: 10.1021/acsenergylett.7b00137.
9. Grätzel, Michael. 2014. "The Light and Shade of Perovskite Solar Cells." *Nature Materials* 13(9):838–42. doi: 10.1038/nmat4065.
10. Im, Jeong Hyeok, Chang Ryul Lee, Jin Wook Lee, Sang Won Park, and Nam Gyu Park. 2011. "6.5% Efficient Perovskite Quantum-Dot-Sensitized Solar Cell." *Nanoscale* 3(10):4088–93. doi: 10.1039/c1nr10867k.
11. Kim, Hui Seon, Chang Ryul Lee, Jeong Hyeok Im, Ki Beom Lee, Thomas Moehl, Arianna Marchioro, Soo Jin Moon, Robin Humphry-Baker, Jun Ho Yum, Jacques E. Moser, Michael Grätzel, and Nam Gyu Park. 2012. "Lead Iodide Perovskite Sensitized All-Solid-State Submicron Thin Film Mesoscopic Solar Cell with Efficiency Exceeding 9%." *Scientific Reports* 2:1–7. doi: 10.1038/srep00591.
12. Park, Nam Gyu. 2015. "Perovskite Solar Cells: An Emerging Photovoltaic Technology." *Materials Today* 18(2):65–72. doi: 10.1016/j.mattod.2014.07.007.
13. Podolsky, B., N. Rosen, J. F. Clauser, A. M. Steinberg, R. Y. Chiao, A. Vaziri, G. Weihs, A. Zeilinger, R. S. Bennink, S. J. Bentley, R. W. Boyd, L. Ratschbacher, A. Fedrizzi, N. K. Langford, A. Zeilinger, M. W. Beijersbergen, R. J. C. Spreeuw, J. P. Woerdman, G. Weihs, A. Zeilinger, L. Leach, G. S. Buller, M. J. Padgett, E. Andersson, F. Miatto, E. R. Eliel, J. P. Woerdman, P. Meystre, K. Schwab, G. S. Agarwal, R. W. Boyd, D. Giovannini, S. M. Barnett, M. J. Padgett, H. C. B. Florijn, M. P. Van Exter, J. Pykacz, S. M. Nomoto, W. H. Schubert, M. D. Novenstern, J. A. Davis, M. A. Bandres, J. Broky, A. Dogariu, D. N. Christodoulides, M. Fiorentino, F. N. C. Wong, T. Herbst, A. Poppe, T. Jennewein, A. Zeilinger, B. Hage, B. Buchler, P. K. Lam, C. Maurer, and S. Bernet. 2012. "References and Notes 1." 338(November):643–48.
14. Heo, Jin Hyuck, Sang Hyuk Im, Jun Hong Noh, Tarak N. Mandal, Choong Sun Lim, Jeong Ah Chang, Yong Hui Lee, Hi Jung Kim, Arpita Sarkar, Md K. Nazeeruddin, Michael Grätzel, and Sang Il Seok. 2013. "Efficient Inorganic-Organic Hybrid Heterojunction Solar Cells Containing Perovskite Compound and Polymeric Hole Conductors." *Nature Photonics* 7(6):486–91. doi: 10.1038/nphoton.2013.80.
15. Burschka, Julian, Norman Pellet, Soo Jin Moon, Robin Humphry-Baker, Peng Gao, Mohammad K. Nazeeruddin, and Michael Grätzel. 2013. "Sequential Deposition as a Route to High-Performance Perovskite-Sensitized Solar Cells." *Nature* 499(7458):316–19. doi: 10.1038/nature12340.

16. Urieta-Mora, J., García-Benito, I., Molina-Ontoria, A., & Martín, N. (2018). *Hole transporting materials for perovskite solar cells: a chemical approach. Chemical Society Reviews.* doi:10.1039/c8cs00262b

17. Ball, James M., Michael M. Lee, Andrew Hey, and Henry J. Snaith. 2013. "Low-Temperature Processed Meso-Superstructured to Thin-Film Perovskite Solar Cells." *Energy and Environmental Science* 6(6):1739–43. doi: 10.1039/c3ee40810h.

18. Liu, Mingzhen, Michael B. Johnston, and Henry J. Snaith. 2013. "Efficient Planar Heterojunction Perovskite Solar Cells by Vapour Deposition." *Nature* 501(7467):395–98. doi: 10.1038/nature12509.

19. Docampo, Pablo, James M. Ball, Mariam Darwich, Giles E. Eperon, and Henry J. Snaith. 2013. "Efficient Organometal Trihalide Perovskite Planar-Heterojunction Solar Cells on Flexible Polymer Substrates." *Nature Communications* 4:1–6. doi: 10.1038/ncomms3761.

20. Malinkiewicz, Olga, Aswani Yella, Yong Hui Lee, Guillermo Mínguez Espallargas, Michael Graetzel, Mohammad K. Nazeeruddin, and Henk J. Bolink. 2014. "Perovskite Solar Cells Employing Organic Charge-Transport Layers." *Nature Photonics* 8(2):128–32. doi: 10.1038/nphoton.2013.341.

21. Saliba, Michael, Taisuke Matsui, Ji Youn Seo, Konrad Domanski, Juan Pablo Correa-Baena, Mohammad Khaja Nazeeruddin, Shaik M. Zakeeruddin, Wolfgang Tress, Antonio Abate, Anders Hagfeldt, and Michael Grätzel. 2016. "Cesium-Containing Triple Cation Perovskite Solar Cells: Improved Stability, Reproducibility and High Efficiency." *Energy and Environmental Science* 9(6):1989–97. doi: 10.1039/c5ee03874j.

22. Song, Zhaoning, Suneth C. Watthage, Adam B. Phillips, and Michael J. Heben. 2016. "Pathways toward High-Performance Perovskite Solar Cells: Review of Recent Advances in Organo-Metal Halide Perovskites for Photovoltaic Applications." *Journal of Photonics for Energy* 6(2):022001. doi: 10.1117/1.jpe.6.022001.

23. Mohamad Noh, Mohamad Firdaus, Chin Hoong Teh, Rusli Daik, Eng Liang Lim, Chi Chin Yap, Mohd Adib Ibrahim, Norasikin Ahmad Ludin, Abd Rashid Bin Mohd Yusoff, Jin Jang, and Mohd Asri Mat Teridi. 2018. "The Architecture of the Electron Transport Layer for a Perovskite Solar Cell." *Journal of Materials Chemistry C* 6(4):682–712. doi: 10.1039/c7tc04649a.

24. Mahmood, Khalid, Saad Sarwar, and Muhammad Taqi Mehran. 2017. "Current Status of Electron Transport Layers in Perovskite Solar Cells: Materials and Properties." *RSC Advances* 7(28):17044–62. doi: 10.1039/c7ra00002b.

25. Yang, Guang, Hong Tao, Pingli Qin, Weijun Ke, and Guojia Fang. 2016. "Recent Progress in Electron Transport Layers for Efficient Perovskite Solar Cells." *Journal of Materials Chemistry A* 4(11):3970–90. doi: 10.1039/c5ta09011c.

26. Kim, Taewan, Jongchul Lim, and Seulki Song. 2020. "Recent Progress and Challenges of Electron Transport Layers in Organic⇓inorganic Perovskite Solar Cells." *Energies* 13(21):1–16. doi: 10.3390/en13215572.

27. Pitchaiya, Selvakumar, Muthukumarasamy Natarajan, Agilan Santhanam, Vijayshankar Asokan, Akila Yuvapragasam, Venkatraman Madurai Ramakrishnan, Subramaniam E. Palanisamy, Senthilarasu Sundaram, and Dhayalan Velauthapillai. 2020. "A Review on the Classification of Organic/Inorganic/Carbonaceous Hole Transporting Materials for Perovskite Solar Cell Application." *Arabian Journal of Chemistry* 13(1):2526–57. doi: 10.1016/j.arabjc.2018.06.006.

28. Yin, Xinxing, Zhaoning Song, Zaifang Li, and Weihua Tang. 2020. "Toward Ideal Hole Transport Materials: A Review on Recent Progress in Dopant-Free Hole Transport Materials for Fabricating Efficient and Stable Perovskite Solar Cells." *Energy and Environmental Science* 13(11):4057–86. doi: 10.1039/d0ee02337j.

29. Urieta-Mora, Javier, Inés García-Benito, Agustín Molina-Ontoria, and Nazario Martín. 2018. "Hole Transporting Materials for Perovskite Solar Cells: A Chemical Approach." *Chemical Society Reviews* 47(23):8541–71. doi: 10.1039/c8cs00262b.

30. Bashir, Z., and Sanjay Rastogi. 2005. “The Explanation of the Increase in Slope at the Tg in the Plot of D-Spacing versus Temperature in Polyacrylonitrile.” *Journal of Macromolecular Science - Physics* 44 B(1):55–78. doi: 10.1081/MB-200044588.

31. Zhao, Jingjing, Xiaopeng Zheng, Yehao Deng, Tao Li, Yuchuan Shao, Alexei Gruverman, Jeffrey Shield, and Jinsong Huang. 2016. “Is Cu a Stable Electrode Material in Hybrid Perovskite Solar Cells for a 30-Year Lifetime?” *Energy and Environmental Science* 9(12):3650–56. doi: 10.1039/c6ee02980a.

32. Li, Hao, Ruihan Yang, Chenyun Wang, Yafei Wang, Hao Chen, Hualin Zheng, Detao Liu, Ting Zhang, Feng Wang, Pengzhan Gu, Jiang Wu, Zhi David Chen, Ping Zhang, and Shibin Li. 2019. “Corrosive Behavior of Silver Electrode in Inverted Perovskite Solar Cells Based on Cu:NiOx.” *IEEE Journal of Photovoltaics* 9(4):1081–85. doi: 10.1109/JPHOTOV.2019.2910192.

33. Li, Jiangwei, Qingshun Dong, Nan Li, and Liduo Wang. 2017. “Direct Evidence of Ion Diffusion for the Silver-Electrode-Induced Thermal Degradation of Inverted Perovskite Solar Cells.” *Advanced Energy Materials* 7(14):1–8. doi: 10.1002/aenm.201602922.

34. Li, Zhen, Sneha A. Kulkarni, Pablo P. Boix, Enzheng Shi, Anyuan Cao, Kunwu Fu, Sudip K. Batabyal, Jun Zhang, Qihua Xiong, Lydia Helena Wong, Nripan Mathews, and Subodh G. Mhaisalkar. 2014. “Laminated Carbon Nanotube Networks for Metal Electrode-Free Efficient Perovskite Solar Cells.” *ACS Nano* 8(7):6797–6804. doi: 10.1021/nn501096h.

35. Luo, Qiang, Ronggen Wu, Lantian Ma, Chaojun Wang, Hu Liu, Hong Lin, Ning Wang, Yuan Chen, and Zhanhu Guo. 2021. “Recent Advances in Carbon Nanotube Utilizations in Perovskite Solar Cells.” *Advanced Functional Materials* 31(6):1–30. doi: 10.1002/adfm.202004765.

36. T. (2019, May 13). DIFFERENCE BETWEEN ITO AND FTO COATED GLASS. TECHINSTRO. https://www.techinstro.com/difference-ito-fto-coated-glass/

37. Asghar, M. I., J. Zhang, H. Wang, and P. D. Lund. 2017. “Device Stability of Perovskite Solar Cells – A Review.” *Renewable and Sustainable Energy Reviews* 77(July 2016):131–46. doi: 10.1016/j.rser.2017.04.003.

38. Hailegnaw, Bekele, Saar Kirmayer, Eran Edri, Gary Hodes, and David Cahen. 2015. “Rain on Methylammonium Lead Iodide Based Perovskites: Possible Environmental Effects of Perovskite Solar Cells.” *Journal of Physical Chemistry Letters* 6(9):1543–47. doi: 10.1021/acs.jpclett.5b00504.

39. Ates, Mehmet, Veysel Demir, Zikri Arslan, Mustafa Camas, and Fatih Celik. 2016. “Toxicity of Engineered Nickel Oxide and Cobalt Oxide Nanoparticles to Artemia Salina in Seawater.” *Water, Air, and Soil Pollution* 227(3). doi: 10.1007/s11270-016-2771-9.

40. Abate, Antonio. 2017. “Perovskite Solar Cells Go Lead Free.” *Joule* 1(4):659–64. doi: 10.1016/j.joule.2017.09.007.

41. The Risk Assessment Information System. (1995, July). Risk Assessment Information System. https://rais.ornl.gov/tox/profiles/nickel_and_nickel_compounds_f_V1.html

42. Dunnick, June K., Michael R. Elwell, Ann E. Radovsky, Janet M. Benson, Fletcher F. Hahn, Kristan J. Nikula, Edward B. Barr, and Charles H. Hobbs. 1995. “Comparative Carcinogenic Effects of Nickel Subsulfide, Nickel Oxide, or Nickel Sulfate Hexahydrate Chronic Exposures in the Lung.” *Cancer Research* 55(22):5251–56.

43. Rao, Haixia, Senyun Ye, Weihai Sun, Weibo Yan, Yunlong Li, Haitao Peng, Zhiwei Liu, Zuqiang Bian, Yongfang Li, and Chunhui Huang. 2016. “A 19.0% Efficiency Achieved in CuOx-Based Inverted CH3NH3PbI3-XClx Solar Cells by an Effective Cl Doping Method.” *Nano Energy* 27:51–57. doi: 10.1016/j.nanoen.2016.06.044.

44. Rajeswari, Ramireddy, Madoori Mrinalini, Seelam Prasanthkumar, and Lingamallu Giribabu. 2017. “Emerging of Inorganic Hole Transporting Materials For Perovskite Solar Cells.” *Chemical Record* 17(7):681–99. doi: 10.1002/tcr.201600117.

45. Becker, Markus, Thorsten Klüner, and Michael Wark. 2017. “Formation of Hybrid ABX3 Perovskite Compounds for Solar Cell Application: First-Principles Calculations of Effective Ionic Radii and Determination of Tolerance Factors.” *Dalton Transactions* 46(11):3500–3509. doi: 10.1039/c6dt04796c.

46. Li, Chonghea, Xionggang Lu, Weizhong Ding, Liming Feng, Yonghui Gao, and Ziming Guo. 2008. “Formability of ABX 3 (X = F, Cl, Br, I) Halide Perovskites.” *Acta Crystallographica Section B: Structural Science* 64(6):702–7. doi: 10.1107/S0108768108032734.

47. Gholipour, Somayeh, and Michael Saliba. 2019. *Bandgap Tuning and Compositional Exchange for Lead Halide Perovskite Materials*. Elsevier Inc.

48. Leijtens, Tomas, Kevin Bush, Rongrong Cheacharoen, Rachel Beal, Andrea Bowring, and Michael D. McGehee. 2017. “Towards Enabling Stable Lead Halide Perovskite Solar Cells; Interplay between Structural, Environmental, and Thermal Stability.” *Journal of Materials Chemistry A* 5(23):11483–500. doi: 10.1039/c7ta00434f.

49. Meloni S, Moehl T, Tress W, Franckevičius M, Saliba M, Lee YH, *et al*. Ionic polarization-induced current–voltage hysteresis in CH3NH3PbX3 perovskite solar cells. Nat Commun 2016 71 [Internet]. 2016 Feb 8 [cited 2021 Aug 2];7(1):1–9. Available from: https://www.nature.com/articles/ncomms10334

50. Wang, Ze, Zejiao Shi, Taotao Li, Yonghua Chen, and Wei Huang. 2017. “Stability of Perovskite Solar Cells: A Prospective on the Substitution of the A Cation and X Anion.” *Angewandte Chemie - International Edition* 56(5):1190–1212. doi: 10.1002/anie.201603694.

51. Pellet, Norman, Peng Gao, Giuliano Gregori, Tae-youl Yang, Mohammad K. Nazeeruddin, Joachim Maier, and Michael Grätzel. 2014. “Mixed-Organic-Cation Perovskite Photovoltaics for Enhanced Solar- Light Harvesting ** Angewandte.” (Arg 247404):3215–21. doi: 10.1002/ange.201309361.

52. Jeon, Nam Joong, Jun Hong Noh, Woon Seok Yang, Young Chan Kim, Seungchan Ryu, Jangwon Seo, and Sang Il Seok. n.d. “Compositional Engineering of Perovskite Materials for High-Performance Solar Cells.” *Nature*. doi: 10.1038/nature14133.

53. Article, Edge, Eric T. Hoke, Daniel J. Slotcavage, Emma R. Dohner, Andrea R. Bowring, Hemamala I. Karunadasa, and Michael D. Mcgehee. 2015. “Chemical Science Halide Hybrid Perovskites for Photovoltaics †.” doi: 10.1039/c4sc03141e.

54. Slotcavage, Daniel J., Hemamala I. Karunadasa, and Michael D. Mcgehee. 2016. “Light-Induced Phase Segregation in Halide- Perovskite Absorbers.” 1–7. doi: 10.1021/acsenergylett.6b00495.

55. Mcmeekin, David P., Golnaz Sadoughi, Waqaas Rehman, Giles E. Eperon, Michael Saliba, Maximilian T. Hörantner, Amir Haghighirad, Nobuya Sakai, Lars Korte, Bernd Rech, Michael B. Johnston, Laura M. Herz, and Henry J. Snaith. 2016. “A Mixed-Cation Lead Mixed-Halide Perovskite Absorber for Tandem Solar Cells.” 351(6269):151–56.

56. Wang P, Lü W, Wang M, Yang L, Wang F, Liu H, *et al*. Novel insights into the role of solvent environment in perovskite solar cells prepared by two-step sequential deposition. J Power Sources. 2020 Dec 31;480:228862

57. Liu R, Li H, Zhang F, Hu T, Yu Y, Liu C, *et al*. The synergistic effect of co-solvent engineering and thermal engineering towards phase control two-dimensional perovskite solar cells. Sol Energy. 2020 Oct 1;209:446–53.

58. He J, Li T, Liu X, Su H, Ku Z, Zhong J, *et al.* Influence of phase transition on stability of perovskite solar cells under thermal cycling conditions. Sol Energy. 2019 Aug 1;188:312–7.

59. Quarti, Claudio, Edoardo Mosconi, James M. Ball, Valerio D. Innocenzo, Chen Tao, Sandeep Pathak, Henry J. Snaith, and Filippo De Angelis. 2016. “Environmental Science Structural and Optical Properties of Methylammonium Lead Iodide across the Tetragonal to Cubic Phase Transition : Implications for Perovskite Solar Cells †.” 2–8. doi: 10.1039/c5ee02925b.

60. Nh, C. H., Sonia R. Raga, Luis K. Ono, Prof Yabing Qi, and See Yabing. 2016. “As Featured in : Energy & Environmental Science.” doi: 10.1039/c6ee02016j.

61. Worsley, David A., and Trystan M. Watson. 2014. “Thermal Evaluation †.” 19338–46. doi: 10.1039/c4ta04725g.

62. Conings, Bert, Jeroen Drijkoningen, Nicolas Gauquelin, Aslihan Babayigit, Jan D. Haen, Lien D. Olieslaeger, Anitha Ethirajan, Jo Verbeeck, Jean Manca, Edoardo Mosconi, Filippo De Angelis, and Hans-gerd Boyen. 2020. “Intrinsic Thermal Instability of Methylammonium Lead Trihalide Perovskite.” 1–8. doi: 10.1002/aenm.201500477.

63. Wang M. Exploring stability of formamidinium lead trihalide for solar cell application. Sci Bull. 2017 Feb 28;62(4):249–55.

64. Akbulatov AF, Martynenko VM, Frolova LA, Dremova NN, Zhidkov I, Tsarev SA, *et al*. Intrinsic thermal decomposition pathways of lead halide perovskites APbX3. Sol Energy Mater Sol Cells. 2020 Aug 15;213:110559.

65. Beal, Rachel E., Daniel J. Slotcavage, Tomas Leijtens, Andrea R. Bowring, Rebecca A. Belisle, William H. Nguyen, George F. Burkhard, Eric T. Hoke, and Michael D. Mcgehee. 2016. “Cesium Lead Halide Perovskites with Improved Stability for Tandem Solar Cells.” 2–7. doi: 10.1021/acs.jpclett.6b00002

66. Tan W, Bowring AR, Meng AC, Mcgehee MD, Mcintyre PC. Thermal Stability of Mixed Cation Metal Halide Perovskites in Air. ACS Appl Mater Interfaces [Internet]. 2018 [cited 2021 Aug 2];10:5491. Available from: www.acsami.org

67. Jørgensen, Mikkel, Kion Norrman, Suren A. Gevorgyan, Thomas Tromholt, Birgitta Andreasen, and Frederik C. Krebs. 2012. “Stability of Polymer Solar Cells.” 580–612. doi: 10.1002/adma.201104187.

68. Bailie, Colin D., Eva L. Unger, Shaik M. Zakeeruddin, Michael Gra, and Michael D. Mcgehee. 2014. “Melt-Infiltration.” 4864–70. doi: 10.1039/c4cp00116h.

69. Jena, Ajay Kumar, Masashi Ikegami, and Tsutomu Miyasaka. 2017. “Severe Morphological Deformation of Spiro-.” 1760–61. doi: 10.1021/acsenergylett.7b00582.

70. Zhou, Weiqi, Zhenhai Wen, and Peng Gao. 2018. “Less Is More : Dopant-Free Hole Transporting Materials for High-Efficiency Perovskite Solar Cells.” 1702512:1–28. doi: 10.1002/aenm.201702512.

71. Yang, Jinli, Braden D. Siempelkamp, Edoardo Mosconi, Filippo De Angelis, and Timothy L. Kelly. 2015. “Origin of the Thermal Instability in CH 3 NH 3 PbI 3 Thin Films Deposited on ZnO.” doi: 10.1021/acs.chemmater.5b01598.

72. You, Jingbi, Lei Meng, Tze-bin Song, Tzung-fang Guo, Yang Michael Yang, Wei-hsuan Chang, Ziruo Hong, Huajun Chen, Huanping Zhou, Qi Chen, Yongsheng Liu, and Nicholas De Marco. 2016. “Solution-Processed Metal Oxide Transport Layers.” 11(January):75–82. doi: 10.1038/nnano.2015.230.

73. Kim, Gee Yeong, Alessandro Senocrate, Tae-youl Yang, Giuliano Gregori, Michael Grätzel, and Joachim Maier. 2018. “In Halide Perovskites and Implications For.” *Nature Materials* 17(May):445–50. doi: 10.1038/s41563-018-0038-0.

74. Aristidou, Nicholas, Christopher Eames, Irene Sanchez-molina, Xiangnan Bu, Jan Kosco, M. Saiful Islam, and Saif A. Haque. 2017. “Fast Oxygen Diffusion and Iodide Defects Mediate Oxygen-Induced Degradation of Perovskite Solar Cells.” *Nature Communications* 8(May):1–10. doi: 10.1038/ncomms15218.

75. Perovskites, Halide, Aron Walsh, David O. Scanlon, Shiyou Chen, X. G. Gong, and Su-huai Wei. 2015. “Self-Regulation Mechanism for Charged Point Defects in Hybrid.” 1791–94. doi: 10.1002/anie.201409740.

76. Ball, James M., and Annamaria Petrozza. 2016. “Defects in Perovskite-Halides and Their Effects in Solar Cells.” (October). doi: 10.1038/NENERGY.2016.149.

77. Zhu, Zonglong, Dongbing Zhao, Chu-chen Chueh, Xueliang Shi, Zhongan Li, Alex K. Jen, Zonglong Zhu, Dongbing Zhao, Chu-chen Chueh, Xueliang Shi, and Zhongan Li. n.d. “Highly Efficient and Stable Perovskite Solar Cells Enabled by All-Crosslinked Charge- Transporting Layers Highly Efficient and Stable Perovskite Solar Cells Enabled by All-Crosslinked Charge-Transporting Layers.” *Joule* 2(1):168–83. doi: 10.1016/j.joule.2017.11.006.

78. Christians, Jeffrey A., Philip Schulz, Jonathan S. Tinkham, Tracy H. Schloemer, Steven P. Harvey, Bertrand J. Tremolet De Villers, Alan Sellinger, Joseph J. Berry, and Joseph M. Luther. 2018. “Solar Cells for > 1 , 000 Hour Operational Stability.” *Nature Energy* 3(January):68–74. doi: 10.1038/s41560-017-0067-y.

79. Bush, Kevin A., Axel F. Palmstrom, Zhengshan J. Yu, Mathieu Boccard, Rongrong Cheacharoen, Jonathan P. Mailoa, David P. Mcmeekin, Robert L. Z. Hoye, Colin D. Bailie, Tomas Leijtens, Ian Marius Peters, Maxmillian C. Minichetti, Nicholas Rolston, Rohit Prasanna, Sarah Sofia, Duncan Harwood, Wen Ma, Farhad Moghadam, Henry J. Snaith, Tonio Buonassisi, Zachary C. Holman, Stacey F. Bent, and Michael D. Mcgehee. 2017. “Tandem Solar Cells with Improved Stability.” 17009(February):1–7. doi: 10.1038/nenergy.2017.9.

80. Leijtens, Tomas, Giles E. Eperon, Nakita K. Noel, Severin N. Habisreutinger, Annamaria Petrozza, and Henry J. Snaith. 2015. “Stability of Metal Halide Perovskite Solar Cells.” 1–23. doi: 10.1002/aenm.201500963.

81. Domanski, Konrad, Essa A. Alharbi, Anders Hagfeldt, Michael Grätzel, and Wolfgang Tress. 2018. “Behaviour of Perovskite Solar Cells.” *Nature Energy* 3(January):61–67. doi: 10.1038/s41560-017-0060-5.

82. Leguy, M. A., Yinghong Hu, Mariano Campoy-quiles, M. Isabel Alonso, Oliver J. Weber, Pooya Azarhoosh, Mark Van Schilfgaarde, Mark T. Weller, Thomas Bein, Jenny Nelson, Pablo Docampo, and Piers R. F. Barnes. 2015. “Reversible Hydration of CH 3 NH 3 PbI 3 in Films, Single Crystals, and Solar Cells.” doi: 10.1021/acs.chemmater.5b00660.

83. Leijtens, Tomas, Eric T. Hoke, Giulia Grancini, Daniel J. Slotcavage, Giles E. Eperon, James M. Ball, Michele De Bastiani, Andrea R. Bowring, Nicola Martino, Konrad Wojciechowski, Michael D. Mcgehee, Henry J. Snaith, and Annamaria Petrozza. 2015. “Mapping Electric Field-Induced Switchable Poling and Structural Degradation in Hybrid Lead Halide Perovskite Thin Films.” 1–11. doi: 10.1002/aenm.201500962.

84. Leijtens, Tomas, Kevin Bush, Rongrong Cheacharoen, Rachel Beal, Andrea Bowring, and Michael D. Mcgehee. 2017. “Environmental , and Thermal Stability.” 11483–500. doi: 10.1039/c7ta00434f.

85. Stoumpos, Constantinos C., Christos D. Malliakas, and Mercouri G. Kanatzidis. 2013. “Semiconducting Tin and Lead Iodide Perovskites with Organic Cations: Phase Transitions, High Mobilities, and Near-Infrared Photoluminescent Properties.”

86. Habisreutinger, Severin N., Tomas Leijtens, Giles E. Eperon, Samuel D. Stranks, Robin J. Nicholas, and Henry J. Snaith. 2014. “Carbon Nanotube/Polymer Composites as a Highly Stable Hole Collection Layer in Perovskite Solar Cells.”

87. Noh, Jun Hong, Sang Hyuk Im, Jin Hyuck Heo, Tarak N. Mandal, and Sang Il Seok. 2013. “Chemical Management for Colorful, E Ffi Cient, and Stable Inorganic − Organic Hybrid Nanostructured Solar Cells.”

88. El-mellouhi, Fedwa, Asma Marzouk, Tayeb Bentria, and Sergey N. Rashkeev. 2016. “Hydrogen Bonding and Stability of Hybrid Organic – Inorganic Perovskites.” 2648–55. doi: 10.1002/cssc.201600864.

89. Leyden, Matthew R., Michael V Lee, Sonia R. Raga, and Yabing Qi. 2015. “Large Formamidinium Lead Trihalide Perovskite Solar Cells Using Chemical Vapor Deposition with High Reproducibility and Tunable Chlorine Concentrations †.” 16097–103. doi: 10.1039/c5ta03577e.

90. Frost, Jarvist M., Keith T. Butler, Federico Brivio, Christopher H. Hendon, Mark Van Schilfgaarde, and Aron Walsh. 2014. “Atomistic Origins of High-Performance in Hybrid Halide Perovskite Solar Cells.”

91. Li, Zhen, Mengjin Yang, Ji-sang Park, Su-huai Wei, Joseph J. Berry, and Kai Zhu. 2016. “Stabilizing Perovskite Structures by Tuning Tolerance Factor: Formation of Formamidinium and Cesium Lead Iodide Solid-State Alloys.” 2. doi: 10.1021/acs.chemmater.5b04107.

92. Lee, Jin-wook, Deok-hwan Kim, Hui-seon Kim, Seung-woo Seo, Sung Min Cho, and Nam-gyu Park. 2015. “Formamidinium and Cesium Hybridization for Photo- and Moisture-Stable Perovskite Solar Cell.” doi: 10.1002/aenm.201501310.

93. Gra, Carole, Shaik M. Zakeeruddin, Ursula Ro, and Michael Gra. 2016. “Environmental Science.” 656–62. doi: 10.1039/c5ee03255e.

94. Kim, Guan-woo, Gyeongho Kang, Mahdi Malekshahi Byranvand, Gang-young Lee, and Taiho Park. 2017. “Gradated Mixed Hole Transport Layer in a Perovskite Solar Cell : Improving Moisture Stability and E Ffi Ciency.” doi: 10.1021/acsami.7b07071.

95. Li, Faming, and Mingzhen Liu. 2017. “Moisture Stability of Perovskite Solar Cells.” *Journal of Materials Chemistry A: Materials for Energy and Sustainability* 5(April 2019):15447–59. doi: 10.1039/C7TA01325F.

96. Leijtens, Tomas, Tommaso Giovenzana, Severin N. Habisreutinger, Jonathan S. Tinkham, Nakita K. Noel, Brett A. Kamino, Golnaz Sadoughi, Alan Sellinger, and Henry J. Snaith. 2016. “Hydrophobic Organic Hole Transporters for Improved Moisture Resistance in Metal Halide Perovskite Solar Cells.” doi: 10.1021/acsami.5b10093.

97. Article, Edge, Eric T. Hoke, Daniel J. Slotcavage, Emma R. Dohner, Andrea R. Bowring, Hemamala I. Karunadasa, and Michael D. Mcgehee. 2015. “Chemical Science Halide Hybrid Perovskites for Photovoltaics †.” doi: 10.1039/c4sc03141e.

98. Barker, Alex J., Aditya Sadhanala, Felix Deschler, Marina Gandini, Satyaprasad P. Senanayak, Phoebe M. Pearce, Edoardo Mosconi, Andrew J. Pearson, Yue Wu, Ajay Ram, Srimath Kandada, Tomas Leijtens, Filippo De Angelis, and Richard H. Friend. 2017. “Defect-Assisted Photoinduced Halide Segregation in Mixed-Halide Perovskite Thin Films.” doi: 10.1021/acsenergylett.7b00282.

99. Yoon, Seog Joon, Masaru Kuno, and Prashant V Kamat. 2017. “Shif t Happens . How Halide Ion Defects In Fl Uence Photoinduced Segregation in Mixed Halide Perovskites.” 1–8. doi: 10.1021/acsenergylett.7b00357.

100. Braly, Ian L., Ryan J. Stoddard, Adharsh Rajagopal, Alexander R. Uhl, John K. Katahara, Alex K. Jen, and Hugh W. Hillhouse. 2017. “Current-Induced Phase Segregation in Mixed Halide Hybrid Perovskites and Its Impact on Two-Terminal Tandem Solar Cell Design.” doi: 10.1021/acsenergylett.7b00525.

101. Limmer, David T., and Naomi S. Ginsberg. 2017. “Origin of Reversible Photoinduced Phase Separation in Hybrid Perovskites.” doi: 10.1021/acs.nanolett.6b04453.

102. Leijtens, Tomas, Giles E. Eperon, Sandeep Pathak, Antonio Abate, Michael M. Lee, and Henry J. Snaith. 2013. “Overcoming Ultraviolet Light Instability of Sensitized TiO2 with Meso-Superstructured Organometal Tri-Halide Perovskite Solar Cells.” *Nature Communications* 1–8. doi: 10.1038/ncomms3885.

103. Correa-baena, Juan-pablo, Roldan Carmona, Giles Richardson, Jamie M. Foster, Filippo De Angelis, James M. Ball, Annamaria Petrozza, Nicolas Mine, Mohammad K. Nazeeruddin, Wolfgang Tress, Ullrich Steiner, Anders Hagfeldt,

and Antonio Abate. 2017. “Environmental Science Migration of Cations Induces Reversible Performance Losses over Day / Night Cycling in Perovskite Solar Cells †.” 604–13. doi: 10.1039/c6ee03352k.

104. Christians, Jeffrey A., Philip Schulz, Jonathan S. Tinkham, Tracy H. Schloemer, Steven P. Harvey, Bertrand J. Tremolet De Villers, Alan Sellinger, Joseph J. Berry, and Joseph M. Luther. 2018. “Solar Cells for > 1 , 000 Hour Operational Stability.” Nature Energy 3(January):68–74. doi: 10.1038/s41560-017-0067-y.

105. Online, View Article, Peng Gao, and Mohammad K. Nazeeruddin. 2014. “Environmental Science Organohalide Lead Perovskites for Photovoltaic Applications.” 1(c):2448–63. doi: 10.1039/c4ee00942h.

106. Istafaul, Mohammed, Haque Ansari, Ahsanulhaq Qurashi, and Mohammad Khaja. 2018. “Journal of Photochemistry and Photobiology C : Photochemistry Reviews Frontiers , Opportunities , and Challenges in Perovskite Solar Cells : A Critical Review.” *“Journal of Photochemistry & Photobiology, C: Photochemistry Reviews”* 35:1–24. doi: 10.1016/j.jphotochemrev.2017.11.002.

107. Snaith, Henry J., Antonio Abate, James M. Ball, Giles E. Eperon, Tomas Leijtens, Nakita K. Noel, Samuel D. Stranks, Jacob Tse-wei Wang, Konrad Wojciechowski, and Wei Zhang. 2014. “Anomalous Hysteresis in Perovskite Solar Cells.” (iii).

108. Tao, Lei, Jian Qiu, Bo Sun, Xiaojuan Wang, Xueqin Ran, Lin Song, Wei Shi, Qi Zhong, Ping Li, Hui Zhang, Yingdong Xia, Peter Müller-buschbaum, and Yonghua Chen. 2021. “Stability of Mixed-Halide Wide Bandgap Perovskite Solar Cells : Strategies and Progress.” *Journal of Energy Chemistry* 61:395–415. doi: 10.1016/j.jechem.2021.03.038.

109. Best Research-Cell Efficiency Chart. (2021). Retrieved 9 August 2021, from https://www.nrel.gov/pv/cell-efficiency.html

110. Miyata, A., Mitioglu, A., Plochocka, P. *et al.* Direct measurement of the exciton binding energy and effective masses for charge carriers in organic–inorganic tri-halide perovskites. *Nature Phys* **11,** 582–587 (2015). https://doi.org/10.1038/nphys3357

111. Li, W., Rao, H., Chen, B., Wang, X., & Kuang, D. (2017). A formamidinium–methylammonium lead iodide perovskite single crystal exhibiting exceptional optoelectronic properties and long-term stability. *Journal Of Materials Chemistry A*, *5*(36), 19431-19438. doi: 10.1039/c7ta04608a

112. Péan, E., De Castro, C., Dimitrov, S., De Rossi, F., Meroni, S., & Baker, J. et al. (2020). Investigating the Superoxide Formation and Stability in Mesoporous Carbon Perovskite Solar Cells with an Aminovaleric Acid Additive. Advanced Functional Materials, 30(12), 1909839. doi: 10.1002/adfm.201909839

113. Liu, C., Fan, J., Zhang, X., Shen, Y., Yang, L., & Mai, Y. (2015). *Hysteretic Behavior upon Light Soaking in Perovskite Solar Cells Prepared via Modified Vapor-Assisted Solution Process. ACS Applied Materials & Interfaces, 7(17), 9066–9071.* doi:10.1021/acsami.5b00375

114. Wu, Y., Xie, F., Chen, H., Yang, X., Su, H., & Cai, M. et al. (2017). Thermally Stable MAPbI3Perovskite Solar Cells with Efficiency of 19.19% and Area over 1 cm2achieved by Additive Engineering. *Advanced Materials*, *29*(28), 1701073. doi: 10.1002/adma.201701073

115. Seo, S., Jeong, S., Bae, C., Park, N., & Shin, H. (2018). Perovskite Solar Cells with Inorganic Electron- and Hole-Transport Layers Exhibiting Long-Term (≈500 h) Stability at 85 °C under Continuous 1 Sun Illumination in Ambient Air. *Advanced Materials*, *30*(29), 1801010. doi: 10.1002/adma.201801010

116. Cheacharoen, R., Boyd, C., Burkhard, G., Leijtens, T., Raiford, J., & Bush, K. et al. (2018). Encapsulating perovskite solar cells to withstand damp heat and thermal cycling. *Sustainable Energy & Fuels*, *2*(11), 2398-2406. doi: 10.1039/c8se00250a

117. Prasanna, R., Leijtens, T., Dunfield, S., Raiford, J., Wolf, E., & Swifter, S. et al. (2019). Design of low bandgap tin–lead halide perovskite solar cells to achieve thermal, atmospheric and operational stability. *Nature Energy*, *4*(11), 939-947. doi: 10.1038/s41560-019-0471-6

118. Raiford, J., Boyd, C., Palmstrom, A., Wolf, E., Fearon, B., & Berry, J. et al. (2019). Enhanced Nucleation of Atomic Layer Deposited Contacts Improves Operational Stability of Perovskite Solar Cells in Air. *Advanced Energy Materials*, *9*(47), 1902353. doi: 10.1002/aenm.201902353

119. V. Zardetto et al., "Towards Large Area Stable Perovskite Solar Cells and Modules," 2019 IEEE 46th Photovoltaic Specialists Conference (PVSC), 2019, pp. 0838-0840, doi: 10.1109/PVSC40753.2019.8981217.

120. Francesco Di Giacomo, Santhosh Shanmugam, Henri Fledderus, Bardo J. Bruijnaers, Wiljan J.H. Verhees, Maarten S. Dorenkamper, Sjoerd C. Veenstra, Weiming Qiu, Robert Gehlhaar, Tamara Merckx, Tom Aernouts, Ronn Andriessen, Yulia Galagan, Up-scalable sheet-to-sheet production of high efficiency perovskite module and solar cells on 6-in. substrate using slot die coating, Solar Energy Materials and Solar Cells, Volume 181, 2018, Pages 53-59, ISSN 0927-0248, https://doi.org/10.1016/j.solmat.2017.11.010.

121. V. Zardetto et al., "Atmospheric Pressure Spatial ALD Layer for Ambient, Thermally and Light Stable p-i-n Planar Perovskite Solar Cells," 2018 IEEE 7th World Conference on Photovoltaic Energy Conversion (WCPEC) (A Joint Conference of 45th IEEE PVSC, 28th PVSEC & 34th EU PVSEC), 2018, pp. 3514-3517, doi: 10.1109/PVSC.2018.8548089.

122. Xin Yan, Jianghui Zheng, LingLing Zheng, Guanhua Lin, Huangding Lin, Guo Chen, Binbin Du, Fengyan Zhang, Optimization of sputtering NiOx films for perovskite solar cell applications, Materials Research Bulletin, Volume 103, 2018, Pages 150-157, ISSN 0025-5408, https://doi.org/10.1016/j.materresbull.2018.03.027.

123. Wang, K., Shen, P., Li, M., Chen, S., Lin, M., Chen, P., & Guo, T. (2014). Low-Temperature Sputtered Nickel Oxide Compact Thin Film as Effective Electron Blocking Layer for Mesoscopic NiO/CH3NH3PbI3Perovskite Heterojunction Solar Cells. *ACS Applied Materials & Interfaces*, *6*(15), 11851-11858. doi: 10.1021/am503610u

124. Zhao, Y., Deng, Q., Guo, R., Wu, Z., Li, Y., & Duan, Y. et al. (2020). Sputtered Ga-Doped SnOx Electron Transport Layer for Large-Area All-Inorganic Perovskite Solar Cells. *ACS Applied Materials & Interfaces*, *12*(49), 54904-54915. doi: 10.1021/acsami.0c19540

125. Richard W. Johnson, Adam Hultqvist, Stacey F. Bent, A brief review of atomic layer deposition: from fundamentals to applications, Materials Today, Volume 17, Issue 5, 2014, Pages 236-246, ISSN 1369-7021, https://doi.org/10.1016/j.mattod.2014.04.026.

126. Whitaker, J., Kim, D., Larson, B., Zhang, F., Berry, J., van Hest, M., & Zhu, K. (2018). Scalable slot-die coating of high performance perovskite solar cells. *Sustainable Energy & Fuels*, *2*(11), 2442-2449. doi: 10.1039/c8se00368h

127. Tao, Yuguo. (2016). Screen-Printed Front Junction n-Type Silicon Solar Cells. 10.5772/63198.

128. Smets, A., Jäger, K., Isabella, O., van Swaaij, R., & Zeman, M. (2016). *Solar Energy: The physics and engineering of photovoltaic conversion, technologies and systems*. UIT Cambridge Limited

129. Mojtaba Abdi-Jalebi, M. Ibrahim Dar, Aditya Sadhanala, Erik M.J. Johansson, Meysam Pazoki, Chapter 3 - Optical absorption and photoluminescence spectroscopy, Editor(s): Meysam Pazoki, Anders Hagfeldt, Tomas Edvinsson, In Micro and Nano Technologies, Characterization Techniques for Perovskite Solar Cell Materials, Elsevier, 2020, Pages 49-79, ISBN 9780128147276, https://doi.org/10.1016/B978-0-12-814727-6.00003-7

130. M. Bodiul Islam, M. Yanagida, Y. Shirai, Y. Nabetani, K. Miyano, Highly stable semi-transparent MAPbI3 perovskite solar cells with operational output for 4000 h, Solar Energy Materials and Solar Cells, Volume 195, 2019, Pages 323-329, ISSN 0927-0248, https://doi.org/10.1016/j.solmat.2019.03.004.

131. Baranwal, A., Kanda, H., Shibayama, N., Masutani, H., Peiris, T., & Kanaya, S. et al. (2018). Thermal Degradation Analysis of Sealed Perovskite Solar Cell with Porous Carbon Electrode at 100 °C for 7000 h. *Energy Technology*, *7*(2), 245-252. doi: 10.1002/ente.201800572

132. Sheikh, A., Munir, R., Haque, M., Bera, A., Hu, W., & Shaikh, P. et al. (2017). Effects of High Temperature and Thermal Cycling on the Performance of Perovskite Solar Cells: Acceleration of Charge Recombination and Deterioration of Charge Extraction. *ACS Applied Materials & Interfaces*, *9*(40), 35018-35029. doi: 10.1021/acsami.7b11250

133. Choi, K., Lee, J., Kim, H., Park, C., Kim, G., & Choi, H. et al. (2018). Thermally stable, planar hybrid perovskite solar cells with high efficiency. *Energy & Environmental Science*, *11*(11), 3238-3247. doi: 10.1039/c8ee02242a

134. Mesquita, I., Andrade, L., & Mendes, A. (2019). Temperature Impact on Perovskite Solar Cells Under Operation. *Chemsuschem*, *12*(10), 2186-2194. doi: 10.1002/cssc.201802899

135. Fang, Y., Wang, X., Wang, Q., Huang, J., & Wu, T. (2014). Impact of annealing on spiro-OMeTAD and corresponding solid-state dye sensitized solar cells. *Physica Status Solidi (A)*, *211*(12), 2809-2816. doi: 10.1002/pssa.201431366

136. Wayesh Qarony, Mohammad I. Hossain, Alberto Salleo, Dietmar Knipp, Yuen Hong Tsang, Rough versus planar interfaces: How to maximize the short circuit current of perovskite single and tandem solar cells, Materials Today Energy, Volume 11, 2019, Pages 106-113, ISSN 2468-6069, https://doi.org/10.1016/j.mtener.2018.10.001.

137. Qian Zhao, Runsheng Wu, Zheling Zhang, Jian Xiong, Zhen He, Baojin Fan, Zhongjun Dai, Bingchu Yang, Xiaogang Xue, Ping Cai, Shiping Zhan, Xiaoling Zhang, Jian Zhang, Achieving efficient inverted planar perovskite solar cells with nondoped PTAA as a hole transport layer, Organic Electronics, Volume 71, 2019, Pages 106-112, ISSN 1566-1199, https://doi.org/10.1016/j.orgel.2019.05.019.

138. International Electrotechnical Commission. (2019). *TC 82 - Solar photovoltaic energy systems* (p. 15). Retrieved from https://webstore.iec.ch/publication/64040

139. Hao, M., Wang, H., Wang, Y., Qin, Y., Zhang, J., & Ai, X. (2020). Effect of energetic distribution of trap states on fill factor in perovskite solar cells. *Journal Of Power Sources*, *479*, 229077. doi: 10.1016/j.jpowsour.2020.229077

140. Chen, B., Yang, M., Priya, S., & Zhu, K. (2016). Origin of J–V Hysteresis in Perovskite Solar Cells. *The Journal Of Physical Chemistry Letters*, *7*(5), 905-917. doi: 10.1021/acs.jpclett.6b00215

141. Unger, E., Hoke, E., Bailie, C., Nguyen, W., Bowring, A., & Heumüller, T. et al. (2014). Hysteresis and transient behavior in current–voltage measurements of hybrid-perovskite absorber solar cells. *Energy Environ. Sci.*, *7*(11), 3690-3698. doi: 10.1039/c4ee02465f

142. Yang, J., & Hu, M. (2017). Temperature-Induced Large Broadening and Blue Shift in the Electronic Band Structure and Optical Absorption of Methylammonium Lead Iodide Perovskite. *The Journal Of Physical Chemistry Letters*, *8*(16), 3720-3725. doi: 10.1021/acs.jpclett.7b01719

143. Yu, M., Wang, H., Zhao, J., Qin, Y., Zhang, J., & Ai, X. (2020). The influence of fullerene on hysteresis mechanism in planar perovskite solar cells. *Chemical Physics Letters*, *750*, 137443. doi: 10.1016/j.cplett.2020.137443

144. Kim, S., Bae, S., Lee, S., Cho, K., Lee, K., & Kim, H. et al. (2017). Relationship between ion migration and interfacial degradation of CH3NH3PbI3 perovskite solar cells under thermal conditions. *Scientific Reports*, *7*(1). doi: 10.1038/s41598-017-00866-6

145. Mahesh, S., Ball, J., Oliver, R., McMeekin, D., Nayak, P., Johnston, M., & Snaith, H. (2020). Revealing the origin of voltage loss in mixed-halide perovskite solar cells. *Energy & Environmental Science*, *13*(1), 258-267. doi: 10.1039/c9ee02162k

146. Ahangharnejhad, R., Friedl, J., Phillips, A., & Heben, M. (2021). Understanding VOC and performance deficit in wide bandgap perovskite photovoltaic devices. *Solar Energy Materials And Solar Cells*, *225*, 111015. doi: 10.1016/j.solmat.2021.111015

147. Tennyson, E., Roose, B., Garrett, J., Gong, C., Munday, J., Abate, A., & Leite, M. (2019). Cesium-Incorporated Triple Cation Perovskites Deliver Fully Reversible and Stable Nanoscale Voltage Response. *ACS Nano*. doi: 10.1021/acsnano.8b07295

148. Tennyson, E., Howard, J., Roose, B., Garrett, J., Munday, J., Abate, A., & Leite, M. (2019). The Effects of Incident Photon Energy on the Time-Dependent Voltage Response of Lead Halide Perovskites. *Chemistry Of Materials*, *31*(21), 8969-8976. doi: 10.1021/acs.chemmater.9b03089

149. Farooq, A., Khan, M., Abzieher, T., Voigt, A., Lupascu, D., & Lemmer, U. et al. (2021). Photodegradation of Triple-Cation Perovskite Solar Cells: The Role of Spectrum and Bias Conditions. *ACS Applied Energy Materials*, *4*(4), 3083-3092. doi: 10.1021/acsaem.0c02813

150. Ginting, R., Jeon, M., Lee, K., Jin, W., Kim, T., & Kang, J. (2017). Degradation mechanism of planar-perovskite solar cells: correlating evolution of iodine distribution and photocurrent hysteresis. *Journal Of Materials Chemistry A*, *5*(9), 4527-4534. doi: 10.1039/c6ta09202k

151. Guo, X., Ngai, K., Qin, M., Lu, X., Xu, J., & Long, M. (2020). The compatibility of methylammonium and formamidinium in mixed cation perovskite: the optoelectronic and stability properties. *Nanotechnology*, *32*(7), 075406. doi: 10.1088/1361-6528/abc50c

152. Namkoong, G., Mamun, A., & Ava, T. (2018). Impact of PCBM/C60 electron transfer layer on charge transports on ordered and disordered perovskite phases and hysteresis-free perovskite solar cells. *Organic Electronics*, *56*, 163-169. doi: 10.1016/j.orgel.2018.02.010

153. Rabenau, T., Simon, A., Kremer, R., & Sohmen, E. (1993). The energy gaps of fullerene C60 and C70 determined from the temperature dependent microwave conductivity. *Zeitschrift F*[illegible]*R Physik B Condensed Matter*, *90*(1), 69-72. doi: 10.1007/bf01321034

154. Shao, S., & Loi, M. (2019). The Role of the Interfaces in Perovskite Solar Cells. *Advanced Materials Interfaces*, *7*(1), 1901469. doi: 10.1002/admi.201901469

155. Yoo, S., Kum, J., & Cho, S. (2011). Tuning the electronic band structure of PCBM by electron irradiation. *Nanoscale Research Letters*, *6*(1), 545. doi: 10.1186/1556-276x-6-545

156. Saliba, M., & Etgar, L. (2020). Current Density Mismatch in Perovskite Solar Cells. *ACS Energy Letters*, *5*(9), 2886-2888. doi: 10.1021/acsenergylett.0c01642

157. Cowan, S., Wang, J., Yi, J., Lee, Y., Olson, D., & Hsu, J. (2013). Intensity and wavelength dependence of bimolecular recombination in P3HT:PCBM solar cells: A white-light biased external quantum efficiency study. *Journal Of Applied Physics*, *113*(15), 154504. doi: 10.1063/1.4801920

158. Hierrezuelo-Cardet, P., Palechor-Ocampo, A., Caram, J., Ventosinos, F., Pérez-del-Rey, D., Bolink, H., & Schmidt, J. (2020). External quantum efficiency measurements used to study the stability of differently deposited perovskite solar cells. *Journal Of Applied Physics*, *127*(23), 235501. doi: 10.1063/5.0011503

159. Paek, S., Cho, N., Choi, H., Jeong, H., Lim, J., & Hwang, J. et al. (2014). Improved External Quantum Efficiency from Solution-Processed (CH3NH3)PbI3 Perovskite/PC71BM Planar Heterojunction for High Efficiency Hybrid Solar Cells. *The Journal Of Physical Chemistry C*, *118*(45), 25899-25905. doi: 10.1021/jp508162p

160. Park, S., Roy, A., Beaupré, S., Cho, S., Coates, N., & Moon, J. et al. (2009). Bulk heterojunction solar cells with internal quantum efficiency approaching 100%. *Nature Photonics*, *3*(5), 297-302. doi: 10.1038/nphoton.2009.69

161. Samu, G., Janáky, C., & Kamat, P. (2017). A Victim of Halide Ion Segregation. How Light Soaking Affects Solar Cell Performance of Mixed Halide Lead Perovskites. *ACS Energy Letters*, *2*(8), 1860-1861. doi: 10.1021/acsenergylett.7b00589

162. Tress, W., Yavari, M., Domanski, K., Yadav, P., Niesen, B., & Baena, J. et al. (2018). Correction: Interpretation and evolution of open-circuit voltage, recombination, ideality factor and subgap defect states during reversible light-soaking and irreversible degradation of perovskite solar cells. *Energy & Environmental Science*, *11*(3), 715-715. doi: 10.1039/c8ee90011f

163. Głowienka, D., Zhang, D., Di Giacomo, F., Najafi, M., Veenstra, S., Szmytkowski, J., & Galagan, Y. (2020). Role of surface recombination in perovskite solar cells at the interface of HTL/CH3NH3PbI3. *Nano Energy*, *67*, 104186. doi: 10.1016/j.nanoen.2019.104186

164. Koster, L., Mihailetchi, V., Xie, H., & Blom, P. (2005). Origin of the light intensity dependence of the short-circuit current of polymer/fullerene solar cells. *Applied Physics Letters*, *87*(20), 203502. doi: 10.1063/1.2130396

165. Wang, Y., Ju, H., Mahmoudi, T., Liu, C., Zhang, C., & Wu, S. et al. (2021). Cation-size mismatch and interface stabilization for efficient NiOx-based inverted perovskite solar cells with 21.9% efficiency. *Nano Energy*, *88*, 106285. doi: 10.1016/j.nanoen.2021.106285

166. Zhao, C., Chen, B., Qiao, X., Luan, L., Lu, K., & Hu, B. (2015). Revealing Underlying Processes Involved in Light Soaking Effects and Hysteresis Phenomena in Perovskite Solar Cells. *Advanced Energy Materials*, *5*(14), 1500279. doi: 10.1002/aenm.201500279

167. Ni, Z., Bao, C., Liu, Y., Jiang, Q., Wu, W., & Chen, S. et al. (2020). Resolving spatial and energetic distributions of trap states in metal halide perovskite solar cells. *Science*, *367*(6484), 1352-1358. doi: 10.1126/science.aba0893

168. Spalla, M., Perrin, L., Planes, E., Matheron, M., Berson, S., & Flandin, L. (2020). Effect of the Hole Transporting/Active Layer Interface on the Perovskite Solar Cell Stability. *ACS Applied Energy Materials*, *3*(4), 3282-3292. doi: 10.1021/acsaem.9b02281

169. W. Nie, J.-C. Blancon, A. J. Neukirch, K. Appavoo, H. Tsai, M. Chhowalla, M. A. Alam, M. Y. Sfeir, C. Katan, J. Even, S. Tretiak, J. J. Crochet, G. Gupta and A. D. Mohite, Lightactivated photocurrent degradation and self-healing in perovskite solar cells, Nat. Commun., 2016, 7, 11574

170. C. Zhao, B. Chen, X. Qiao, L. Luan, K. Lu and B. Hu, Revealing Underlying Processes Involved in Light Soaking Effects and Hysteresis Phenomena in Perovskite Solar Cells, Adv. Energy Mater., 2015, 5, 1500279

171. Kim, S., Jang, J., Wu, Z., Lee, M., Woo, H., & Hwang, I. (2021). Interfacial Defects Change the Correlation between Photoluminescence, Ideality Factor, and Open-Circuit Voltage in Perovskite Solar Cells. *Small*, 2101839. doi: 10.1002/smll.202101839

172. Patidar, R., Burkitt, D., Hooper, K., Richards, D., & Watson, T. (2020). Slot-die coating of perovskite solar cells: An overview. *Materials Today Communications*, *22*, 100808. doi: 10.1016/j.mtcomm.2019.100808